UNIVERSITÀ DEGLI STUDI DI MILANO

Doctoral School of Computer Science
Department of Computer Science

Dissertation submitted in partial fulfillment of the requirements for the degree of
Doctor of Philosophy in Computer Science
(XXIX Cycle)

ADAPTIVE MODEL-BASED CARDIAC SIGNALS ANALYSIS AND FEATURE EXTRACTION

INF/01

DOCTORAL DISSERTATION OF:
Ebadollah Kheirati Roonizi

ADVISOR:
Prof. Roberto Sassi

DIRECTOR OF DOCTORAL SCHOOL:
Prof. Paolo Boldi

Academic Year 2016/'17

ABSTRACT

Signal modeling and feature extraction are among the most crucial and important steps for stochastic signal processing. In this thesis, a general framework that employs adaptive model-based recursive Bayesian state estimation for signal processing and feature extraction is described. As a case study, the proposed framework is studied for the problem of cardiac signal analysis. The main objective is to improve the signal processing aspects of cardiac signals by developing new techniques based on adaptive modelling of electrocardiogram (ECG) wave-forms. Specially several novel and improved approaches to model-based ECG decomposition, waveform characterization and feature extraction are proposed and studied in detail. In the concept of ECG decomposition and wave-forms characterization, the main idea is to extend and improve the signal dynamical models (*i.e.* reducing the non-linearity of the state model with respect to previous solutions) while combining with Kalman smoother to increase the accuracy of the model in order to split the ECG signal into its waveform components, as it is proved that Kalman filter/smoother is an optimal estimator in minimum mean square error (MMSE) for linear dynamical systems. The framework is used for many real applications, such as: ECG components extraction, ST segment analysis (estimation of a possible marker of ventricular repolarization known as T/QRS ratio) and T-wave Alternans (TWA) detection, and its extension to many other applications is straightforward.

Based on the proposed framework, a novel model to characterization of Atrial Fibrillation (AF) is presented which is more effective when compared with other methods proposed with the same aims. In this model, ventricular activity (VA) is represented by a sum of Gaussian kernels, while a sinusoidal model is employed for atrial activity (AA). This new model is able to track AA, VA and fibrillatory frequency simultaneously against other methods which try to analyze the atrial fibrillatory waves (f-waves) after VA cancellation.

Furthermore we study a new ECG processing method for assessing the spatial dispersion of ventricular repolarization (SHVR) using $\mathcal{V}$-index and a novel algorithm to estimate the index is presented, leading to more accurate estimates. The proposed algorithm was used to study the diagnostic and prognostic value of the $\mathcal{V}$-index in patients with symptoms suggestive of Acute Myocardial Infraction (AMI).

CONTENTS

LIST OF TABLES

1 INTRODUCTION

1.1 CARDIAC SIGNALS

The heart is one of the most important organs in the body, which pumps blood through the vessels of the circulatory system. The pumped blood provides all the vital materials which is necessary for functioning human bodies (*e.g.* oxygen, glucose, sodium, calcium, potassium and amino acids) and removes the waste products which is non-necessity. The heart is essentially a muscle that contracts regularly and continuously, to fulfill the pumping function of the blood. The pumping action is caused by a ionic activity that repeats itself. It is called cardiac cycle and its frequency described by the heart rate. The cardiac cycle starts with contraction of the atria and ends with relaxation of the ventricles. In the case of arrhythmia such as premature atrial contractions (PAC), premature ventricular contractions[1] (PVCs), atrial fibrillation (AF), paroxysmal supraventricular tachycardia (PSVT) and ventricular fibrillation (VF), the electrical activity can affect the heart's ability to pump properly. Fortunately, the electrical activity of the heart muscles can be measured by an array of electrodes placed on the body surface. It is represented by a graphical signal known as electrocardiogram (ECG). Fig. (1.1) shows how one cycle of the ECG is completed. It also shows how the heart chambers involve to create the ECG beat. As a result ECG can be used for studying the function of heart and doctors and clinicians can look at the ECG signal to asses the normality or abnormality of the heart.

1 A PVC is a heart beat which is autonomously triggered in the ventricles, and not in the sinus node. PVCs are common events which do not necessarily imply a negative heart condition [1].

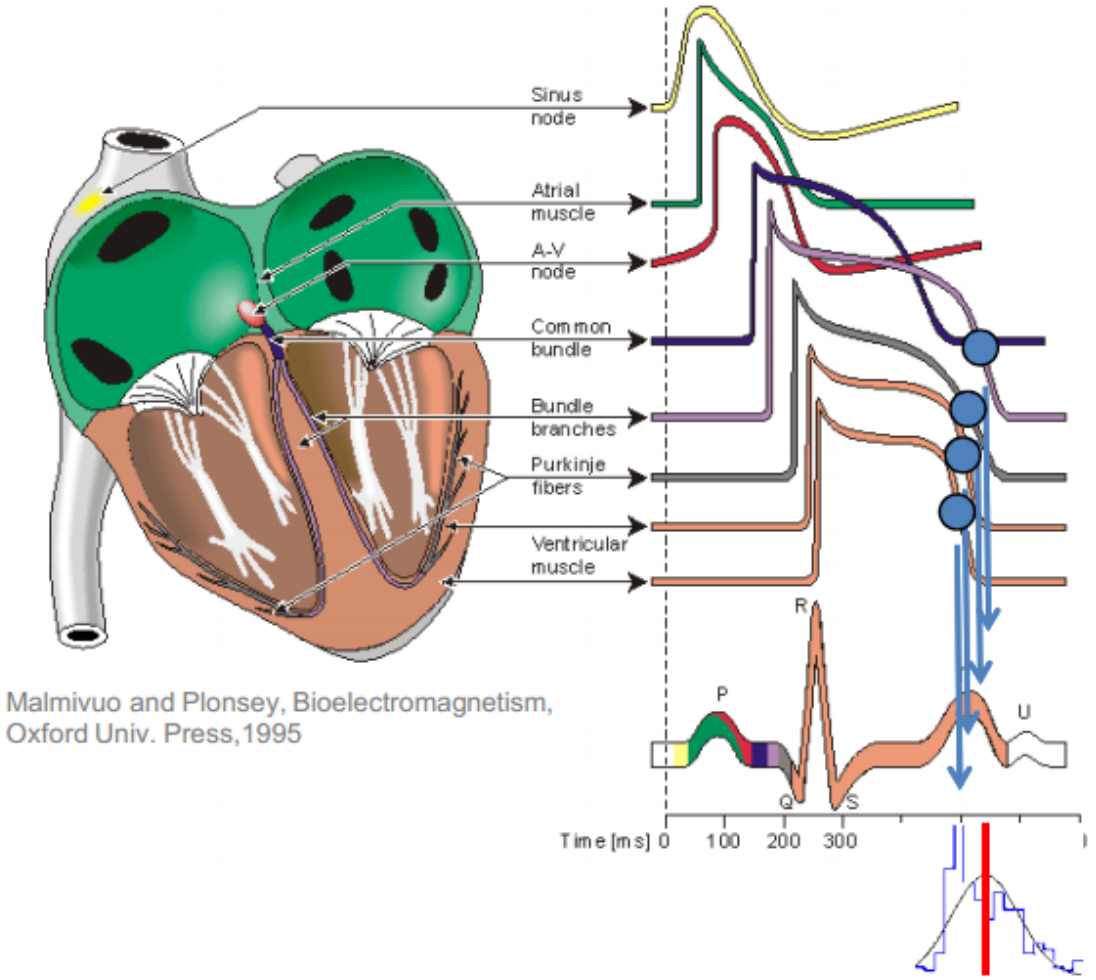

Figure 1.1: A typical representation of the ECG waves.

1.2 STATE OF THE ART

1.2.1 PRIOR WORKS FOR ECG DELINEATION

The ECG is a non-stationary signal and composed of a P wave, which represents depolarization of the atrial musculature, a QRS complex [2] which is the combined result of the repolarization of the atria and depolarization of the ventricles, which occur almost simultaneously and a T wave which is the positive deflection after each QRS complex and represents the ventricular repolarization. Most of the clinically relevant information can be found within the amplitudes, shapes and intervals between these waveforms. Some of these features are shown in Fig. (1.2). These features can be used for many applications (*e.g.* ST-waveform analysis for intrapartum fetal monitoring [2, 3], changes in P wave morphology due to various conditions [4, 5], QT interval analysis [6, 7] and T wave alternans (TWA) [8]). So an accurate and robust procedure for automatic ECG labeling is an important goal for clinicians and biomedical engineers.

2 QRS complex is the combination of the Q, R and S wave.

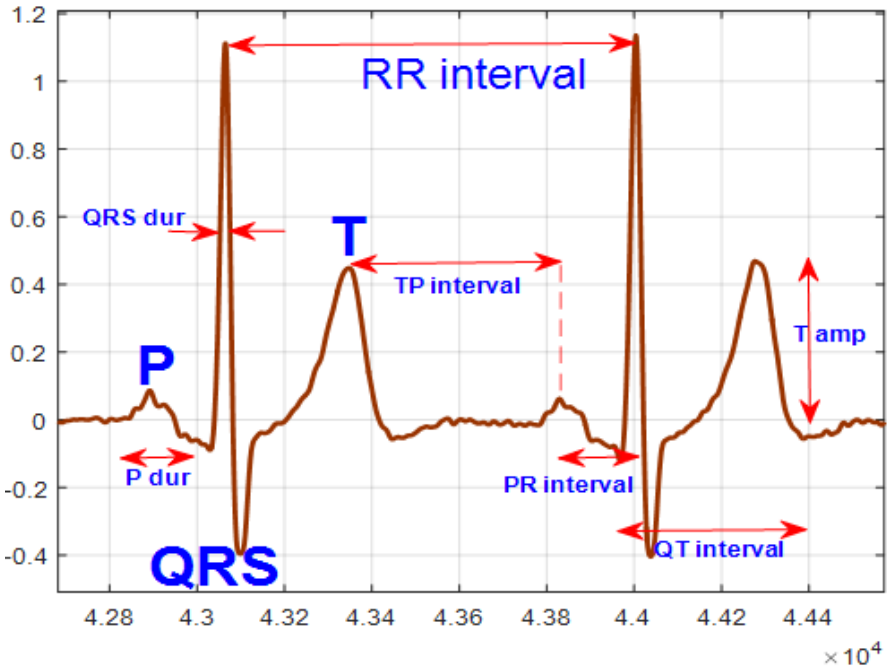

Figure 1.2: A single ECG beat with its waveforms and intervals.

A preliminary ECG components extraction phase, where the different waves are separated from each other, could surely simplify the task. Hence most of the cardiac disease classification algorithms begin with the separation or delineation of the individual ECG signal components (P, QRS and T wave). There are many methods in the literature to characterize the ECG waveform components.

One of the popular methods for QRS complex detection was proposed by Pan-Tompkins [9]. The fact that the typical frequency components of a QRS complex is about 10-25 Hz, the temporal derivative based method is used to attenuate the noise and artifacts out of this ranges. Digital filters have also been used for the same aim [10, 11, 12]. High-pass filters are typically used to attenuate P and T wave components as well as baseline wander. In [13, 14], neural network has been used for QRS detection. It can be considered as an adaptive nonlinear signal processing method.

Wavelet transform has been widely used to characterize the ECG component features. One of the early applications of wavelet transform in ECG analysis was proposed by Meste *et al.* to highlight ventricular late potentials and to observe temporal and frequency variability in the ECG [15]. Senhadji *et al.* compared the ability of different mother wavelets (like Daubechies, spline and Morlet) to recognize and describe isolated cardiac beats [16]. In [17], a technique based wavelet to obtain a multiresolution representation of some example patterns for the automatic detection of any recurrent pattern in ECG time series has been discussed. The main advantage of the technique is that it solves the problem of automatic P wave detection in Holter ECG recordings. The mother wavelets which have been used for ECG delineation are wavelet Gaussian function [18, 19] and quadratic Spline [20, 21]. The quadratic spline was originally proposed in [22].

Another examples are: adaptive filters [23], hidden Markov models (HMM) [24, 25, 26], zero crossing [27], Kalman filter [28, 29], dynamic time warping (DTW) [30, 31], support vector machine (SVM) [32], particle filters [33], Particle swarm optimization (PSO) with extended Kalman filter (EKF) [34] and partially collapsed Gibbs sampler (PCGS) [35, 36].

1.2.2 PRIOR WORKS FOR ATRIAL FIBRILLATION ANALYSIS

Atrial fibrillation (AF) is one of the most common forms of supraventricular arrhythmia and an important cause of morbidity and hospitalizations in the world, affecting approximately 5 percent of its population over 50 years of age [37, 38]. AF is a heart rhythm abnormality and is associated with an increased risk of stroke and heart failure [39]. The studies have shown that there is a close relationship between AF and obesity [40], obstructive sleep apnea [41], and long-term alcoholism [42]. This arrhythmia may appear in three different forms: paroxysmal, permanent and persistent AF. During AF, the conduction in the atria is irregular and often composed of several spiralling patterns, resulting in an irregular heartbeat. The atrial activity (AA), as detected on the surface electrocardiogram (ECG), is characterized by a baseline fluctuating in the range $3-12$ Hz, f-waves, instead of P-waves. In atrial flutter, which is another type of atrial tachyarrhythmia, the P waves are replaced by f-waves which are slower and more regular than the f-waves during AF. The separation of atrial activity from the surface ECGs, recorded during AF for further analysis, is an important task to help physicians and clinicians. In recent years, several methods have been proposed for extracting [43, 44, 45, 46, 47] and analyzing [48, 49, 50, 51] f-waves. Actually atrial and ventricular activities overlap in both time and frequency domains. As a result, one needs to extract f-waves from the mixture of ventricular (QRS-T) and atrial signals, and, due to the much higher amplitude of the ventricular activity (VA) signals, most of the existing procedures deal with the cancellation of QRS-T [52], instead of the direct extraction of f-waves.

The procedures for analyzing f-waves can be divided into two parts. First, cancellation of QRS-T in time domain [53] and then analyzing the residual AF waveforms in frequency domain [54, 55, 56]. The existing QRS-T cancellation or f-waves extraction approaches in the literature can be categorized by their methodologies, which include linear or nonlinear decomposition and adaptive filtering [50, 57]. The number of ECG leads for ventricular activity cancellation is an important issue which should be considered. The QRS-T cancellation can be performed using single or multi channel ECG recordings. Most methods try to remove ventricular activity using multi-channel recordings such as spatiotemporal QRS-T cancellation [58] and Blind source separation (BSS) [44, 45]. For instance, BSS derives a global atrial signal with contributions from all leads. Other methods include principal component analysis (PCA) [59] and echo state neural network [60]. Although the algorithms that deal with extracting atrial activity using multi channel recordings often outperform those methods exploiting single channel recordings, the performance of the former will decrease when the number of leads is reduced (*e.g.*, in specific applicative context as telemedicine or mobile applications).

The issue is particularly important: (i) to analyze Holter recordings in which only two or three leads are usually available; (ii) for the detection of AF in atrial implantable cardioverter defibrilators and specialized monitors [61]; (iii) in all those operative conditions where collecting ECGs with a very limited number of ECG channels is the only viable option (especially outside healthcare premises in wearable devices).The earlier method for single lead applications was average beat subtraction (ABS) [46, 58, 62]. It removes ventricular activity by subtracting an average beat representative of the ventricular activity from each individual beat. Adaptive singular value decomposition (SVD) is an extended version of ABS which removes the ventricular activity using an adaptive SVD [63]. Adaptive singular value cancellation (ASVC) which is applied to each single beat was proposed by Alcareaz et al. in order to overcome the limitations of ABS [63, 64].

Atrial fibrillation signal extraction based on wavelet transform has been presented in [65]. In [66] a method based on event synchronous adaptive filter (ESAF) is proposed for AF detection from single ECG lead. Alternative methods for extracting AA signal from single lead ECG recordings are weighed average beat subtraction (WABS) and the extraction algorithm based on maximum likelihood estimation (MLE) proposed by H. Dai *et al.* [67]. In WABS, the variation of QRS complexes in different beat cycles is also considered by modulating the ABS template with a coefficient obtained by minimizing the mean square error. In MLE method, first, the probability distribution functions (PDFs) of AA and VA signals are modeled using a generalized Gaussian model in training stage. Then, AA signal is extracted by maximizing the likelihood function.

Once earned the atrial signal by removing QRS-T, the extracted atrial activity (residual ECG) is used to detect the atrial fibrillatory frequency, *i.e.* the repetition rate of the f-waves. The AF frequency can be used for monitoring drug effects, as well as for predicting spontaneous or drug-induced AF termination; A low AF frequency has proved to be a predictor of spontaneous AF termination [68]; also the likelihood of successful pharmaceutical cardioversion is higher when the AF frequency is below 6 Hz; the risk of early AF recurrence is higher for patients with higher AF frequency.

The AF frequency is usually determined from the periodogram of the residual ECG, thus precluding the detection of changes in AF frequency, unless using more complex techniques [54, 69].

1.2.3 PRIOR WORKS ON HETEROGENEITY OF VENTRICULAR REPOLARIZATION

The morphology of ECG components related to ventricular repolarization (*e.g.* J point, ST-segments and T wave) changes under various pathophysiologic conditions [70]. In this thesis, two important ventricular repolarization analysis are discussed.

1.2.3.1 T-WAVE ALTERNANS ANALYSIS

Repolarization abnormalities produce periodic alternation of the T-wave morphology on the ECG (T-wave Alternans, TWA). Most often, the size of such alterations is small ($\approx$ 10μV) and buried into noise. The detection of such alternans is very important to identify those patients at higher risk for Sudden Cardiac Death (SCD). In the last

three decades, a variety of non-invasive indices have been proposed to identify the patients with higher risk of SCD from electrocardiographical recordings, such as T-peak to T-end time, QT dispersion, heart rate variability and T Wave Alternans [71]. In particular, TWA is the manifestation of a repolarization abnormality [72]. One of the recent methods which is employed for detecting TWA is Extended Kalman filter (EKF). The necessary dynamical models of the ECG for using in Kalman filter structure is an extension version of the ECG dynamical model (EDM) proposed by McSharry *et al.*. McSharry's model was based on a set of nonlinear state space equations in Cartesian coordinates [73] and later simplified by Sameni *et al.* [74] by reducing the number of state variables using the polar coordinate system. Thereafter, application of the modified ECG dynamical model has been studied in conjunction with a Bayesian filtering framework, such as Extended Kaman Filter (EKF), for ECG denoising [74], generating multi-channel ECG as well as simulating abnormal rhythms [75]. Application of the so-called modified EDM in EKF filter for ECG estimation were restricted to the estimation of the whole ECG beat and its corresponding phase. However, extracting the physiological components, such as P wave, QRS complex and T wave, is of great importance in some clinical applications as discussed in previous section. To overcome this limitation, Sayadi *et al.* introduced a modified EKF structure (EKF17), which employs the parameters α, b and θ of Gaussian kernels, corresponding to P, Q, R, S and T waves, as hidden state variables [29]. Subsequently extended Kalman filter (EKF) has been modified and used for TWA detection [76, 77, 78].

1.2.3.2 HETEROGENEITY OF VENTRICULAR REPOLARIZATION

The differences in ventricular repolarization times is referred to ventricular repolarization heterogeneity and may have an arrhythmogenic meaning (favoring reentry). In normal hearts, the ventricular repolarization is a relatively smooth, continuous process, during which the ventricles repolarize almost simultaneously. However several cardiac diseases or drugs may disturb the repolarization and thus increase the heterogeneity of ventricular repolarization. On the other hand the T-wave morphology and its duration depend on differences in the repolarization times of the ventricular myocardial cells. Hence the ECG signals can be used to assess this repolarization heterogeneity. Several electrocardiographic indices for assessing the repolarization heterogeneity have been proposed in the literature such as: T-wave amplitude, T-wave area, T-wave complexity and T-wave symmetry ratio, QT dispersion, and the Tapex-end interval. Recently a new index so called $\mathcal{V}$-index has been proposed for the same aim which is derived from a biophysical model Sassi2011.

1.3 OBJECTIVE OF THIS THESIS

Electrocardiogram is an important biomedical tool for the diagnosis of heart disorders. The detection of cardiac disease has been explored using computers and algorithms. However the problem is still challenging and the existing algorithms needs to be improved.

Modeling and feature extraction are among the most crucial and important steps for ECG analysis specially in noisy environment. They can help to enhance the diagnostic capability. The objective of this thesis can be summarized as follows:

- **ECG waveform components separation:**

  The analysis of ECG waveforms information (amplitude, time interval and patterns) for further analysis and feature extraction has been the subject of many intense research. Our objective is to build a robust framework based on adaptive models while combining it with a Bayesian smoother to split the ECG signal into its waveform components. Such framework is useful for many applications in ECG signal analysis. For this purpose, a signal decomposition model based Bayesian framework for ECG components separation is presented in chapter 2, section 2.4, 2.5 and 2.6.

- **Atrial fibrillation detection**

  In patients with atrial fibrillation, the repetition rate of the atrial fibrillatory waves (f-waves) or fibrillatory frequency plays an important role when analyzing AF from the electrocardiogram. The fibrillatory frequency is useful for non-invasive assessment of electrical remodeling in AF. It can be assessed by signal processing tools such as power spectral analysis and short time Fourier transform (STFT) from the surface ECG after ventricular activity (QRS-T complex) cancellation. Our objective is to devise a method for tracking the fibrillatory frequency while ignoring the step of VA cancellation. Chapter 3, section 3.2, present a nonlinear Bayesian framework for tracking VA, AA and dominant atrial fibrillatory frequency, simultaneously.

- **T-wave alternans detection**

  Abnormality of ventricular repolarization in the ECG have been shown to be related to cardiovascular mortality. Our objective is to improve the model of cardiac signal and combine it with a Bayesian filtering framework in order to detect TWA. In chapter 4, section 4.1.6, A new signal decomposition model based extended Kalman smoother is presented for T-wave alternans detection.

- **Improving the $\mathcal{V}$-index computation:**

  Spatial heterogeneity of ventricular repolarization (SHVR) can be assessed from surface ECGs using the $\mathcal{V}$-index. The index is derived from a biophysical model and its computation needs to solve an inverse problem (fitting a model by a Taylor expansion). Our objective is to estimate the $\mathcal{V}$-index using an analytical model while considering as much as possible Taylor terms with ease. Such model is theoretically expected to improve the accuracy of estimates. For this purpose, a new model based sinusoidal functions for $\mathcal{V}$-index computation is presented in chapter 5 , section 5.2.

1.4 THESIS OVERVIEW

In the following, the chapters of this thesis are briefly described.

- **Chapter 2:** In this chapter, we review the previous ECG models and introduce a signal decomposition model-based Bayesian filtering framework for splitting ECG into its waveform components (P, Q, R, S and T).
- **Chapter 3:** In this chapter, we introduce an extended nonlinear Bayesian filtering framework for Atrial fibrillation characterization which is able to estimate the fibrillatory frequency while ignoring the step of VA cancellation.
- **Chapter 4:** In this chapter, we describe the application of ECG signal decomposition based Kalman smoother for T-wave alternans (TWA) detection.
- **Chapter 5:** In this chapter, first, a biophysical model for the time evolution of the electrical properties of the myocardial muscle is described. Then the $\mathcal{V}$-index (*i.e.* an estimator of the dispersion of repolarization time) formulation is described. Finally a novel model based sinusoidal signal is presented for improving the computation of the $\mathcal{V}$-index.
- **Chapter 6:** Finally this chapter concludes all the proposed methods in this thesis and explains the future works.

2

MODEL-BASED ECG WAVEFORMS CHARACTERIZATION

This chapter describes a signal decomposition model-based Bayesian framework for splitting ECG into its waveform components. The rest of the chapter is organized as follows. In section 2.1, we give a brief overview of signal modelling and its applications to signal processing. A brief history of ECG dynamical modelling is presented in section 2.2. Section 2.4, 2.5 and 2.6 respectively, present the theory, implementation and applications of the signal decomposition for cardiac signal analysis. Finally the chapter is closed with some general remarks.

2.1 SIGNAL MODELLING

In signal processing, a model is a mathematical description that provides an efficient approximation of a signal. Most of the modelling process is divided into two steps. The first step is to choose a suitable parametric form and the second one is to find the model parameters that provides the best approximation of the signal. The unknown parameters are usually found by minimizing a criteria such as mean square error (MSE) between desired and observed signals, as a function of the parameters. As an example, consider the class of sinusoidal signals. A finite segment x_n of each signal can be represented as a linear combination of sinusoidal functions:

$$\hat{x}_n = \sum_{k=1}^{N} \alpha_k \cos(\omega_k n + \phi_k), \tag{2.1}$$

where α_k, ϕ_k and $\omega_k = 2\pi f_k$ are respectively, the amplitude, phase and frequency of the sinusoidal model. As a result each sinusoid has three parameters. Other examples are autoregressive (AR) models, moving average (MA) models and autoregressive moving average (ARMA) modelling, which are useful for stochastic signal modelling. Although the models can also be nonparametric, the parametric forms are more com-

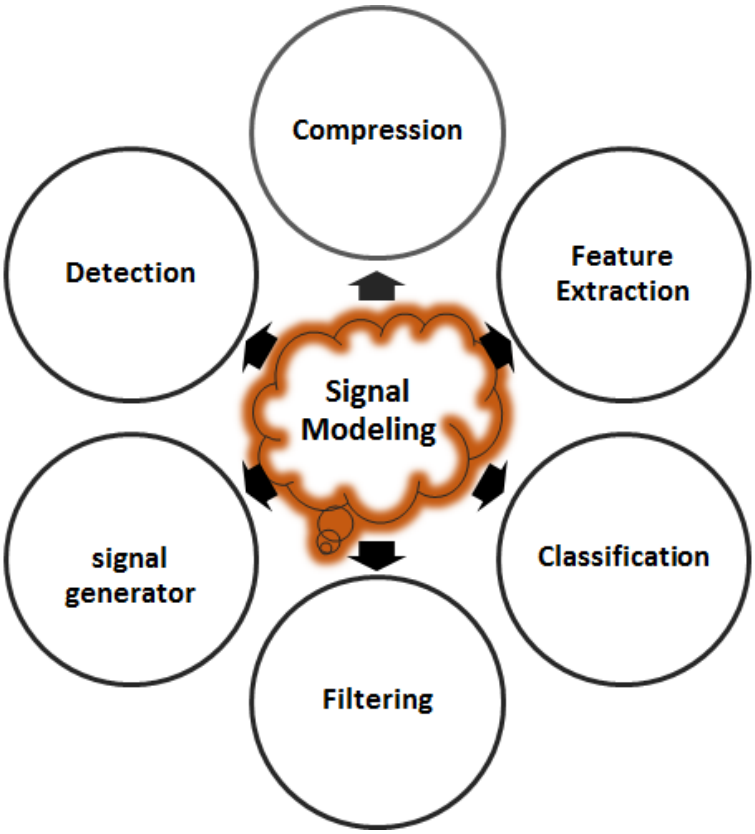

Figure 2.1: Modelling and its applications.

mon in practical applications. Hence we are most interested in parametric forms. In general, models can be divided into two categories: Linear or Nonlinear. A good model should have some properties such as: i) it should be able to represent the signal with a small number of parameters, ii) computing the model parameters should be easy (low computational requirements), iii) the model parameters should have a physically meaningful interpretation.

Modelling has a broad range of applications in signal processing. Some of them are shown in Fig. 2.1 and listed bellow:

1. **Prediction:** Prediction models have been widely used in real applications such as public health, clinical practice, and medical research [79]. They are useful for forecasting the future behavior. In this context the well-known example is classical time series modelling methods (*e.g.* AR, ARMA, ARIMA and MA). Of course they assume that the past results are relevant for predicting the future. Hence they are more suitable for stationary time series. For instance short-term density forecasting of wave energy flux can be done by ARMA-GARCH models [80]. Another example is ARIMA model for time series forecasting of Ibovespa [81].

2. **Reconstruction:** The models can be used to determine the original signal from a sequence of real samples. For instance, a signal can be reconstructed from its discrete Fourier transform (DFT) model.

3. **Understanding:** Real signals are generated from a physical mechanism (*e.g.* musical, speech and medical signals). Having a model for the signal can help to achieve a better understanding of the mechanism of the physical source. For instance, ECG models are helpful to understand the function of the heart.

4. **Filtering:** One of the applications of modelling is to remove the noise from signal. The parametric models are usually based on combination of smooth functions and can be useful to neglect the noise.

5. **Compression:** One of the most important areas in information theory and computer science is data compression. In this context the models can be used to get an efficient representation of the signals for data compression.

6. **Synthetic signal generator:** The models are useful for synthesizing artificial signals similar to the real ones. Synthetic signals can be used for evaluating the signal processing methods before applying on real data (*e.g.* medical signals).

7. **Detection:** Signal detection has been widely applied in real world problems such as face recognition. It can be performed using modelling.

8. **Pattern recognition applications:** The extracted parameters of a model can be used for feature extraction and classification [82, 83, 84]

The terms "signal" can include speech, audio, musical, image, video, sonar, radar, medical and communication signals. In this thesis, we are most interested in biomedical signals and specially in cardiac signals.

2.2 A REVIEW OF SYNTHETIC ELECTROCARDIOGRAM MODELLING

ECG is the most studied signals in the field of biological signals due to the well-shaped pseudo-periodic structure of the ECG and the fact that the ECG morphology conveys clinical information. ECG modelling has been extensively used for many applications in cardiac studies such as evaluating bio-instrumentation systems [85], biosignal denoising [74], classification [86] and compression [87]. In the following section we review some ECG dynamical models (EDMs).

2.2.1 MCSHARRY'S MODEL

The EDM was first proposed by McSharry *et al.* in 2003 [73]. It is able to produce ECG signals of arbitrary morphology and heart rate [73, 88]. The model is based on a set of nonlinear state space equations in Cartesian coordinates. The basic idea behind it, is to

construct a dynamical model that repeats the single beat in a pseudo-periodic manner. The model is described as follows:

$$\begin{cases} \dot{x} = \rho x - \omega y \\ \dot{y} = \omega x + \rho y \\ \dot{z} = -\sum_{i \in \{P,Q,R,S,T\}} \alpha_i \Delta\theta_i \exp\left[-\frac{\Delta\theta_i^2}{2b_i^2}\right] - (z - z_0) \end{cases} \tag{2.2}$$

where x, y and z are the state variables, $\rho = 1 - \sqrt{x^2 + y^2}$, $\Delta\theta_i = (\theta - \theta_i) \mathrm{mod}\ 2\pi$, $\theta = \arctan(y, x)$ and ω is the angular velocity corresponding to heart rate variability (HRV). Accordingly, the state variable z models ECG as a summation of the Gaussian kernels, where α_i, b_i and θ_i adapt amplitude, width and center of the Gaussian kernels to the different morphological ECG signals and z_0 models the baseline wander.

The McSharry model was used for many applications such as filtering, compression, classification [89, 90] and generating rather realistic synthetic electrocardiogram signals in many normal and abnormal cases [75].

2.2.2 EKF2 DERIVED MODEL

The EDM was modified by Sameni *et al.* [74] by reducing the number of state variables using polar coordinate system:

$$\begin{cases} \theta_{k+1} = (\theta_k + \omega\sigma) \mod 2\pi \\ z_{k+1} = z_k - \sum_{i \in \{P,Q,R,S,T\}} \delta \frac{\alpha_i \omega}{b_i^2} \Delta\theta_i \exp\left[-\frac{\Delta\theta_i^2}{2b_i^2}\right] + \eta \end{cases} \tag{2.3}$$

where θ is the *cardiac phase* defined as an explicit state variable that indicates the angular location of the P, Q, R, S and T components and models intra beat variations. z, as before, is the amplitude of the ECG signal, δ is the sampling period and η is a noise term corresponding to the inaccuracy of the model (such as baseline wander). Comparing it to (2.2), (2.3) is much simpler and its interpretation is straightforward. The summation is taken over a finite number of Gaussian signals used for modelling P, Q, R, S and T waves. Thereafter, application of the modified ECG dynamical model has been studied in conjunction with Bayesian filtering frameworks such as Extended Kaman Filter (EKF) and Extended Kalman Smoother (EKS), for modelling fetal ECG [88], ECG denoising [91, 74], removing cardiac contaminants [92], generating multi-channel ECG as well as simulating abnormal rhythms [93, 75]. However, applications of the so-called modified EDM in EKF filter for ECG denoising are restricted to the whole ECG beat and their corresponding phases [87]. While extracting the physiological components such as P wave, QRS complex and T wave is of great importance in some clinical applications.

2.2.3 EKF17 DERIVED MODEL

Sayadi *et al.* modified the polar form of McSharry's model (EKF2) while considering the parameters of Gaussian functions as hidden states and introduced "EKF17" (as it uses 17 state variables). They considered an AR model for each parameter (a random walk). It is assumed that the Gaussian parameters can fluctuate very small in each beat. The equations of EKF17 are defined as follows:

Process equation:

$$\begin{cases} \theta_{k+1} = \theta_k + \omega\delta \\ z_{k+1} = z_k - \sum\limits_{i=\in P,Q,R,S,T} \alpha_i \omega \dfrac{\theta_k - \theta_i}{b_i^2} \exp\left[-\dfrac{(\theta_k-\theta_i)^2}{2b_i^2}\right] + \eta_z \\ \alpha_{i,k+1} = \alpha_{i,k} + u_{j,k}, \qquad j \in \{1,2,3,4,5\} \\ b_{i,k+1} = b_{i,k} + u_{j,k}, \qquad j \in \{6,7,8,9,10\} \\ \theta_{i,k+1} = \theta_{i,k} + u_{j,k}, \qquad j \in \{11,12,13,14,15\} \end{cases}, \tag{2.4}$$

Observation equation:

$$\begin{cases} \psi_k = \theta_k + v_{1,k} \\ s_k = z_k + v_{2,k} \end{cases}, \tag{2.5}$$

EKF17 was successfully used for ECG compression and denoising [87], as well as for ECG beat segmentation [29].

2.2.4 EKF4 DERIVED MODEL

Another approach which is more suitable when applying the model to filtering arrhythmias, is to consider different events of the ECG separately as hidden state variables. This idea has been proposed by Sayadi *et al.* for robust detection of premature ventricular contractions [94], as well as modelling the temporal dynamics of ECG [95]. In this case the ECG beats are modeled using seven Gaussian kernels, one Gaussian kernel for modelling symmetric component (Q, R, S) and two Gaussian kernels for modelling the asymmetries components for P or T waves (indicated by $^+$ and $^-$ superscripts). The model is described as follows:

Process equation:

$$\begin{cases} \theta_{k+1} = \theta_k + \omega_k \delta \\ P_{k+1} = P_k - \sum_{i \in \{P^-, P^+\}} \alpha_i \omega \frac{\theta - \theta_i}{b_i^2} \exp\left[-\frac{(\theta - \theta_i)^2}{2b_i^2}\right] + \eta_P \\ C_{k+1} = C_k - \sum_{i \in \{Q,R,S\}} \alpha_i \omega \frac{\theta - \theta_i}{b_i^2} \exp\left[-\frac{(\theta - \theta_i)^2}{2b_i^2}\right] + \eta_C \\ T_{k+1} = T_k - \sum_{i \in \{T^-, T^+\}} \alpha_i \omega \frac{\theta - \theta_i}{b_i^2} \exp\left[-\frac{(\theta - \theta_i)^2}{2b_i^2}\right] + \eta_T \end{cases}, \tag{2.6}$$

Observation equation:

$$\begin{cases} \psi_k = \theta_k + \nu_{1,k} \\ s_k = P_k + C_k + T_k + \nu_{2,k} \end{cases}, \tag{2.7}$$

Since the number of state variables is four, the method was termed EKF4. The parameters α_i, b_i, and θ_i are identified before applying the Kalman filter. To this aim, after QRS complex detection, an ECG waveform template is obtained by averaging the time-warped beats [74] and then used to fit the parameters by nonlinear least square estimation. It is possible to compute the parameters of the model using an iterative linear least square estimation [96]. The procedure of estimating the parameters of sum of Gaussian to fit the model to the single ECG beat is described in [96].

Morphological changes in abnormal ECG beats or artifacts, which are included when computing the average ECG beat, can change the value of these parameters. So they are considered as process noise in EKF2 and EKF4. Since the parameters appear in the time update (2.6), their changes can affect the filter performance. This is particularly true for the amplitudes α_i. To further clarify the issue, the synthetic ECG in Fig. 2.2a displays an episode of alternation of T-wave forms (macroscopic T-wave alternans, TWA). It was inspired by figure 2 in [97]. Such alterations often precede torsade de pointes and sudden cardiac death and their detection is clearly relevant. During the episode depicted in Fig. 2.2a or its noisy version in Fig. 2.2b, the T wave amplitude changes in time. The different polarity affects the value of the average template in Fig. 2.2c, which is obtained by averaging the noisy signal in Fig. 2.2b. The components waveforms (CWs) obtained with EKF4/EKS4 are shown in Fig. 2.3a and 2.3b. Unfortunately, the low amplitude of the T waves detected is evident. Morphological changes, especially in abnormal ECG sequences, lead to large errors on the updating state variables and low accuracy on the corresponding ECG component separation. In 2.4.2, a new EDM, which no longer depends on the amplitude of the Gaussian kernels will be introduced and used with EKS.

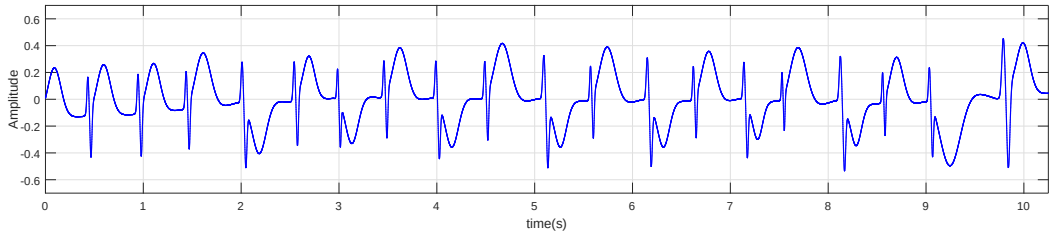

(a) Synthetic ECG

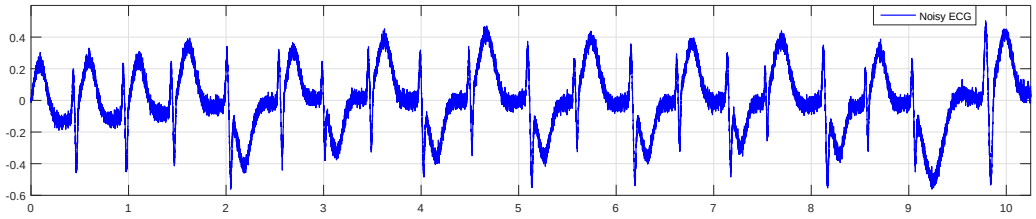

(b) Noisy ECG

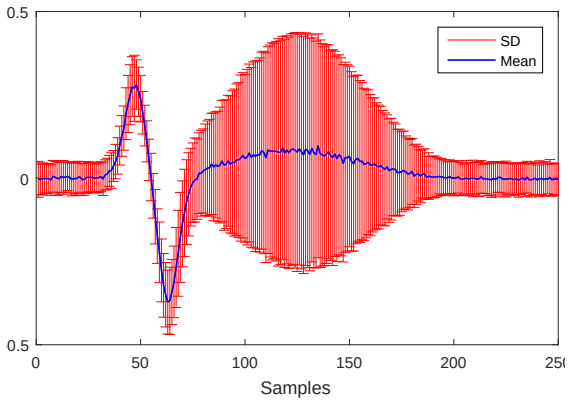

(c) Mean ECG pattern

Figure 2.2: Synthetic signal corrupted by noise with SNR = 18 dB and mean ECG pattern for noisy ECG.

2.3 A MORE COMPREHENSIVE APPROACH TO ECG MODELLING

Digital computers (IBM 704) was first used for analyzing the ECG data in 1959 [98]. Thereafter ECG waveforms representation and analysis became the subject of many researches [99, 100, 101, 102]. In 1963, the first model using basis function was presented by Young *et al.*, who studied the problem of ECG representation within a linear combination of basis functions [103]. Homomorphic analysis and modelling of ECG signals of normal, inverted T-wave, and PVCs was studied in [104]. In [105], the shape of QRS complex was described by morphological modelling of ECG using Gaussian function. A model based polynomial functions were studied in [106] for extraction of QRS complex. A general approach to modeling the ECG waveforms based on the method of

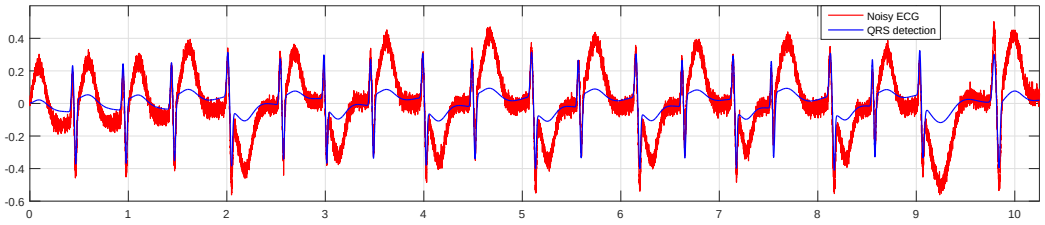

(a) QRS extraction provided by EKS4

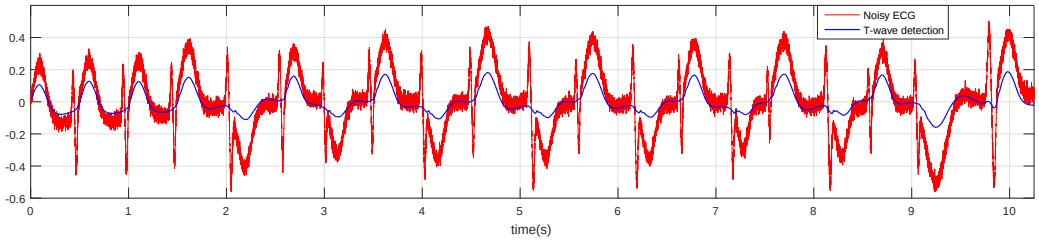

(b) T wave extraction provided by EKS4

Figure 2.3: QRS complex and T-wave estimates provided by EKS4, when applied to a synthetic signal corrupted by noise with SNR = 18 dB (Fig. 2.2).

Gaussian pulse decomposition was presented in [107]. In 2003 EDM was introduced by McSharry *et al.* which was based on modelling ECG waveforms using Gaussian functions [73]. Recently, Kheirati Roonizi and Sameni have presented a general framework for ECG modelling using a signal decomposition perspective [108]. The framework has been used for morphological modelling of cardiac signals and for generating a realistic synthetic ECG. A single ECG beat can be represented as the linear combination of basis functions:

$$z = \sum_{i=0}^{N-1} \alpha_i \phi_i(t), \tag{2.8}$$

where $\{\phi_i\}_{i=0}^{N-1}$ is a set of functions used for signal expansion and α_i are the expansion coefficients. The basic idea behind the framework is to use a *priori* information about cardiac signals, such as their pseudo-periodic structure, to present the average beat as a sum of basis functions, and repeat it in a pseudo-periodic manner to generate multiple subsequent beats. To apply this idea one need to use the notion of *cardiac phase*[1] signal defined in [88, 109]. The angular speed of the phase signal is

$$\dot{\theta} = 2\pi f \tag{2.9}$$

1 The cardiac phase $\theta \in [-\pi, \pi]$ is a monotonically increasing functional assigned to each ECG beat. In the simplest case, θ can have a constant slope in each beat, which starts from $-\pi$ and ends at $+\pi$, with the R-peak fixed at $\theta_t = 0$ and each phase value assigned to the critical waveforms of the ECG.

where f is the heart rate in Hertz, which can fluctuate from beat to beat. The general model can be represented as

$$z = \sum_{i=0}^{N-1} \alpha_i \phi_i(\theta) \tag{2.10}$$

where θ is, as before, the cardiac phase which is defined between $-\pi$ and π. Accordingly, by updating θ using the dynamics in (2.9), multiple beats with arbitrary heart rates are achieved. The cardiac phase maps the arbitrary ECG beats to $[-\pi, \pi]$, *i.e.*, time-scaling all ECG beats regardless of the beat-to-beat variations of the heart rate.

For applications such as Kalman filtering, it is more efficient to augment the cardiac phase dynamics in (2.9) with the dynamical form of (2.10), resulting in a unified dynamic model of the ECG[2]

$$\begin{cases} \dot{\theta} = 2\pi f \\ \dot{\phi}(\theta) = g(\phi(\theta), \theta) \cdot \dot{\theta} \\ z = \alpha^T \phi(\theta) \end{cases} \tag{2.11}$$

where based on Leibniz's notation $g = \frac{d\phi}{d\theta}$ and

$$\begin{aligned} \phi &= [\phi_0(t), \phi_1(t), ..., \phi_{N-1}(t)]^T \\ \alpha &= [\alpha_0, \alpha_1, ..., \alpha_{N-1}]^T \end{aligned} \tag{2.12}$$

are vectors of the basis functions and their corresponding coefficients respectively. This model is useful for generating multiple ECG beats. For this purpose, different basis functions such as polynomial splines, sinusoidal and Gaussian functions can be employed to model synthetic ECG waves. Having a parametric model of a single ECG waveform, using the heart rate dynamics, the ECG beats can be repeated successively to generate a continuous ECG. An example of a Bézier, B-spline and sinusoidal model with a real heart rate dynamics, to model a realistic ECG, is shown in Fig. 2.4. By detecting the R-peaks, the beat-to-beat heart rate and the cardiac phase signal θ are calculated. The phase signal θ is used to calculate the average ECG beat. Finally, Bézier, B-spline and sinusoidal models are fitted over the average beat and repeated successively at the real ECG heart beats. The resulting ECG beats are shown in Fig. 2.4.

Unfortunately, real ECG signals can be highly non-stationary in practice. So fixing the parameters of a single beat and repeating it to generate multiple beats, is largely an approximation. For example, it is known that the QT-interval changes significantly under varying heart rates [6].

2 In (2.11), the chain rule has been used to convert the derivative with respect to θ to the derivative with respect to t.

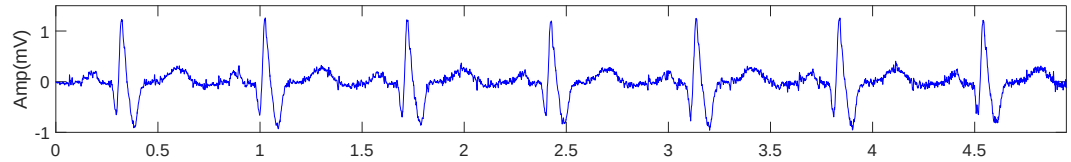

(a) Original ECCG

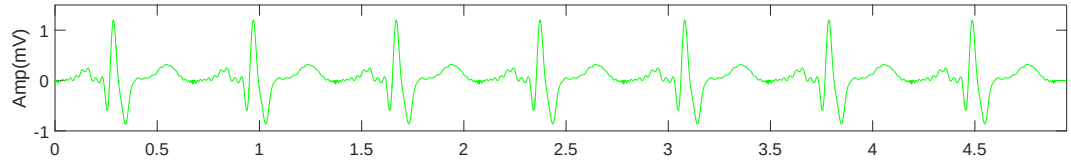

(b) Bézier model

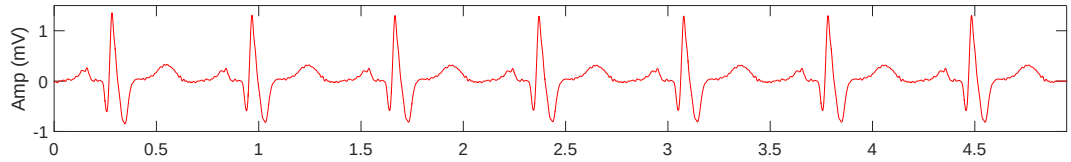

(c) Sinusoidal model

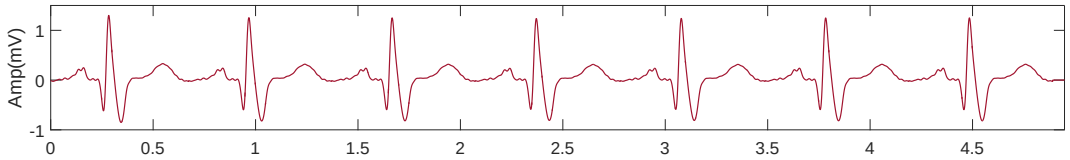

(d) B-spline model

Figure 2.4: ECG modelling using Bézier, sinusoidal and B-spline basis functions.

2.4 ECG WAVEFORM COMPONENTS SEPARATION

The discussed EDMs can be used to separate the ECG waveform components. However since real ECG signals can be highly non-stationary, repeating the average beat to generate multiple ECG is not optimal. One of the solution is to update the parameters of the EDM on a beat-to-beat basis. It can be performed using Bayesian estimation. In the following, first, a brief description of Bayesian filtering framework is prresented. Then we introduce a new EDM and study the application of the proposed model-based Kalman smoother for separating such waveform components, for further analysis and easier feature extraction.

2.4.1 KALMAN FILTER

In 1960, Kalman reformulated the Wiener problem and proposed a recursive procedure based on state transition to avoid the limitations of the Wiener filter (which is suitable for stationary systems) [110]. Kalman filter is an optimal estimator in the minimum mean square error (MMSE) sense applied to a dynamical system that involves random perturbations [111]. It gives a linear, unbiased, and minimum error variance recursive

algorithm to optimally estimate the unknown states of a dynamical system from noisy data taken at discrete instants. It has been a fundamental tool for analyzing and solving a broad class of estimation problems in engineering and science such as for traffic management [112], training recurrent neural network channel equalizers [113], sensor fusion in a human tracking system [114], state estimation of a nuclear reactor [115], dynamic and secure smart grid state estimation [116], bad-data detection in power system [117], underwater navigation systems [118, 119], tracking relative errors in internet coordinate systems, human motion tracking [120], eye tracking [121] and fault detection and isolation (FDI) logic [122].

Let us now consider the undriven non-linear deterministic/stochastic system. Specifically, let us consider the state-space description

$$\begin{cases} x_{k+1} = f(x_k, k) \\ y_k = g(x_k, k) \end{cases}$$

and its associated "noisy" system

$$\begin{cases} x_{k+1} = f(x_k, w_k, k) \\ y_k = g(x_k, v_k, k) \end{cases}, \tag{2.13}$$

where

- x_k is the unobserved or hidden state vector;
- y_k is the observation vector at time instant k;
- $f(\cdot)$ is the evolution state function;
- $g(\cdot)$ represents the relationship between the hidden state and observations;
- w_k is process noise with the corresponding covariance matrices $Q_k = E\{w_k w_k^T\}$;
- v_k is measurement noise with the corresponding covariance matrices $R_k = E\{v_k v_k^T\}$.

For nonlinear systems, the *extended* Kalman filter, which is applied after linearization of the model, might be employed instead. The extended Kalman filter for (2.13) is given as follows [123]:

Time Update:

$$\begin{cases} \hat{x}_{k+1}^- = f_k(\hat{x}_k^+, w, k)_{|w=0} \\ H_{k+1}^- = A_k H_k^+ A_k^T + F_k Q_k F_k^T \end{cases} \tag{2.14}$$

Measurement update:

$$\begin{cases} \hat{x}_k^+ = \hat{x}_k^- + K_k \left[y_k - g(\hat{x}_k^-, v_k, k)_{|v=0} \right] \\ K_k = H_k^- C_k^T \left(C_k H_k C_k^T + G_k R_k G_k^T \right)^{-1} \\ H_k^+ = H_k^- - K_k C_k H_k^- \end{cases} \tag{2.15}$$

where

$$\begin{cases} A_k = \dfrac{\partial f(x, \hat{w}_k, k)}{\partial x}\Big|_{x=\hat{x}_k} \\ F_k = \dfrac{\partial f(\hat{x}_k, w, k)}{\partial w}\Big|_{w=\hat{w}_k} \\ C_k = \dfrac{\partial g(x, \hat{v}_k, k)}{\partial x}\Big|_{x=\hat{x}_k} \\ G_k = \dfrac{\partial g(\hat{x}_k, v, k)}{\partial v}\Big|_{v=\hat{v}_k} \end{cases} \tag{2.16}$$

- $\hat{x}_k^- = E\{x_k | y_{k-1}, \cdots y_1\}$ is a *prior* estimate of x at time instant k given the previous observations y_1 to y_{k-1};
- $\hat{x}_k^+ = E\{x_k | y_k, \cdots y_1\}$ is a *posterior* estimate that is obtained by correction of $\hat{x}_k^+$ after observing y_k;
- The matrices $H_k^- = E\{(x_k - \hat{x}_k^-)(x_k - \hat{x}_k^-)^T\}$ is the *prior* state covariance matrices;
- $H_k^+ = E\{(x_k - \hat{x}_k^+)(x_k - \hat{x}_k^+)^T\}$ is the *posterior* state covariance matrices.

Suppose that the observation signal y_k is available for $k = 1, 2, ..., N$. The optimal estimate of the state vector x_k using all the observations (*i.e.* past, present, and future) is called a smoothing estimate of x_k. Extended Kalman smoother (EKS) consists of a forward EKF stage followed by a backward recursive smoothing stage. Since EKS uses information brought by "future" observations, it provides better estimates of the current states and follows the ECG morphology more accurately than EKF in noisy scenarios [95].

2.4.2 A NEW ECG DYNAMICAL MODEL (EKS6)

In this section, we introduce a new EDM and combine it with the Bayesian filtering framework to estimate the states of the model, in order to split the ECG signal into its components, on a beat-to-beat basis. A single ECG beat can be modeled as a sum of N Gaussian functions with different amplitudes and widths centered at specific points in time [108]. According to (2.8) and merging the coefficients into the basis functions

$$\phi_i \equiv \alpha_i \exp\left[-\frac{(\theta - \theta_i)^2}{2b_i^2}\right],$$

where α_i, b_i and θ_i were previously defined in (2.2). ϕ_i can be coupled with a model of the heart rate dynamics, to synthesize multiple ECG beats with arbitrary heart rates [73]

$$\begin{cases} \dot{\theta} = \omega \\ \phi_i = \alpha_i \exp\left[-\dfrac{(\theta-\theta_i)^2}{2b_i^2}\right], \\ z = \displaystyle\sum_{i=0}^{N-1} \phi_i \end{cases}.$$

where θ was defined before and ω is the angular speed of the *phase signal*. The main advantage of this model is that the amplitudes now pertain to the basis functions.

Taking again the derivative of ϕ_i, instead of the signal z, the EDM becomes

$$\begin{cases} \dot{\theta} = \omega \\ \dot{\phi}_i = -\alpha_i \omega \left(\dfrac{\theta-\theta_i}{b_i^2}\right) \exp\left[-\dfrac{(\theta-\theta_i)^2}{2b_i^2}\right], \\ z = \displaystyle\sum_{i=0}^{N-1} \phi_i \end{cases} \tag{2.17}$$

which, in our notation, is similar to the model (2.6) that is used in EKS4. Nonlinearity is decreased significantly by substituting $\alpha_i \exp[-(\theta-\theta_i)^2/(2b_i^2)]$ with ϕ_i in the second equation. Our final EDM model, which is capable of generating continuous ECG waveforms, is thus as follows

$$\begin{cases} \dot{\theta} = \omega \\ \dot{\phi}_i = -\omega \left(\dfrac{\theta-\theta_i}{b_i^2}\right) \phi_i \\ z = \displaystyle\sum_{i=0}^{N-1} \phi_i \end{cases}. \tag{2.18}$$

It no longer depends on α_i, which are absorbed completely into the state ϕ_i.

2.5 DISCRETIZATION AND IMPLEMENTATION OF THE FRAMEWORK

The model derived in the previous section was in the continuous time domain. Hence its discretized version is needed for EKS. The modified EKS is defined by process and observation equations:

Process equation:

$$\begin{cases} \theta_{k+1} = (\theta_k + \omega\delta) \mod 2\pi \\ \phi_{i,k+1} = \left(1 - \omega\delta\dfrac{\theta_k-\theta_i}{b_i^2}\right)\phi_{i,k} + \eta_{i,k}, \end{cases} \tag{2.19}$$

where θ_k and $\phi_{i,k}, i \in \{P, Q, R, S, T\}$ are state variables, $\eta_{i,k}$ are i.i.d. Gaussian random variables considered to be random additive noise. The proposed discrete EDM consists of six hidden state variables (one for each of P, Q, R, S and T components), plus the cardiac phase θ_k. For this reason, in the following the model will be named EKS6. In some cases, specially for abnormal ECGs more Gaussian basis functions are needed to have an accurate representation. However, this will increase the cost and the complexity of the overall scheme, as well as the risk of over fitting.

Observation equation:

$$\begin{cases} \psi_k = \theta_k + v_{1,k} \\ s_k = \sum\limits_{i \in \{P,Q,R,S,T\}} \phi_{i,k} + v_{2,k} \end{cases}, \tag{2.20}$$

where

- s_k is the noisy observation (the recorded ECG);
- ψ_k is the noisy cardiac phase at time instant k;
- $v_{1,k}$ and $v_{2,k}$ are zero mean random variables considered to be observation noise.

As a result, the state variables vector, x_k, the observation vector, y_k, the process noise vector, w_k, and the observation noise vector, v_k, are defined as follows:

$$\begin{aligned} x_k &= [\theta_k, \phi_{P,k}, \ldots, \phi_{T,k}] \\ y_k &= [\psi_k, s_k] \\ w_k &= [b_P, \ldots, b_T, \theta_P, \ldots, \theta_T, \eta_P, \ldots, \eta_T, \omega] \\ v_k &= [v_{1,k}, v_{2,k}] \end{aligned}.$$

The non-linear discrete dynamical system which is suitable to combine with the EKF framework is as follows:

$$\begin{cases} \theta_{k+1} = (\theta_k + \omega\delta) \mod 2\pi \\ \phi_{i,k+1} = \left(1 - \omega\delta \dfrac{\theta_k - \theta_i}{b_i^2}\right) \phi_{i,k} + \eta_{i,k} \\ \psi_k = \theta_k + v_{1,k} \\ s_k = \sum\limits_{i \in \{P,Q,R,S,T\}} \phi_{i,k} + v_{2,k} \end{cases}. \tag{2.21}$$

The dynamical model in (2.21) is still nonlinear. However, the nonlinearity is largely reduced with respect to (2.6), and it is limited to the product $\theta_k \phi_{i,k}$. To linearize it, and then build the EKS, we first reformulate it into the terminology of (2.13):

$$\begin{cases} \theta_{k+1} = f_1(\theta_k, \omega, k) \\ \phi_{i,k+1} = f_i(\theta_k, \phi_{i,k}, \omega, b_i, \theta_i, \eta_{i,k}, k) \\ \psi_k = g_1(\theta_k, k) \\ s_k = g_2(\theta_k, \phi_{i,k}, k) \end{cases}.$$

Then, following (2.16):

$$\frac{\partial f_1}{\partial \theta_k} = 1 \qquad \frac{\partial f_i}{\partial \theta_k} = \frac{-\omega\delta}{b_i^2}\phi_{i,k}$$
$$\frac{\partial f_1}{\partial \phi_{i,k}} = 0 \qquad \frac{\partial f_i}{\partial \phi_{i,k}} = \left(1 - \omega\delta\frac{\theta_k - \theta_i}{b_i^2}\right)$$
$$\frac{\partial f_1}{\partial b_i} = 0 \qquad \frac{\partial f_i}{\partial b_i} = \frac{2\omega\delta(\theta_k - \theta_i)}{b_i^3}\phi_{i,k}$$
$$\frac{\partial f_1}{\partial \theta_i} = 0 \qquad \frac{\partial f_i}{\partial \theta_i} = \frac{\omega\delta}{b_i^2}\phi_{i,k}$$
$$\frac{\partial f_1}{\partial \eta_{i,k}} = 0 \qquad \frac{\partial f_i}{\partial \eta_{i,k}} = 1$$
$$\frac{\partial f_1}{\partial \omega} = \delta \qquad \frac{\partial f_i}{\partial \omega} = \frac{-\delta(\theta_k - \theta_i)}{b_i^2}\phi_{i,k}$$
$$\frac{\partial g_1}{\partial \theta_k} = 1 \qquad \frac{\partial g_1}{\partial \phi_{i,k}} = 0$$
$$\frac{\partial g_2}{\partial \theta_k} = 0 \qquad \frac{\partial g_2}{\partial \phi_{i,k}} = 1$$
$$\frac{\partial g_1}{\partial v_{1,k}} = 1 \qquad \frac{\partial g_1}{\partial v_{2,k}} = 0$$
$$\frac{\partial g_2}{\partial v_{1,k}} = 0 \qquad \frac{\partial g_2}{\partial v_{2,k}} = 1$$

so that the matrices A_k, F_k, C_k and G_k are obtained as follows:

$$A_k = \begin{bmatrix} 1 & O_{1\times5} \\ \gamma_{5\times1} & M_{5\times5} \end{bmatrix}_{6\times6}$$
$$F_k = \begin{bmatrix} O_{1\times5} & O_{1\times5} & O_{1\times5} & \delta \\ \Gamma_{5\times5} & \Lambda_{5\times5} & I_{5\times5} & \beta_{5\times1} \end{bmatrix}_{6\times16'}$$
$$C_k = \begin{bmatrix} 1 & O_{1\times5} \\ 0 & 1_{1\times5} \end{bmatrix}_{2\times6}$$
$$G_k = I_{2\times2}$$

where

$$\gamma_{5\times1} = \left[\frac{-\omega\delta}{b_i^2}\phi_{i,k}\right]^T$$
$$M_{5\times5} = \text{diag}\left[1 - \omega\delta\frac{\theta_k - \theta_i}{b_i^2}\right]$$
$$\Gamma_{5\times5} = \text{diag}\left[\frac{2\omega\delta(\theta_k - \theta_i)}{b_i^3}\phi_{i,k}\right]$$
$$\Lambda_{5\times5} = \text{diag}\left[\frac{\omega\delta}{b_i^2}\phi_{i,k}\right]$$
$$\beta_{5\times1} = \left[\frac{-\delta(\theta_k - \theta_i)}{b_i^2}\phi_{i,k}\right]$$

and I, O are identity and zero matrices, respectively. EKS6 has several advantages. The state matrix A_k is not anymore a constant diagonal matrix, as it was for EKS4. As a result it changes at each step k. It is amplitude independent. These properties allow the EKS6 scheme to be more capable of adapting to changes in amplitude in the ECG waveforms.

Before using the Kalman filter/smoother, we need to initialize the parameters of the model and the Kalman filter. The initial value for the state vector, kernels as well as the covariance matrices of the process and the measurement noise were set using the procedure described in [74] and [94]. First of all, the initial values of the model needs a single beat of ECG signal. The best option is to use the average template of ECG. An ECG average template waveform, $\overline{ECG}(\theta)$, and its standard deviation, $\sigma_{ECG}(\theta)$, were obtained by averaging the time-warped beats. For this, one need to detect the position of QRS complexes in the signal. The R-peak selection algorithm proposed by Pan-Tompkins can be used for this purpose [9]. Then, nonlinear least squares was employed (due to the nonlinear dependence) to fit the model

$$z_k = \sum_{i\in\{P,Q,R,S,T\}} \alpha_i \exp[-(\theta_k - \theta_i)^2/(2b_i^2)]$$

to the ECG template and get the initial values of the parameters of the Gaussian kernels. The angular frequency of the model was set to $\omega = 2\pi/\langle RR\rangle$, where $\langle RR\rangle$ is the average RR-interval of the whole signal, while θ_0 was set to $-\pi$.

The process noise covariance matrix Q_k was set to $E\{w_k w_k^T\} =$

$\text{diag}(\sigma^2_{b_p}, ..., \sigma^2_{b_T}, \sigma^2_{\theta_p}, ..., \sigma^2_{\theta_T}, \sigma^2_{\eta_p}, ..., \sigma^2_{\eta_T}, \sigma^2_{\omega})$, where the values were found by computing the magnitude of the amount of deviation of the parameters of $\phi_{i,k}$ around $\overline{ECG}(\theta)$, to stay within the upper and lower bound of $\overline{ECG}(\theta) \pm \sigma_{ECG}(\theta)$ [87, 74]. With respect to the measurement noise covariance matrix R_0, $E\{v^2_{1,k}\}$ was set to $(\omega\delta)^2/12$, implying a uniform error in the location of the R-peak. Then, $E\{v^2_{2,k}\}$ was set to the average variance of the perturbation found around baseline, across the different beats used to build the template. The measurement noise covariance matrix R_k was considered to be diagonal as in [74]. After linearization and setting the parameters, the state variables are propagated in time using equations (2.14) and (2.15). This is equivalent

to having a set of basis functions updated over time in sense of MMSE, such that they are distinctly estimated from sample to sample. Therefore ECG components can be extracted even in noisy scenarios, leading to a higher accuracy of the fitting of the model.

2.6 PERFORMANCE ANALYSIS AND RESULTS

The proposed framework (EKS6-based decomposition) can be used for many applications in ECG processing (*e.g.* ECG waveform components extraction, T/QRS ratio calculation, denoising or QT interval measurement). This section describes the results and comparison of the proposed method with previous works for ECG waveforms separation. The same scheme of parameter selection procedure, discussed in previous section, was used for the Kalman filter for other models.

2.6.1 PERFORMANCE MEASURES

As discussed before, EKS4 has four hidden state variables while EKS6 has six hidden states. Hence to make the comparison between EKS6 and EKS4 fair, after applying the former, the Q, R and S waveforms were combined to obtain the QRS complex. Thus, we had three components for each ECG (P wave, QRS complex, and T wave). We produced signals varying the power of $v_{2,k}$ in (2.20). The signal-to-noise ratio (SNR) was modulated from -10 to 50 dB. For evaluating the performance of the proposed method, we used three different measures.

1. $\mathrm{SNR}_i^{\mathrm{dif}}$

   To simplify the definition of the error metrics, we group together the estimated components into the matrix $\hat{\Phi}$ and we call Φ the corresponding matrix of "true" components. The estimates $\hat{\Phi}$ are taken to be the linear combination of the true components plus noise v, that is

   $$\hat{\Phi} = U\Phi + Dv,$$

   where

   $$\begin{aligned}
   \hat{\Phi} &= [\hat{\phi}_P, \hat{\phi}_{QRS}, \hat{\phi}_T]^T = [\hat{\phi}_1, \hat{\phi}_2, \hat{\phi}_3]^T \\
   \Phi &= [\phi_P, \phi_{QRS}, \phi_T]^T = [\phi_1, \phi_2, \phi_3]^T \\
   U &= [u_{ij}]_{3\times 3}, \qquad i,j = 1,2,3 \\
   D &= [d_i]_{3\times 1}, \qquad i = 1,2,3
   \end{aligned}$$

   and the coefficient matrix U and D have to be estimated. Given the fact that the ECG components only minimally overlap in time, we can take their inner product to be approximatively zero. Moreover, ECG components and noise are assumed to be orthogonal. Under these conditions, the estimator $\hat{\Phi}$ achieves minimum

mean square error (MMSE) if and only if $E\{(\hat{\Phi}-\Phi)^T\hat{\Phi}\}=0$. Hence the MMSE estimates of the matrices of coefficients U and D are:

$$\hat{u}_{ij}=\frac{E\{\hat{\phi}_i^T\phi_j\}}{E\{\phi_j^T\phi_j\}},$$
$$\hat{d}_i=\frac{E\{\hat{\phi}_i^T\nu\}}{E\{\nu^T\nu\}}.$$

In a successful component extraction procedure, the interference of undesired components should be minimal, as well as the contribution of noise to the desired component. In other words, in the output of $\hat{\phi}_i$, the power of $\hat{u}_{ii}\phi_i$ (target component) should be much larger than the power of $\sum_{j=1,j\neq i}^{3}\hat{u}_{ij}\phi_j+\hat{d}_i\nu$ (other components). That is, in an optimal component separation, the coupling matrix U should be close to the identity matrix and D close to a null vector. The input signal-to-noise ratio and output signal-to-noise ratio are, respectively, defined as follows:

$$SNR_i^{in}=\frac{P_{\phi_i}}{\sum_{j=1,j\neq i}^{3}P_{\phi_j}+P_\nu},$$
$$SNR_i^{out}=\frac{\hat{u}_{ii}^2P_{\phi_i}}{\sum_{j=1,j\neq i}^{3}\hat{u}_{ij}^2P_{\phi_j}+\hat{d}_i^2P_\nu},$$

where P_{ϕ_1}, P_{ϕ_2}, P_{ϕ_3} and P_ν denote powers of P wave, QRS complex, T wave and noise respectively. SNR_i^{in} characterizes the problem at hand before performing any separation of components: some components might be very small with respect to the others and thus difficult to detect. A large SNR_i^{out} indicates instead that the power of the estimated component $\hat{\phi}_i$ is high against other components and noise. We further define the improvement $SNR_i^{dif}=SNR_i^{out}-SNR_i^{in}$.

2. *NSR_i*

   Another measures of improvement is given by

$$NSR_i=\left[\frac{\sum_k\left(\phi_{i,k}-\hat{\phi}_{i,k}\right)^2}{\sum_k\phi_{i,k}^2}\right]^{\frac{1}{2}},$$

   is a classical ratio between the power of the reconstruction error and the power of the component $\phi_{i,k}$ (a noise-to-signal ratio).

3. *imp_i*

   The third measure is defined by [95]

$$imp_i=-10\log_{10}\frac{\sum_k\left(\hat{\phi}_{i,k}-\phi_{i,k}\right)^2}{\sum_k\left(s_k-\phi_{i,k}\right)^2}\ (dB), \tag{2.22}$$

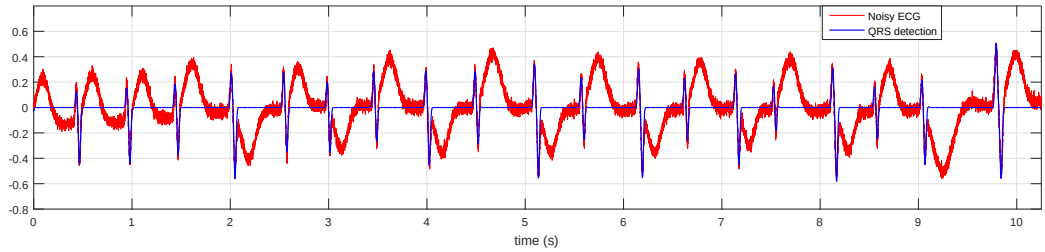

(a) QRS extraction provided by EKS6

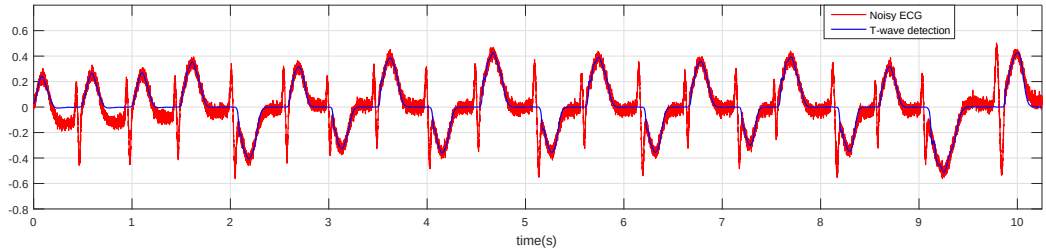

(b) T wave extraction provided by EKS6

Figure 2.5: QRS complex and T-wave estimates provided by EKS6, when applied to a synthetic signal corrupted by noise with SNR = 18 dB (Fig. 2.2).

which instead considers the ratio between the power of the reconstruction error and the power of the other components contained in the original signal s_k, defined in (2.20), including the noise $v_{2,k}$.

2.6.2 RESULTS AND DISCUSSION

As discussed before, T-wave alternans is one of the abnormality in ECG and its detection is relevant. We applied EKS6 to detect the changes in T-waves for such abnormalities. Fig. 2.5a and 2.5b show the result of applying EKS6 to the synthetic ECG displaying alternation of T-wave forms. The T wave component follows more precisely, when compared to EKS4 in Fig. 2.3a and 2.3b, the ECG morphology, due to the independence of the model from the amplitude. The detected QRS complex produced by EKS6 is also more close to the original one, comparing to EKS4.

We also applied the model on real data. Fig. 2.6 and 2.7 shows the results of the decomposition for a specific case (record 08378m from MIT-BIH Atrial Fibrilation Database [124]), using EKS4 and EKS6. EKS4 leads to the distortion of T waves before premature ventricular contractions (PVC), while EKS6 does not, as highlighted using black circles.

For evaluating the performance of the proposed method, we applied it on simulated data, which permits to quantify the decomposition error directly (no gold-standard is available for the decomposition of ECG components of real recordings).

For synthetic data generation, we used the single channel ECG dynamic model presented by McSharry *et al.* and combined it with signal decomposition based model suggested by Kheirati Roonizi and Sameni [108]. In 250 synthetic signal the sampling

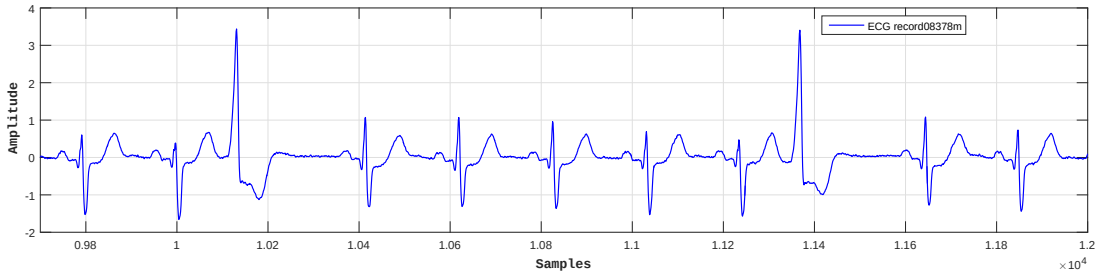

(a) ECG record 08378m.

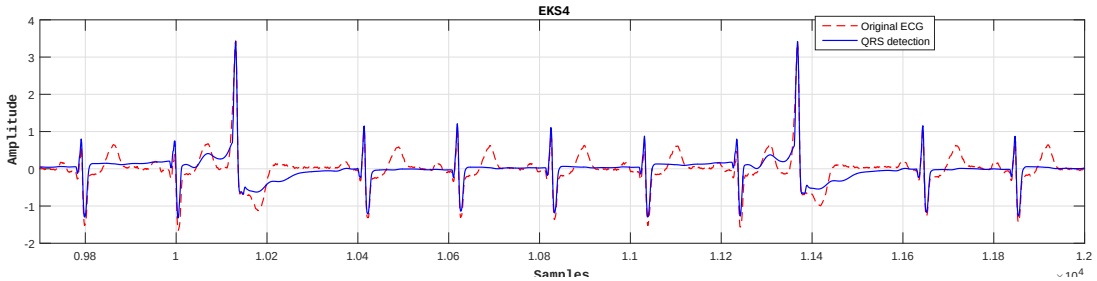

(b) QRS extraction provided by EKS4

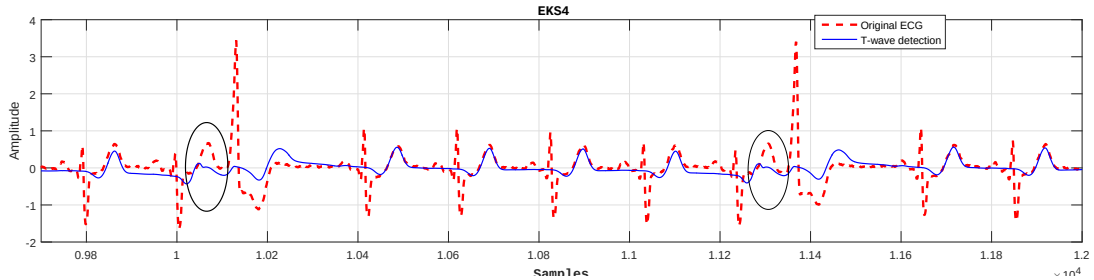

(c) T wave extraction provided by EKS4

Figure 2.6: QRS complex and T-wave estimates provided by EKS4 for record 08378m from the MIT-BIH Atrial Fibrilation Database (afdb).

rate was set to 1000. The RR interval durations were allowed a random fluctuation of up to 5% in each beat. A summary of the results of the components extraction procedures on synthetic data using the first metrics (SNR_i^{dif}) is reported in Fig. 2.8. SNR_i^{dif} for EKS6 outperformed EKS4. Fig. 2.9 shows the results of components estimation using the second metrics (NSR_i). The results, reported in Fig. 2.9, show that the reconstruction improvement continues for EKS6 even when the noise corrupting the input signal is small, while it saturates for EKS4. In fact, the results are referred to components separation, not ECG modelling. A wrong component detection or the mixing in the components detected might happen also when little noise is contaminating the input signal. A similar result is conveyed in Fig. 2.10 by the third metrics (imp_i). From a practical point of view, EKS6 outperformed EKS4 in the tests we performed. For example, components were sometimes mixed up by EKS4 but not by EKS6, as shown for QRS and T waves in Fig. 2.2 and 2.6. Surely, EKS6 has two extra state variables with respect to EKS4 (a price to pay for removing amplitude from the model), and, in

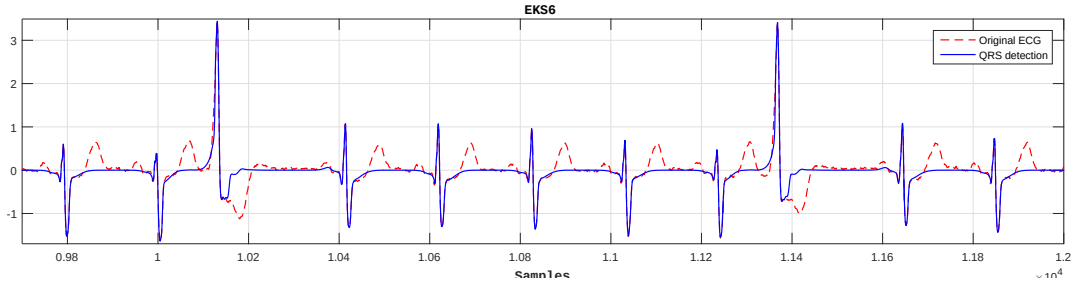

(a) QRS extraction provided by EKS6

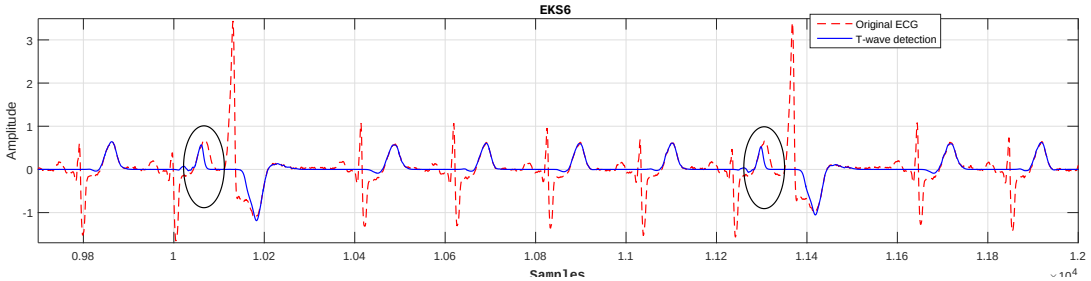

(b) T wave extraction provided by EKS6

Figure 2.7: QRS complex and T-wave estimates provided by EKS6 for record 08378m from the MIT-BIH Atrial Fibrilation Database (afdb).

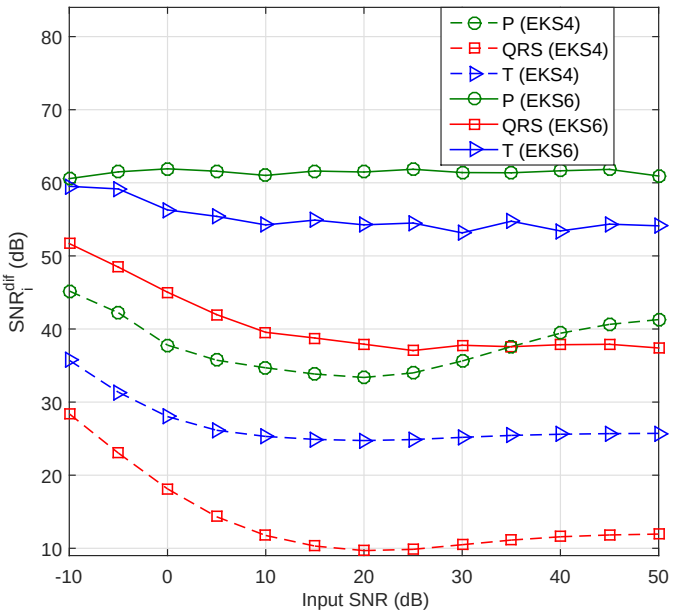

Figure 2.8: Mean values of SNR_i^{dif} for ECG components estimated by EKS6 and EKS4, as a function of the power of the broadband noise corrupting the input signal.

principle, a larger number of degrees of freedom surely helps EKS6 in better following the ECG components. However, this is not the main source of the performance gain, but the improvement is due to the new EDM proposed in (2.18). To support this claim, we increased the number of hidden state variables of EKS4 to six, by using the EDM in (2.17), which in our notation corresponds to (2.6). The results are reported in Fig.

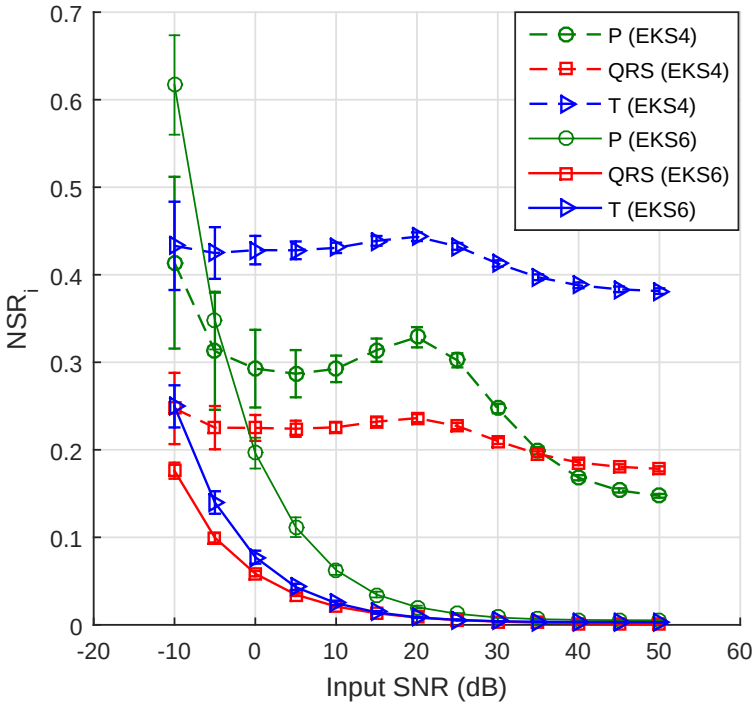

Figure 2.9: Mean values of NSR_i for ECG components estimated by EKS6 and EKS4, as a function of the power of the broadband noise corrupting the input signal.

2.11. EKS6 still outperformed the previously suggested solution, even when the number of hidden state variables was made equal. The same figure also contains the partial results (only related to QRS to make the figure easier to read), obtained employing the method described in [125], our preliminary attempt based on (2.18) and six hidden state variables. Also in this second case, EKS6 displayed better performance. These two further tests support the idea that the improvements derive from the new EDM model itself, possibly underlining the importance of the complete removal of the amplitude dependence.

Although the proposed method is more suitable for ECG components separation, but it is also useful for ECG denoising as shown in Fig. 2.12.

2.7 SUMMARY

In this chapter, an adaptive model-based Bayesian filtering framework was described for ECG analysis and feature extraction. While it could be employed for multiple purposes, like features extraction and denoising, it is particularly suited for extracting electrocardiogram (ECG) wave-forms (P, Q, R, S and T waves) from ECG recordings. In the proposed method, the ECG components are directly utilized as hidden state variables, and simultaneously estimated as a time series through an EKS. The simulation results demonstrated that EKS6 has the capability of correctly tracking ECG component waveforms, on a beat-to-beat basis.

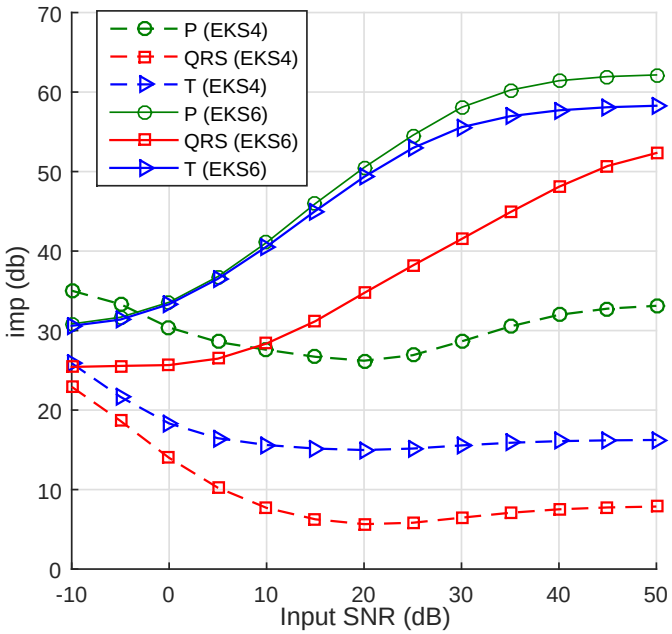

Figure 2.10: Mean values of SNR_i^{dif}, NSR_i and imp_i for ECG components estimated by EKS6 and EKS4, as a function of the power of the broadband noise corrupting the input signal.

There are some theoretical advantages that EKS6 has over other recent works in this context. As compared with EKS2, that uses only two state variables, six state variables are employed, with the advantage of permitting ECG components separation (and not only ECG filtering). The matrix A_k in EKS6 is not constant in time, making it able to better model the nuances in the ECG signal. Finally, EKS linearizes the dynamical system at an operating point by approximating the state model through a first order Taylor series approximation. The truncation of the Taylor series is a poor approximation for most non-linear functions. In fact, the accuracy of the linearization depends on the amount of local nonlinearity in the functions being approximated. Then, the posterior mean and covariance estimations become suboptimal and model errors are introduced. This can lead to instability, particularly when the system dynamics are strongly nonlinear [126]. The EDM proposed here for EKS6 was derived to reduced the nonlinearity of the state model with respect to previous solutions.

A second technical reason favoring EKS6, might be related to what reported recently by [127], where an EDM, similar to (2.6), was found to produce a baseline drift in non-invasive fetal ECG, obtained from a similar Bayesian framework.

In the experiments performed in this work, six hidden state variables were employed. The number could be increased to have a more accurate representation of ECG components, at the cost of an increased complexity of the overall scheme. However, this might cause the model to follow undesired observation noises. Information on the measurement and process noises (v_k and w_k) might help in selecting the values of the matrixes Q_k and R_k, and hence the actual smoothness of the results. The eigenvalues of R_k^{-1} should be large when the SNR is high, *i.e.*, little measurement noise v_k is assumed,

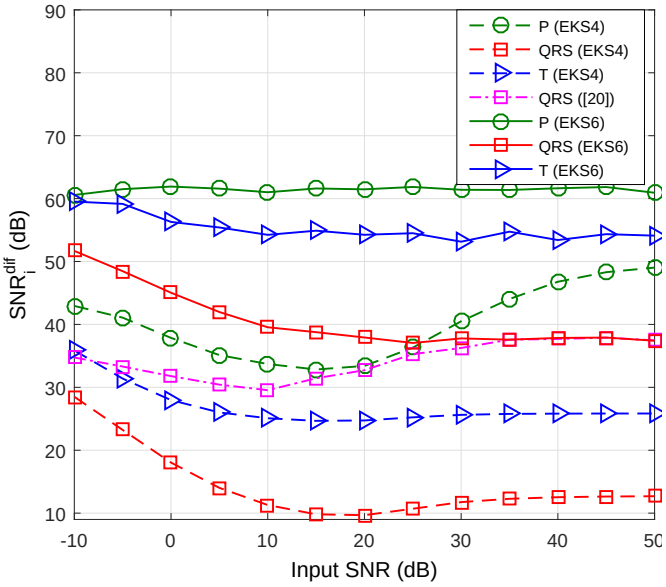

Figure 2.11: Mean SNR_i^{dif} for ECG components estimated by EKS6 and EKS4. For the latter the number of hidden state variables was increased to six, so that it did not differ from what used in the former. The picture also reports the mean SNR_i^{dif} value obtained when estimating the QRS component using the preliminary EKS described in [125].

while the eigenvalue of Q_k^{-1} should be large when the state model is accurate, *i.e.*, w_k is supposed to be small in (2.13).

The tests on data coming from real world problems including T/QRS ratio calculation will be discussed in the next chapters. They confirmed that ECG components separation through EKS6 is feasible.

In the next chapter we extend the framework to Atrial fibrillation and propose a new model for Atrial fibrillation analysis. The framework can also be extended to fetal ECG components separation. For this purpose, one could modify the parallel EKS introduced in [128] using the new EDM model in (2.18) for fetal ECG and the one in (2.3) for maternal ECG.

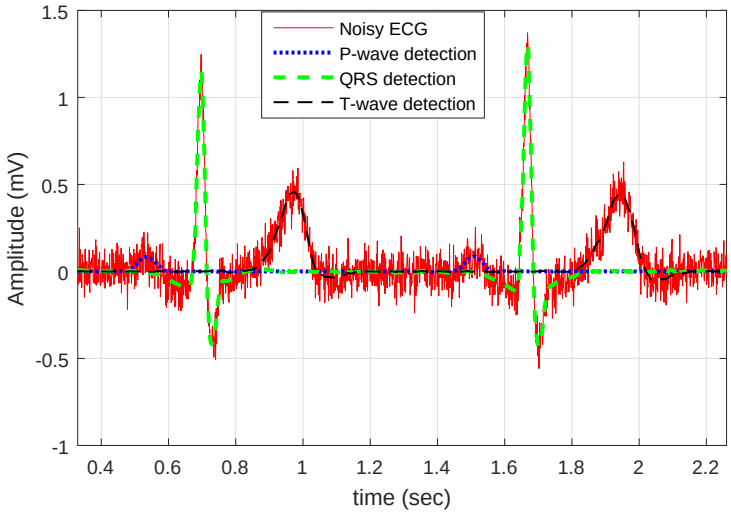

(a) Noisy ECG beats (SNR = 10 dB) with QRS and T-waves components overlaid, as extracted by means of EKS6.

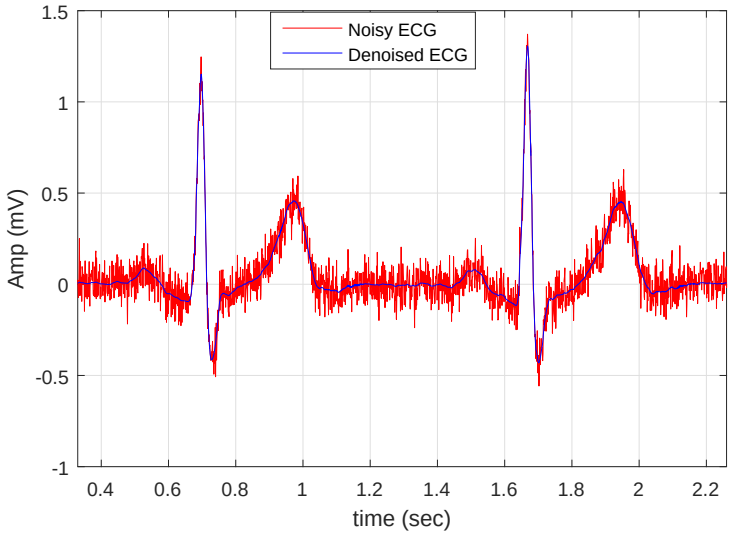

(b) The same noisy ECG overlaid with its de-noised version (the superposition of components produced by EKS6).

Figure 2.12: ECG denoising using EKS6.

3

MODEL-BASED ATRIAL ACTIVITY CHARACTERIZATION

In patients with atrial fibrillation the repetition rate of the atrial fibrillatory waves is very important for analyzing AF from surface ECG. The fibrillatory frequency (FF) is useful for non-invasive assessment of electrical remodeling in AF. FF can be assessed by signal processing tools such as power spectral analysis and short time Fourier transform (STFT) from ECG after ventricular activity (QRS-T complex) cancellation. The existing methods for ventricular activity cancellation (or AF extraction) are based on single or multi-channel recordings. Although the algorithms that deals with extracting atrial activity (AA) using multi-lead ECG recordings often outperform those methods exploiting single lead ECG, the performance of the former will decrease when the number of leads is reduced.

In this chapter, we describe the theory and application of a new model for single lead ECG analysis in patients with atrial fibrillation (AF). The rest of the chapter is organized as follows. In section 3.1, we review a common method in the literature that extracts the atrial activity using single channel recordings. Section 3.2 presents an original model-based extended Kalman filter for tracking the fibrillatory frequency (FF) while separating atrial and ventricular activity in atrial fibrillation. Section 3.3 shows the results of the proposed method for real and simulated data. A summary of the chapter is given in the final section.

3.1 QRS-T CANCELLATION USING AVERAGE BEAT SUBTRACTION (ABS) FROM SINGLE LEAD ECG RECORDINGS

ABS is one of the common methods for cancellation of ventricular activity from the surface electrocardiogram during AF. The idea was initially proposed by Slocum *et al.*, for identification of P-wave during ventricular tachycardia [129]. Atrial and ventricular activities during AF can be considered, in first approximation, statistically uncorrelated. The idea of ABS is to construct a template of an average beat and then subtract it

from the original signal, on a beat to beat basis. The remainder ECG, with subtracted ventricular activity, is taken to be the f-wave. The ECG average template waveform is computed by averaging the time-warped beats, thus assuming that the beat morphologies have been clustered. The main point is that prior to subtraction, the average beat and each QRST complex should be well-aligned in time to each other. Otherwise the resulting atrial signal will contain QRST residuals. Therefore, temporal alignment is required in any method that involves subtraction of the average beat. The alignment problem is defined by [130]

$$\epsilon^2 = \min_{\tau} \|x - J_\tau \bar{x}\|^2, \tag{3.1}$$

where ϵ^2 denotes quadratic error defined by the vector norm and the vector x denotes N samples of the observed signal $x(n)$,

$$x = [x(0), x(1), ...x(N-1)]. \tag{3.2}$$

The average beat $\bar{x}$ contains 2Δ additional samples so as to allow for temporal alignment of x relative $\bar{x}$ using the shift matrix J_τ,

$$J_\tau = [0_{N\times(\Delta+\tau)} \qquad I_{N\times N} \qquad 0_{N\times(\Delta-\tau)}] \tag{3.3}$$

where τ denotes an integer time shift. The two matrices 0 and I denote the zero and identity matrix, respectively. The maximal alignment error that can be corrected with this formulation is $\pm\Delta$. The minimization is performed as a grid search over all admissible values of τ, thus determining the N samples of $\bar{x}$ which best fit x. However, one of the necessary assumption that should be considered when using ABS is the stationarity of ECG signals. ABS assumes that the morphology of the ECG signal changes little in time. In other word, ECG is considered as a stationary signal. Unfortunately, real ECG signals can be highly non-stationary in practice, and QRST morphology varies beat by beat. As a result, ABS might produce a poor cancellation of ventricular activity, since it introduces high power residues. Hence, atrial activity signals extracted by ABS often have serious distortions, especially for weak atrial activity [131]. This might then affect the frequency analysis of the extracted f-waves.

3.2 A NEW FRAMEWORK FOR ATRIAL FIBRILLATION DETECTION

In this section, a new algorithm based on an extended Kalman smoother (EKS) is introduced for AF analysis. Using the EKS, together with a dynamical model describing the surface electrocardiogram waveform and fibrillatory wave (generated by the activity of the atria while fibrillating), allows the decomposition of the original ECG signal and a much more accurate detection of atrial fibrillation.

3.2.1 VENTRICULAR ACTIVITY MODEL

As mentioned before, normal ECG beats are composed of different waves, classically labeled as P, Q, R, S and T, which can be modeled by a linear combination of Gaussian kernels with different amplitudes and widths centered at specific points in time. During AF, the P-waves are absent. However, QRS-T can still be modeled using sum of Gaussian functions:

$$\begin{cases} \theta_{k+1} = (\theta_k + \omega\delta) \mod 2\pi \\ z_{k+1} = z_k - \omega\delta \sum_{i\in\{Q,R,S,T\}} \alpha_i \frac{\theta_k - \theta_i}{b_i^2} e^{-\frac{(\theta_k-\theta_i)^2}{2b_i^2}} \end{cases}, \tag{3.4}$$

where ω is the angular velocity of the trajectory as it moves around the limit cycle, θ is the cardiac phase, which is defined between $-\pi$ and π, f_s is the sampling rate, $\delta = 1/f_s$ the sampling interval, α_i, b_i and θ_i adapt amplitude, width and center of the Gaussian kernels to the different ECG morphologies [88].

3.2.2 ATRIAL ACTIVITY MODEL

It has been shown that surface ECG f-waves are not completely random and display a periodical behaviour with a dominant frequency within a range of 3-12 Hz [132]. This fact motivated us to consider the following sinusoidal model for f-waves, characterized by a fundamental frequency f_c, plus $N-1$ of its harmonics:

$$\zeta_k = \sum_{n=1}^{N} p_n \cos(n w_c k + \varphi_n), \tag{3.5}$$

where $w_c = 2\pi f_c/f_s$. p_n and φ_n are respectively the amplitude and phase of the n^{th} harmonic. To derive a corresponding dynamical model, we recast (3.5) into:

$$\begin{cases} \phi_{n,k} = p_n \cos(n w_c k + \varphi_n) \\ \zeta_k = \sum_{n=1}^{N} \phi_{n,k} \end{cases}, \tag{3.6}$$

Then, a possible dynamical models of f-wave is:

$$\begin{cases} \phi_{n,k+1} + \phi_{n,k-1} = 2\cos(n w_c)\phi_{n,k} \\ \zeta_k = \sum_{n=1}^{N} \phi_{n,k} \end{cases}. \tag{3.7}$$

The model no longer depends on amplitude and phase of the harmonics. Moving one step further, with the objective of being able to track in time the fundamental frequency, we propose the following autoregressive (AR) dynamics for w_c

$$\begin{cases} w_{c,k+1} = w_{c,k} + \eta_{w_c} \\ \phi_{n,k+1} = 2\cos(nw_c)\phi_{n,k} - \phi_{n,k-1} + \eta_\phi \\ \zeta_k = \sum_{n=1}^{N} \phi_{n,k} \end{cases} \tag{3.8}$$

where η_{w_c} and η_ϕ are i.i.d. Gaussian random variables and represent the possible model errors, including minor frequency, amplitude and phase deviation. We assumed that the fibrillatory frequency can be considered as a times series that its value is regressed on its previous values. To emphasize that the value of w_c can change over time, we used an AR model of order one.

3.2.3 LINEARIZATION OF THE FRAMEWORK AND DERIVATION OF THE KF

Our goal is to combine the ventricular and atrial activity model, (3.4) and (3.8), for using them in a EKS algorithm to track the ventricular activity (z_k), the fibrillatory wave (ζ_k) and the AF fundamental frequency (w_c). Putting together eq. (3.4) and (3.8) the full ECG dynamical model is:

$$\begin{cases} \theta_{k+1} = (\theta_k + \omega\delta) \mod 2\pi \\ w_{c,k+1} = w_{c,k} + \eta_{w_c} \\ z_{k+1} = z_k - \omega\delta \sum_{i\in\{Q,R,S,T\}} \alpha_i \frac{\theta_k - \theta_i}{b_i^2} e^{-\frac{(\theta_k-\theta_i)^2}{2b_i^2}} \\ \begin{bmatrix} \phi_{n,k+1} \\ \phi_{n,k} \end{bmatrix} = \begin{bmatrix} 2\cos(nw_{c,k}) & -1 \\ 1 & 0 \end{bmatrix} \begin{bmatrix} \phi_{n,k} \\ \phi_{n,k-1} \end{bmatrix} + \begin{bmatrix} 1 \\ 0 \end{bmatrix} \eta_\phi \end{cases} . \tag{3.9}$$

The dynamical model is now complete and may be applied to ECG signals using classical iterative KF. At each time step k, the state variables which need to be estimated are: the ventricular activities z_k, the atrial activity components $\phi_{n,k}$, the AF fundamental frequency $w_{c,k}$ and the cardiac phase θ_k.

The corresponding observation equation is:

$$\begin{cases} \psi_k = \theta_k + v_{1,k} \\ s_k = z_k + \sum_{n=1}^{N} \phi_{n,k} + v_{2,k} \end{cases}, \tag{3.10}$$

where s_k is the noisy observation (the real ECG) and ψ_k is the noisy cardiac phase at time instant k. $v_{1,k}$ and $v_{2,k}$ are zero mean random variables considered to be observation noise.

Summarizing, in the terminology of EKF structure, we have:

$$\begin{cases} \theta_{k+1} = f_1(\theta_k, \omega, k) \\ w_{c,k+1} = f_2(w_{c,k}, \eta_{w_c}, k) \\ z_{k+1} = f_3(\theta_k, z_k) \\ \phi_{n,k+1} = f_n^1(w_{c,k}, \phi_{n,k}, \phi_{n,k-1}, \eta_{\phi_n}, k) \\ \phi_{n,k} = f_n^2(\phi_{n,k}, k) \\ \psi_k = g_1(\theta_k, k, v_{1,k}) \\ s_k = z_k + g_2(\phi_{n,k}, k, v_{2,k}) \end{cases},$$

and

$$\begin{aligned} x_k &= [\theta_k, w_{c,k}, z_k, \phi_{n,k}, \phi_{n,k-1}] \\ y_k &= [\psi_k, s_k] \\ w_k &= [\alpha_Q, \ldots, \alpha_T, b_Q, \ldots, b_T, \theta_Q, \ldots, \theta_T, \eta_{n,k}, \eta_{w_c}, \eta_{z,k}, \omega] \\ v_k &= [v_{1,k}, v_{2,k}]. \end{aligned}$$

The dynamical model in (3.9) is nonlinear. To linearize it and build the EKS, following eq. (4) in [133]:

$$\begin{aligned} \frac{\partial f_1}{\partial \theta_k} &= \frac{\partial f_2}{\partial w_{c,k}} = 1 & \frac{\partial f_2}{\partial v_{2,k}} &= \frac{\partial f_3}{\partial z_k} = 1 \\ \frac{\partial f_3}{\partial \eta_z} &= \frac{\partial f_2}{\partial w_{c,k}} = 1 & \frac{\partial f_3}{\partial z_k} &= \frac{\partial f_n^2}{\partial \phi_{n,k}} = 1 \\ \frac{\partial g_1}{\partial \theta_k} &= \frac{\partial g_1}{\partial v_{1,k}} = 1 & \frac{\partial f_n^1}{\partial \eta_{\phi_n}} &= \frac{\partial g_2}{\partial z_k} = 1 \\ \frac{\partial f_n^1}{\partial \phi_{n,k}} &= 2\cos(n w_{c,k}) & \frac{\partial f_n^1}{\partial w_{c,k}} &= -2n \sin(n w_{c,k}) \phi_{n,k} \\ \frac{\partial f_n^1}{\partial \phi_{n,k-1}} &= -1 & \frac{\partial f_1}{\partial \omega} &= \delta \\ \frac{\partial f_3}{\partial \alpha_i} &= -\omega\delta \frac{\theta_k - \theta_i}{b_i^2} \exp\left[-\frac{(\theta_k - \theta_i)^2}{2b_i^2}\right] \\ \frac{\partial f_3}{\partial \theta_i} &= \delta \frac{\alpha_i \omega}{b_i^2}\left[1 - \frac{(\theta_k - \theta_i)^2}{b_i^2}\right] \exp\left[-\frac{(\theta_k - \theta_i)^2}{2b_i^2}\right] \\ \frac{\partial f_3}{\partial b_i} &= 2\delta\alpha_i\omega \frac{\theta_k - \theta_i}{b_i^3}\left[1 - \frac{(\theta_k - \theta_i)^2}{b_i^2}\right] \exp\left[-\frac{(\theta_k - \theta_i)^2}{2b_i^2}\right] \\ \frac{\partial f_3}{\partial \omega} &= -\delta \sum_{i \in \{Q,R,S,T\}} \alpha_i \frac{\theta_k - \theta_i}{b_i^2} \exp\left[-\frac{(\theta_k - \theta_i)^2}{2b_i^2}\right] \end{aligned}$$

where we did not report the terms which were equal to zero.

3.2.4 PARAMETERS INITIALIZATION

Before implementation of the filter, it is necessary to select the values of the model parameters, process and measurement noise covariance matrices. The initial value for the state vector, kernels as well as the covariance matrices of the process and the measurement noise were initialized using the procedure described in [133, 74].

The initial parameters of Gaussian functions of ventricular activity model were computed by fitting the model

$$z_k = \sum_{i \in \{Q,R,S,T\}} \alpha_i \exp[-(\theta_k - \theta_i)^2/(2b_i^2)]$$

to the ECG template, which is obtained after R-peaks detection. The ECG template contains ventricular activity, supposing that the effect of atrial activity signal is attenuated by taking the average along the beats. The angular frequency of the model was set to $\omega = 2\pi/\overline{RR}$, where $\overline{RR}$ is the average RR-interval of the whole signal and we set $\theta_0 = -\pi$.

The process noise covariance matrix Q_k was set to

$$E\{w_k w_k^T\} = \quad \text{diag}(\sigma^2_{\alpha_Q}, ..., \sigma^2_{\alpha_T}, \sigma^2_{b_Q}, ..., \sigma^2_{b_T}, \sigma^2_{\theta_Q}, ..., \sigma^2_{\theta_T}, ..., \sigma^2_{w_c}, \sigma^2_{\omega}, \sigma^2_{\eta_\phi}),$$

where $\sigma^2_{\alpha_T}, \sigma^2_{b_Q}, ..., \sigma^2_{b_T}, \sigma^2_{\theta_Q}, ..., \sigma^2_{\theta_T}$ were derived from the amount of deviation of the parameters during the fitting procedure of the model to the template [74], while σ^2_{ω} was computed by taking the standard deviation of heart rate. $\sigma^2_{w_c}, \sigma^2_{\eta_\phi}$ are the parameters that represent the imprecision of the atrial activity dynamical model. We can consider them as zero-mean Gaussian random variable with an appropriate variance. With respect to the measurement noise covariance matrix R_0, $E\{v^2_{1,k}\}$ was set to $(\omega\delta)^2/12$, implying a uniform error in the location of the R-peak. The measurement noise covariance matrix R_k, $E\{v^2_{2,k}\}$ was considered to be diagonal as in [74].

For estimating the initial parameters of the atrial activity model, we selected the TQ segments[1] of 10 first beats of ECG and estimated the frequency of each segment by fitting a single sinusoid to each segment. Finally, the average of these 10 frequencies was considered as initial fundamental frequency. The algorithms for fundamental frequency estimation can be split into two categories: **time domain based estimators** (*e.g.*, zero crossing, autocorrelation, *etc.*) and **frequency domain based estimators** (*e.g.*, Fast Fourier Transform (FFT), harmonic product spectrum, cepstrum, *etc.*). Another examples include adaptive filter and models of the human ears [134].

In the following section, a simple algorithm is proposed for estimating the parameters of a single tone and its performance is compared with nonlinear least squares estimation from time domain and FFT from the frequency domain based estimator.

1 Assuming that ventricular activity is absent in the TQ interval.

3.2.5 A SIMPLE ALGORITHM FOR ESTIMATING THE FUNDAMENTAL FREQUENCY OF A SINGLE TQ SEGMENT

Our hypothesis for estimating the fundamental frequency of TQ segment is to fit a single sinusoidal model to the segment. The model is described as follows:

$$\hat{\zeta}(t) = p_s \cos(w_s t + \phi_s), \tag{3.11}$$

where p_s, w_s and ϕ_s are respectively, the amplitude, frequency and phase of the sinusoid. $\hat{\zeta}$ is a single sinusoid function for modelling TQ segment, which the frequency is the desired fundamental frequency.

The main goal is to approximate the unknown frequency w_s in equation (3.11). Noting that $\hat{\zeta}$ is nonlinear with respect to w_s, this problem is generally associated with the solution of an over determined system of nonlinear equations, which is generated by substituting the observed data (TQ segment) into (3.11). In this section, we propose an original algorithm for estimating w_s which is composed of two iterative steps, each of them linear. The algorithm is as follows:

Taking twice partial derivative of both sides of (3.11) yields:

$$\frac{\partial^2}{\partial t^2}\hat{\zeta} = -w_s^2\hat{\zeta}. \tag{3.12}$$

Taking twice integral of both sides of (3.12) yields:

$$\hat{\zeta} = a_1 + a_2 t - w_s^2 \int_0^t \int_0^v \hat{\zeta}(u)\,du\,dv; \tag{3.13}$$

(3.13) is more robust to noise, since it is described by an integral equation against (3.12) which is described by a derivative equation.

The new fitting algorithm is as follows:

$$\hat{\zeta}(t) = \sum_{k=0}^{2} c_k \phi_k(t) \tag{3.14}$$

where

$$\begin{cases} \phi_k(t) = t^k, & 0 \leqslant k \leqslant 1 \\ \phi_2(t) = \int_0^t \int_0^v \hat{\zeta}(u)\,du\,dv \end{cases} \tag{3.15}$$

and

$$\begin{cases} c_0 = a_1 \\ c_1 = a_2 \\ c_2 = -w_s^2 \end{cases}. \tag{3.16}$$

(3.14) can be expressed as:

$$\hat{\zeta}(t) = c^T \Phi(t), \tag{3.17}$$

where

$$\begin{aligned} c &= [c_0, c_1, c_2]^T \\ \Phi(t) &= [\phi_0(t), \phi_1(t), \phi_2(t)]^T \end{aligned} \tag{3.18}$$

According to (3.17) the error function is defined as

$$e(t) = \hat{\zeta}(t) - c^T \Phi(t) \tag{3.19}$$

The following cost function can be minimized to find the parameters that minimize the energy of the residual error

$$\begin{aligned} SMSSE(\hat{\zeta}|c) &= \int_{-\infty}^{\infty} |e(t)|^2 dt \\ &= \int_{-\infty}^{\infty} |\zeta(t) - c^T \Phi(t)|^2 dt \end{aligned} \tag{3.20}$$

The criterion is expressed more cleanly in matrix terms as

$$SMSSE(\hat{\zeta}|c) = \|\hat{\zeta} - c^T \Phi\|^2 \tag{3.21}$$

By direct calculation, the minimization of (3.21) leads to the following optimal solution:

$$c_{opt} = (\Phi^T \Phi)^{-1} \Phi^T \hat{\zeta}. \tag{3.22}$$

$\phi_2(t)$ depends on $\hat{\zeta}(t)$ and $\hat{\zeta}(t)$ is unknown. That is why we replace $\hat{\zeta}(t)$ with $\zeta(t)$, the fundamental frequency of TQ segment can be computed using $w_s = \sqrt{-c_2}$, with respect to (3.16). The only unknown parameters in (3.5) are the coefficients (p_n and q_n) which are estimated using a linear optimization. Note that the Eq (3.13) has $\hat{\zeta}(t)$ on both the left hand side and the right. This may appear on the face of it to require an iterative method for improving the accuracy of estimation.

To assess the accuracy of the proposed method in comparison with the FFT and nonlinear least squares estimation, synthetic datasets were employed. Several sets of single tone signal over time interval $[0, 5]$ sec with sampling rates (1kHz) were generated. Each set includes 101 sinusoidal curves with different frequencies ranging between $\omega_i = (0 : 0.01 : 1) \times \pi$. Also we generated different phases ranging between $\phi_i = (0 : 0.01 : 1) \times \pi$ to see the handling ability of the method to estimate sinusoidal functions. In this experiment, we produced the signals with different SNR changing from -10 to 40 dB.

For evaluating the performance of the proposed method, we used the SNR improvement measure given by:

$$\text{imp(dB)} = \text{SNR}_{out} - \text{SNR}_{in} = 10\log \frac{\sum_{k=1}^{N} (f_n[k] - \hat{f}[k])^2}{\sum_{k=1}^{N} (f[k] - \hat{f}[k])^2} \text{dB} \tag{3.23}$$

where N is the number of samples, $f_n[k]$, $f[k]$ and $f\hat{[k]}$ are the noisy, original and reconstructed discretized signals, respectively. The equations mentioned in (3.12) and (3.13), both can be used to estimate the frequency. We also compared the performance of these two proposed models in estimating the frequency, amplitude and phase of the single tones with other methods. Fig. 3.1 shows the results of performance comparison . The results show that the proposed algorithm with integral equation outperforms other methods. Compared to nonlinear least square estimation, the precision of this new method is equivalent while enjoying an improvement in computational time as shown in Fig. 3.2. As another weaknesses of nonlinear least square estimation is that its performance strongly depends on the initial conditions and it may diverge.

The FFT divides the frequency domain into equal intervals on a linear scale. The frequency bin containing the most energy is used to find the peak frequency. In our experiment, the resolution which is defined by $\Delta f = \frac{fs}{N}$ is 0.2, containing the sample time window of 5 sec. The FFT sample time window (where the tone should ideally remain constant) is the inverse of the frequency difference Δf and it is possible that the desired frequency does not fall in a frequency bin. In other words, FFT is constrained by the limited time resolution and produces inaccurate estimates. Finally the state variables are propagated in time using equations (2) and (3) in [133]. This is equivalent to having a set of basis functions updated over time, such that they are distinctly estimated from sample to sample.

3.3 RESULTS

The signals used in this study were taken from PhysioNet PTB Diagnostic ECG Database [135] (sampling frequency: 1000 Hz; resolution: 16-bit). Several ECG segments, each with duration of 10s, were selected from the twelve conventional leads, at the beginning of each recording. P-waves were separated and removed from segments using the approach proposed for ECG components separation in [133]. Synthetic f-waves were generated using a sawtooth model introduced in [58, 60], and replaced instead of P-waves to study the performance of the proposed filter. In specific, the synthetic f-wave model is described by a fundamental oscillating components and its $M-1$ harmonics

$$\xi_{d,k} = \sum_{m=1}^{M} a_{m,k} \sin\left[m\omega_0 k + \frac{\delta_f}{f_f}\sin(\omega_f k)\right] \tag{3.24}$$

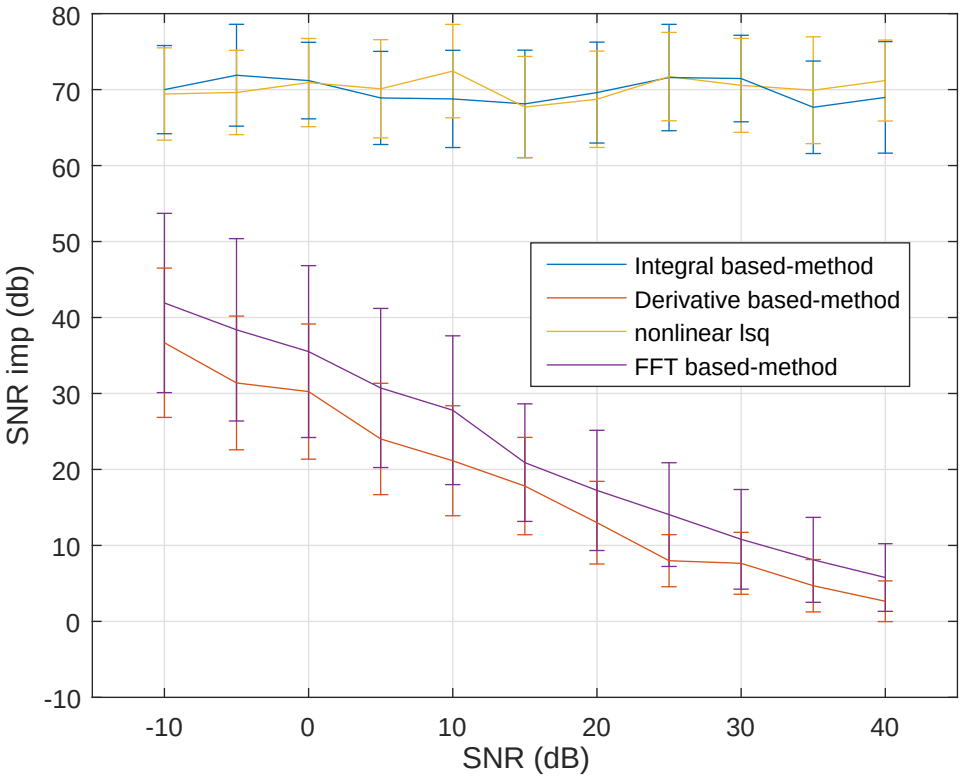

Figure 3.1: The average of SNR improvement versus the simulated SNR for four methods the proposed derivative (3.12), the proposed integral (3.13), FFT and nonlinear least square estimation.

where the fundamental frequency $\omega_0 = 2\pi f_0$ has the maximum frequency deviation δ_f and the modulation frequency $\omega_f = 2\pi f_f$. Furthermore the amplitude $a_{m,k}$ is defined so that a signal with sawtooth characteristic is produced

$$a_{m,k} = \frac{2}{m\pi}\left[a + \delta a \sin(\omega_a k)\right], \tag{3.25}$$

where a denotes the sawtooth amplitude, δa modulates the peak amplitude and $\omega_a = 2\pi f_a$ is the amplitude modulation frequency. Finally, the realistic synthetic mixtures of real ECG and synthetic f-wave with added white Gaussian noise were generated for different situations.

3.3.1 VENTRICULAR AND ATRIAL ACTIVITY SIGNAL SEPARATION

As preliminary example, the synthetic ECG with real QRS-T, synthetic f-wave and white Gaussian noise in Fig. 3.3 displays an episode of AF. Fig. 3.3a and Fig. 3.3b illustrate the synthetic f-wave produced by (3.24) and the original QRS-T. Fig. 3.3c shows the ECG mixture of ventricular activity and atrial activity signals and Fig. 3.3d shows the ECG corrupted by noise (SNR = 0 dB).

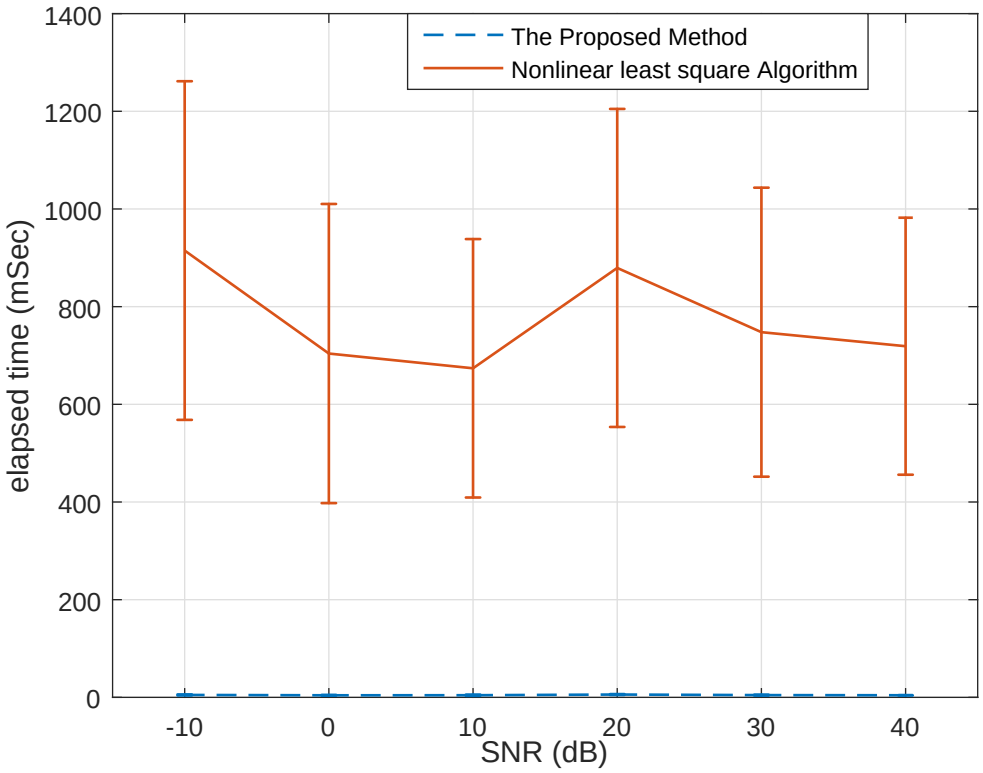

Figure 3.2: The mean and standard deviation of the computational complexity versus the simulated SNR for nonlinear least square estimation and the proposed scheme (3.13).

Finally, Fig. 3.4a and 3.4b show the result of applying EKS to the noisy ECG displaying AF. The QRS-T wave component follows precisely the ECG morphology and the result of f-wave detection is reliable.

Furthermore, we produced signals varying the power of $v_{2,k}$ in (3.10). The signal-to-noise ratio (SNR) was modulated from -10 to 20 dB. Inspired by [133], the estimated QRS-T and f-waves signals, $\hat{z}$ and $\hat{\zeta}$, are assumed to be the linear combination of z, ζ, and noise, such that

$$\hat{z} = u_{11}z + u_{12}\zeta + u_{13}n$$
$$\hat{\zeta} = u_{21}z + u_{22}\zeta + u_{23}n$$

where the coefficients $u_{ij}, i = 1, 2$ and $j = 1, 2, 3$ have to be estimated. The coefficients can be estimated using

$$\hat{u}_{11} = \frac{E\{\hat{z}^T z\}}{E\{z^T z\}} \qquad \hat{u}_{12} = \frac{E\{\hat{z}^T \zeta\}}{E\{\zeta^T \zeta\}} \qquad \hat{u}_{13} = \frac{E\{\hat{z}^T n\}}{E\{n^T n\}}$$
$$\hat{u}_{21} = \frac{E\{\hat{\zeta}^T z\}}{E\{z^T z\}} \qquad \hat{u}_{22} = \frac{E\{\hat{\zeta}^T \zeta\}}{E\{\zeta^T \zeta\}} \qquad \hat{u}_{23} = \frac{E\{\hat{\zeta}^T n\}}{E\{n^T n\}}$$

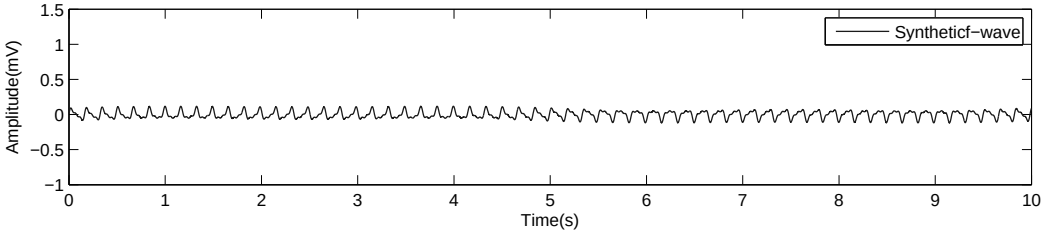

(a) Synthetic f-wave generated by (3.24)

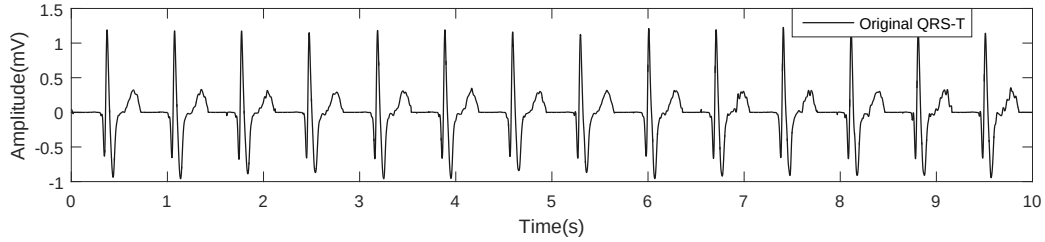

(b) Original QRS-T

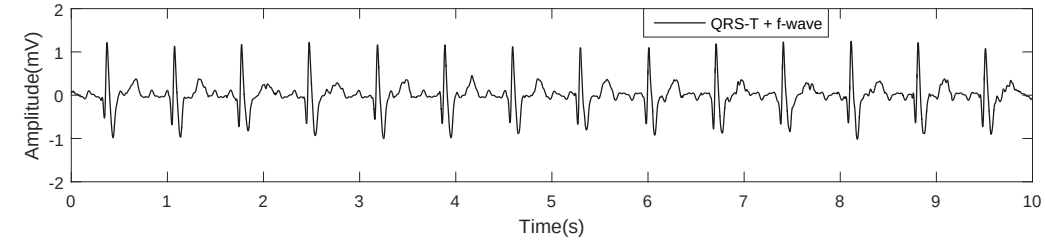

(c) Original QRS-T plus synthetic f-wave

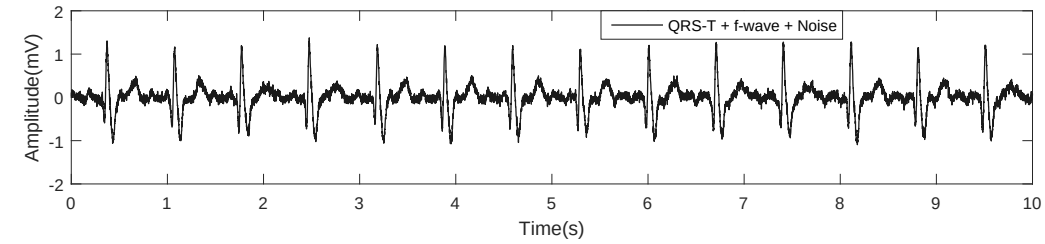

(d) Noisy Signal

Figure 3.3: An episode of AF signal simulated from original QRS-T and synthetic f-wave.

In a successful ventricular activity and atrial activity extraction procedure, the interference of undesired signals should be minimal, as well as the contribution of noise to the desired signal. The input signal-to-noise ratio and output signal-to-noise ratio are, respectively, defined as follows:

$$\mathrm{SNR}_z^{\mathrm{in}} = \frac{P_z}{P_z + P_\zeta + P_\nu}, \qquad \mathrm{SNR}_\zeta^{\mathrm{in}} = \frac{P_\zeta}{P_z + P_\zeta + P_\nu}$$

$$\mathrm{SNR}_z^{\mathrm{out}} = \frac{\hat{u}_{11}^2 P_z}{\hat{u}_{12}^2 P_\zeta + \hat{u}_{13}^2 P_\nu}, \qquad \mathrm{SNR}_\zeta^{\mathrm{out}} = \frac{\hat{u}_{22}^2 P_\zeta}{\hat{u}_{21}^2 P_z + \hat{u}_{23}^2 P_\nu}$$

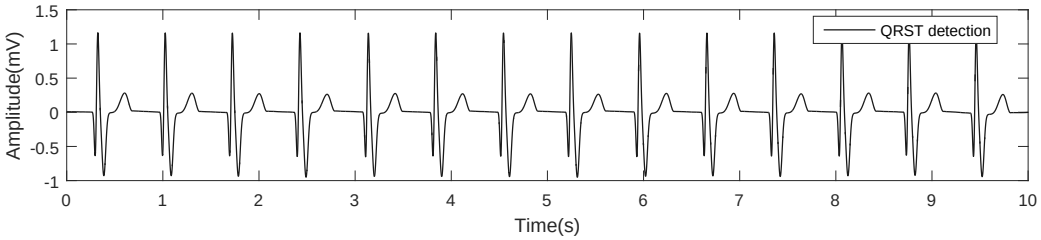

(a) QRS-T extraction provided by proposed EKS

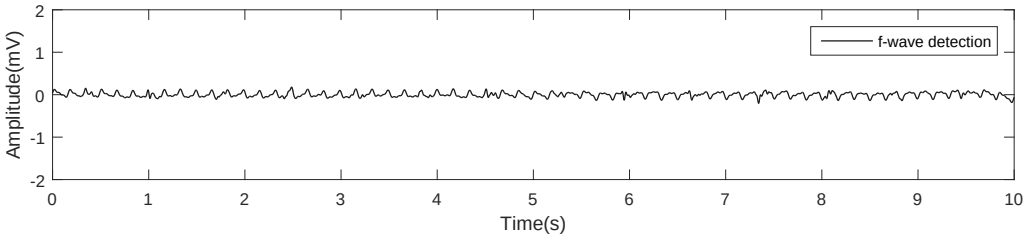

(b) f-wave extraction provided by proposed EKS

Figure 3.4: Atrial and Ventricular activity waveforms separation provided by proposed EKS, when applied to a real QRS-T plus synthetic f-wave corrupted by noise with SNR = 0 dB Fig.(3.3).

where P_z, P_ζ and P_ν denote powers of QRS-T (z), f-waves (ζ) and noise (n) respectively. We further define the improvement $SNR_Y^{dif} = SNR_Y^{out} - SNR_Y^{in}$, $Y \in \{z, \zeta\}$. A summary of the results of the signals extraction procedures on synthetic data is reported in Fig. 3.5 and 3.6. SNR_Y^{dif} for EKS outperformed ABS in both f-wave and QRS-T extraction.

For evaluating the performance of the proposed method, we also used another measures of improvement given by

$$NSR_Y = \sqrt{\frac{1}{k}\sum_k \left[Y - \hat{Y}\right]^2},$$

The mean and standard deviation (SD) of the RMSE versus different input SNRs are plotted in Fig. 3.7 and 3.8. The results of this measure also show that the proposed EKS outperforms ABS in VA and AA extraction. Specially in low SNRs, the performance of EKS is much better than ABS. Also the proposed EKS hass the advantage of enjoying of tracking the fibrillatory frequency in parallel with AA and VA extraction.

3.3.2 FUNDAMENTAL FREQUENCY TRACKING OF ATRIAL FIBRILLATORY WAVES

We also studied the performance of the proposed filter for tracking the fundamental frequency of atrial fibrillatory waves. For this purpose, we generated four types of fundamental frequency, as shown in Fig 3.9: I) constant frequency $f_c = 7$ Hz, II) stepwise changing frequency, III) gradually decreasing frequency $f_c = 7 - 2(1 - \exp[-0.1n/f_s]^2)$; and IV) time varying frequency $f_c = 7 \pm 0.5\sin[0.6\pi n/f_s]$. Then, f-waves with four different frequency trends were created and added to the original ECGs. The frequency trends of the simulated signals are shown in Fig 3.9. We compared the ability of filter to

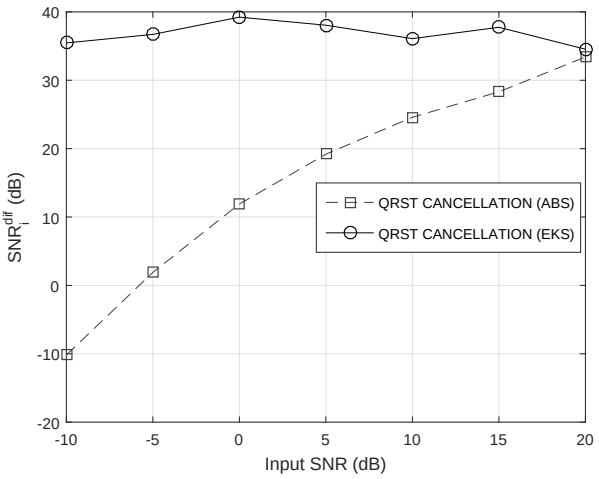

Figure 3.5: Mean SNR_i^{dif} for QRS-T Detection

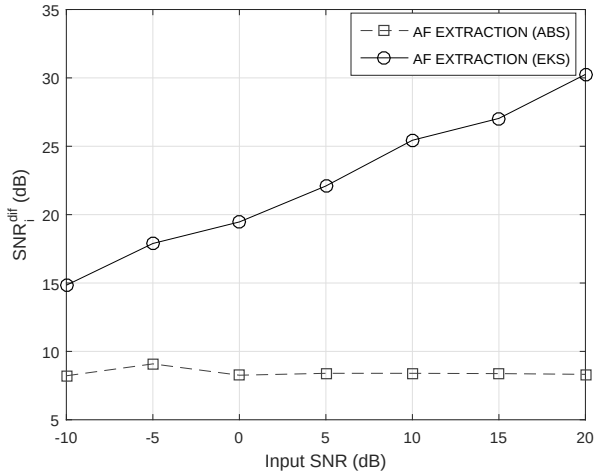

Figure 3.6: Mean SNR_i^{dif} for f-waves Detection

estimate the fundamental frequency in present of noise. To quantify the performances of the method, we employed the root mean square error (RMSE) defined as:

$$\text{RMSE} = \sqrt{\frac{1}{n}\sum_{n}\left(f_{c,n} - \hat{f}_{c,n}\right)^2},$$

where $f_{c,n}$, $\hat{f}_{c,n}$ are the original and the estimated fundamental frequency. The additive Gaussian noise was added with varying SNR (from 0 to 40 dB). The mean and standard deviation (SD) of the RMSE versus different input SNRs achieved over 250 ECG segments are plotted in Fig. 3.10. The results show that the filter is able to track the fundamental frequency even in present of noise. The filter is more able to track the fundamental frequency when it is constant or it changes gradually in time, However its performance is decreased in the case of time-varying frequency.

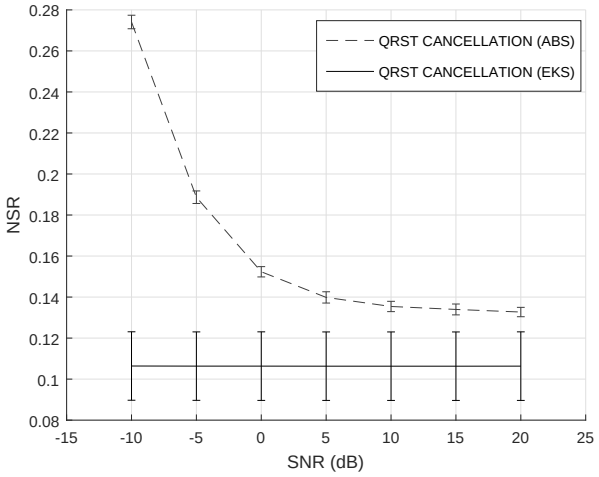

Figure 3.7: Mean SNR_i^{dif} for QRS-T Detection

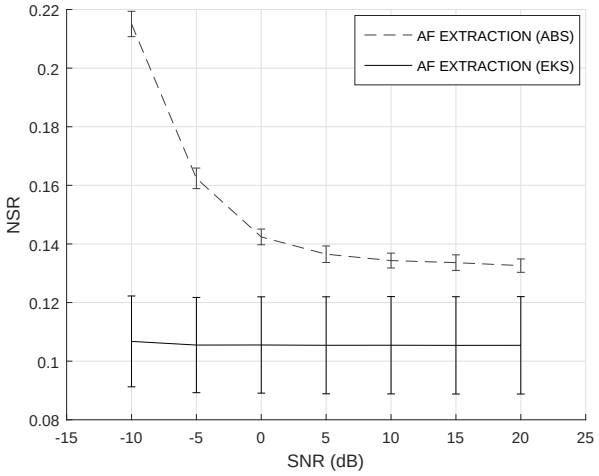

Figure 3.8: Mean SNR_i^{dif} for f-waves Detection

3.3.3 REAL DATA

The efficiency of the proposed method in tracking the fundamental frequency of atrial f-waves, and separating AA and VA was tested also on real data. For this purpose the AF termination challenge database [136] was considered. The database consists of two-channels one-minute ECG recordings of patients undergoing an episode of atrial fibrillation, sampled at 128 Hz. We considered the records in groups S and T (10 records in each), and built 10 two-minutes records, by connecting each S and T record belonging to the same subject (they were separated for the challenge). Clearly, for real signals, AA, VA and the frequency of the true AF signal are not known. Hence we evaluated the quality of the frequency tracking by a visual qualitative comparison of the corresponding AF frequency estimated using short time Fourier transform (STFT), after VA cancellation (we selected the frequency of the main peak in the range 3-12 Hz). An ABS method based on two different windows [51], one for QRS- and one for the

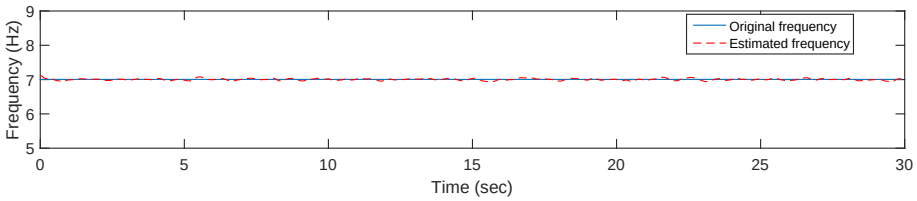

(a) Type I) Constant frequency

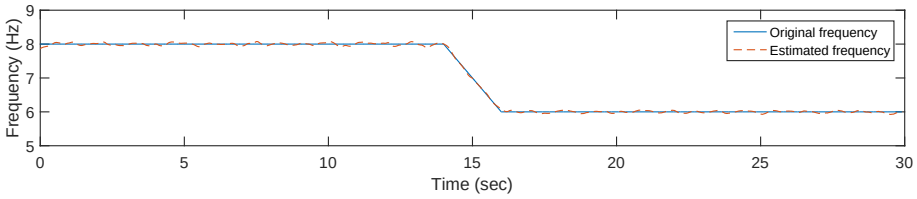

(b) Type II) Stepwise changing frequency

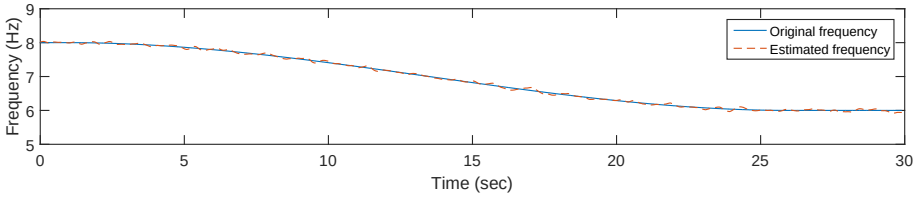

(c) Type III) Gradually changing frequency

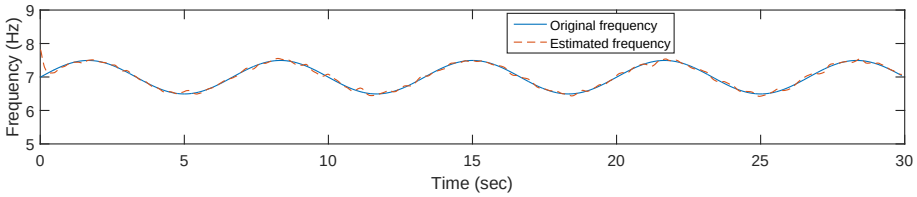

(d) Type IV) Varying frequency

Figure 3.9: Frequency trends of the simulated AF signal with (a) constant frequency, (b) stepwise changing frequency, (c) gradually changing frequency, (d) varying frequency.

T-wave, was used for VA cancellation. As an illustration, fig. 3.11 and 3.12 show the fibrillatory frequency estimated for subject 2 and 7 (both channel), compared with the one obtained using ABS. Equivalent results were obtained for the other 8 cases. The results show that the proposed EKS is able to track the fundamental frequency in real ECG recordings. Comparing to ABS-STFT, EKS method is basically a smoothed out estimate. ABS-STFT is constrained by the limited time resolution which can be obtained and by the large theoretical variance of the periodogram. Thus it produces "way noisier and inaccurate estimates than the EKS".

3.4 QT/RR ESTIMATION

The ECG analysis is extensively used as a diagnostic tool to provide information on the heart function. The cardiac cycle begins with the P wave, followed by the QRS complex

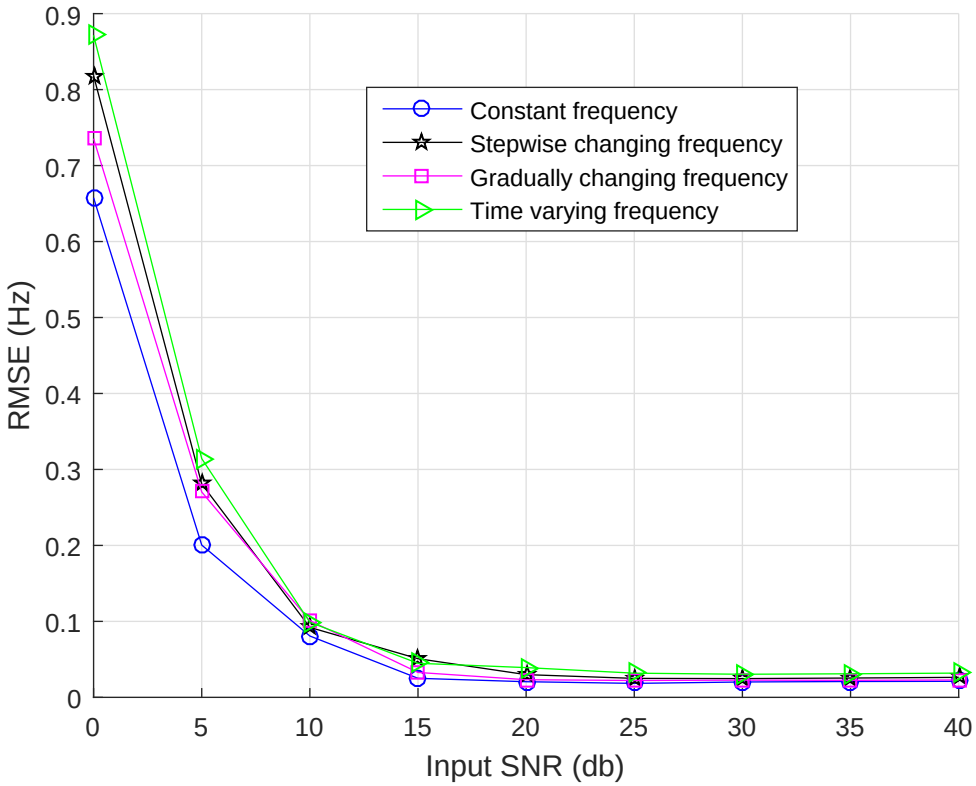

Figure 3.10: Mean and standard deviation of RMSE in frequency estimation for three types of frequency by means of EKS, as a function of the broadband noise contaminating the input signal.

and T wave whose characteristics are clinically relevant. Most of the clinically relevant information can be found within the amplitudes, shapes and intervals between these waveforms. In particular, the time interval between the onset of the QRS complex and the T wave end, known as QT interval, is considered to express the duration of ventricular repolarization. QT-interval (QT) versus RR-interval (RR) is an interesting index during Atrial fibrillation [137, 138, 139]. However the main problem is that finding the T-peak or T-offset is difficult due to atrial signal which disturbs T-waves. In fact atrial signals (or f-waves) can change the T-wave amplitude and its offset. The determination of RR and QT intervals requires the detection and delineation of ECG waves and limits. The approach proposed in this chapter, could help to improve QTI/RRI measurement, since it is able to separate ventricular activity and atrial activity precisely, improving T-peak and T-offset detection.

We computed the QT/RR ratio using the proposed filter. The details of ECG data were described before. The QT/RR computation was repeated two times. First, it was performed directly on the original ECG data. Then, synthetic f-wave and white Gaussian noise were added to the ECG signal ("noisy ECG") and the QT/RR was recomputed. Finally, f-wave and QRS-T wave were automatically separated by EKS, starting from the noisy ECG signal, and the QT/RR was computed a second time finding the time of the peak position of T and Q waves. In every case, the Q and T peaks were

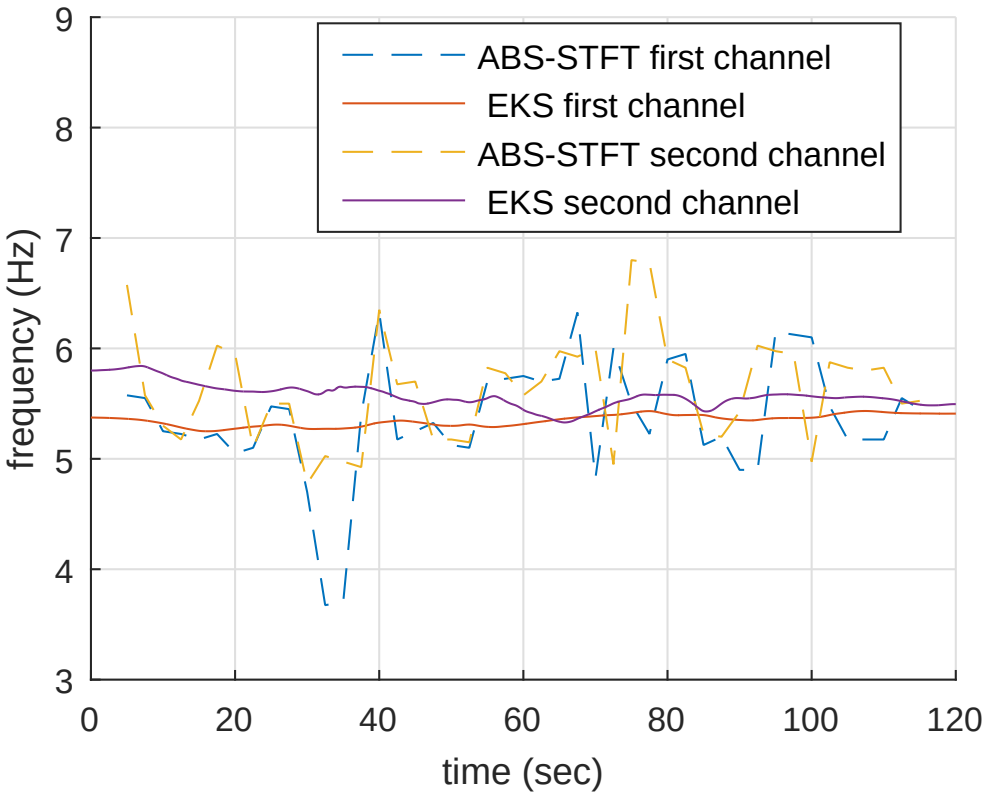

Figure 3.11: Frequency tracking of f-waves provided by ABS-STFT and EKS, for record afrecord2 from the AF Termination Challenge Database (aftdb).

located as the maximum values in the Q and T waveforms which are separated using EKS, respectively. A Butterworth 3rd order bandpass filter (0.5 to 40 Hz) was employed as preprocessing step when EKS was not used. In Fig. 3.13, scatter plots of the QT/RR are compared for the original and noisy ECG. The results are aligned along a straight line, which indicates that the model rendered the results more resilient to atrial signal and noise.

3.5 P WAVE MORPHOLOGY ASSESSMENT

The P wave is the first characteristic waveform found in each beat of an ECG recording. It corresponds to the spread of ionic currents through the atrial musculature (activation or depolarization), after the firing of the sinoatrial (SA) node. The P-wave duration has been commonly employed as a marker of atrial conduction, and its prolongation associated with the remodelling induced by an history of AF. However, a slower propagation is not necessarily linked to paroxysmal episodes of AF. The study of the entire P-wave morphology is therefore gaining momentum, in particular for detecting local conduction disturbances which might then lead to AF, but also for characterizing a larger class of pathologies, *i.e.*, ischemic heart disease and congestive heart failure [140, 141].

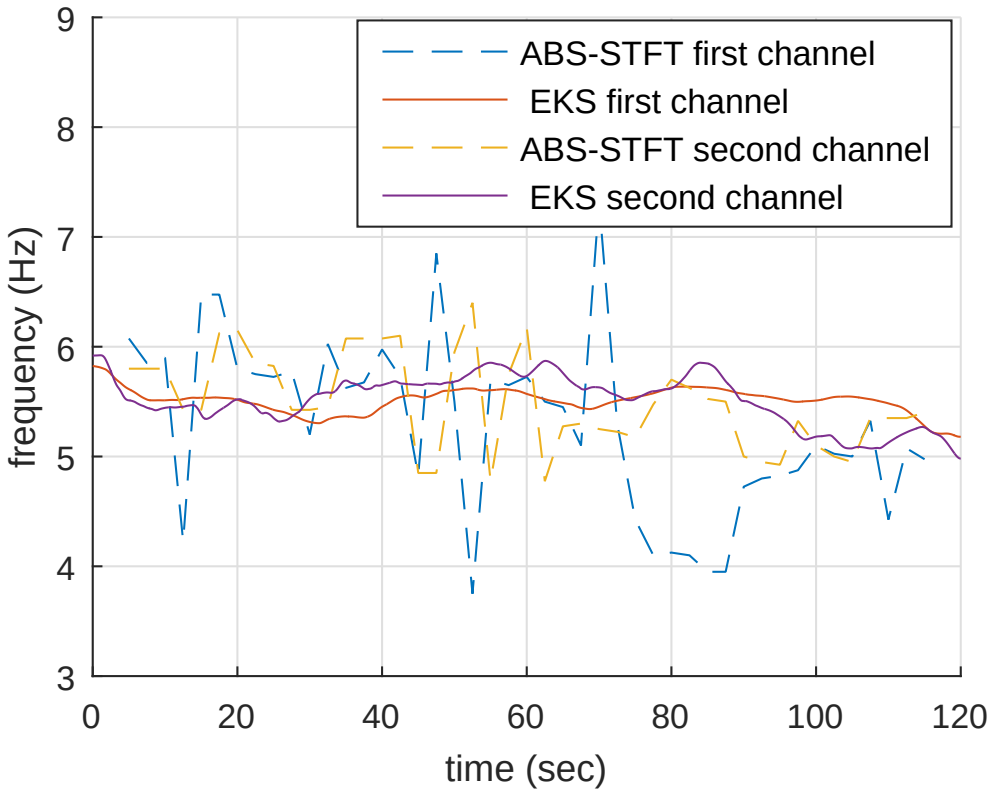

Figure 3.12: Frequency tracking of f-waves provided by ABS-STFT and EKS, for record afrecord7 from the AF Termination Challenge Database (aftdb).

Hence, a standardized method for signal-averaged P wave analysis has been called for, especially in the clinical management of elderly patients [142].

On the other hand, the analysis of the P wave presents technical challenges due to the small ECG amplitude and the consequently lower signal to noise (SNR) ratio. Signal-averaged P wave analysis, where consecutive P wave are averaged to decrease the impact of noise, was the first solution suggested to cope with this issue. More recently, techniques based on fitting a mathematical model capable of capturing the main morphological features emerged. The morphological features are derived directly from the model. For example, Censi *et al.* presented a P wave model, based on a linear combination of Gaussian functions [4]. Alternatively, Carlson *et al.* tried to model directly the conduction system, of which the P wave is a sort of "impulse response" [143].

In this section, we aim to compare different models for a morphological description of the P wave, from a signal decomposition perspective. Possible morphological parameters, which can be subsequently derived from the models, were not considered, as they depend on the specific class of patients under analysis.

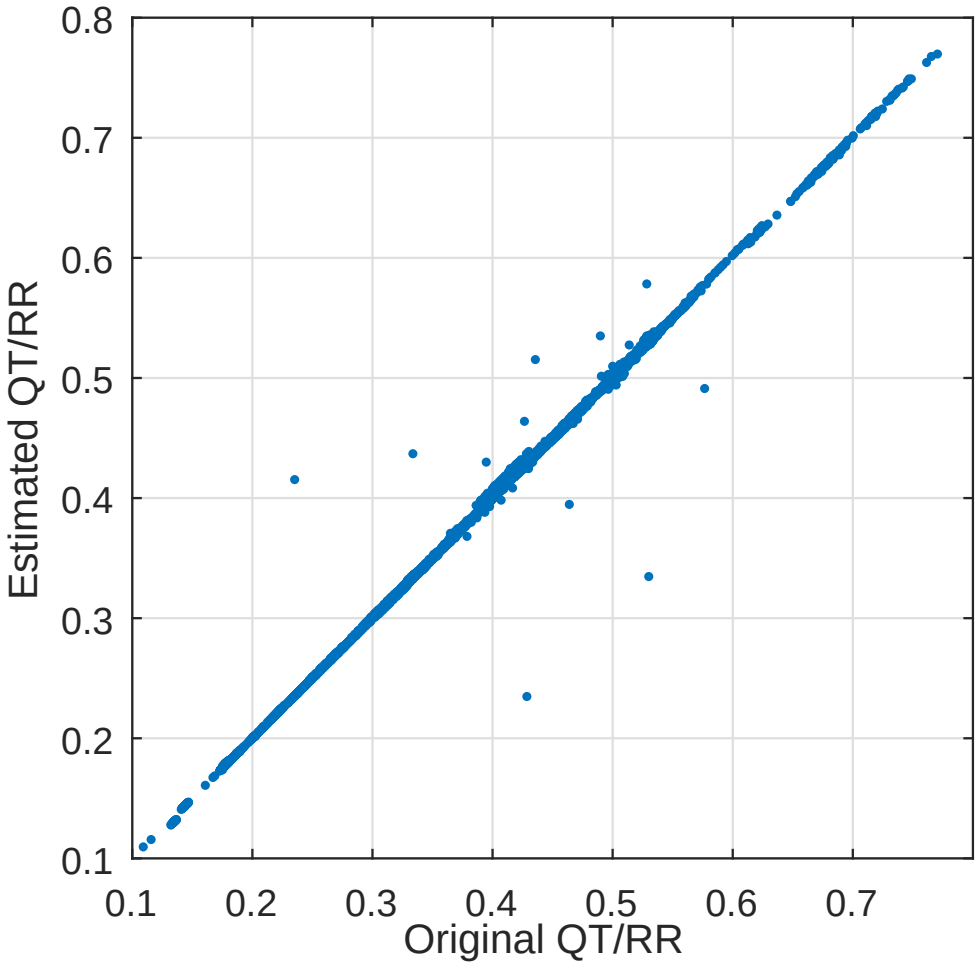

Figure 3.13: QTI/RRI estimated with EKS for 250 ECG recordings with SNR = 5 dB. Notice the alignment of the actual and estimated QTI/RRI using the proposed model.

3.5.1 FUNCTIONAL MODELS FOR MORPHOLOGICAL MODELLING OF P-WAVE

Let us consider the P wave samples $x(t_i)$, collected in the $(1 \times n)$ vector x. Our goal is to model them with $\hat{x}(t_i)$, produced by the linear combination of basis functions $\phi_k(t)$, that is

$$\hat{x}(t_i) = \sum_{k=0}^{N-1} c_k \phi_k(t_i) \quad \text{or} \quad \hat{x} = c^T \Phi, \tag{3.26}$$

where c_k are N scalar coefficients and c their corresponding $(N \times 1)$ vector. Φ is a $(N \times n)$ matrix containing on each row the basis functions sampled at the instants t_i. The only unknown parameters are the coefficients c_k and they can be obtained

Table 3.1: Performances (mean PRD over all P-waves and leads) of the different approximations for different models' orders.

Model	N					
	6	9	12	15	18	21
Gaussian	24.9±0.9%	15.3±0.9%	10.02± 1.0%	7.00±0.7%	5.40±0.6%	4.01±0.7%
Bézier	17.76±1.1%	11.06±0.7%	7.62± 0.6%	5.32±0.4%	3.46±0.2%	2.09±0.2%
B-spline	11.74±0.8%	7.58±0.6%	4.77± 0.3%	2.34±0.2%	1.29±0.1%	0.86±0.1%
Trigonom.	10.98±0.4%	5.88±0.3%	3.13± 0.2%	1.64±0.2%	0.91±0.2%	0.58±0.1%

by minimizing the energy of the residual signal $\hat{x}(t_i) - x(t_i)$, that is the scalar cost function

$$\begin{aligned} \mathrm{SMSSE}(x|c) &= \left\| x^T - \Phi^T c \right\|_2^2 \\ &= (x - c^T\Phi)(x^T - \Phi^T c). \end{aligned}$$

Taking the derivative of $\mathrm{SMSSE}(x|c)$ with respect to c, and after algebraic manipulations, we get

$$c = (\Phi^T)^+ x^T = (\Phi^+)^T x^T = \Phi(\Phi^T\Phi)^{-1}x^T \tag{3.27}$$

The P wave is a continuous function defined on a compact support $[a, b]$. If the functions $\{\phi_k(t)\}$ are a *complete* set of $\mathbb{L}^2\{[a, b]\}$ then any finite energy signal $x(t)$, defined over $[a, b]$, can be approximated at a selected precision with (3.26). Moreover, if $\{\phi_k(t)\}$ also form an *orthonormal basis*, the expansion is not redundant and the relative amplitudes of c_k convey information about the relevance of each of the basis functions in the construction of the signal.

In the following several basis functions will be considered: polynomial splines (Bézier and B-spline), trigonometric and Gaussian functions. However the framework can be extended to other functions such as wavelets.

3.5.1.1 POLYNOMIAL SPLINE BASIS FUNCTIONS

Polynomial splines have been extensively used for curve fitting and interpolation [144]. Among the different types of polynomial splines, Bézier and B-splines satisfy many of the aforementioned properties required for signal modelling. For a finite support signal $x(t)$ defined for $t \in [a, b]$, Bézier basis functions of order p (also known as Bernstein polynomials [144, Ch. 5]) are defined as:

$$\phi_k(t) = \binom{p}{k} \left(\frac{t-a}{b-a}\right)^k \left(\frac{b-t}{b-a}\right)^{p-k}. \tag{3.28}$$

Therefore, following (3.26), the resulting signal's model is

$$\hat{x}(t) = \sum_{k=0}^{N-1} c_k \binom{p}{k} \frac{(t-a)^k (b-t)^{p-k}}{(b-a)^p}. \tag{3.29}$$

The Bézier spline in (3.29) is a polynomial of order $N-1$. However local control is not achieved by Bézier curves, since the change of the control points (which are fixed) will affect the whole curve shape [145]. B-Spline curves can be used to solve this issue.

Once selected a non-decreasing sequence of real numbers $\{t_j\}_{j=0}^{N+p}$, known as *knots* or *node sequences*, a B-spline of order p is recursively defined as:

$$\phi_j^p(t) = \frac{t-t_j}{t_{j+p-1}-t_j}\phi_j^{p-1}(t) + \frac{t_{j+p}-t}{t_{j+p}-t_{j+1}}\phi_{j+1}^{p-1}(t),$$

where

$$\phi_j^0(t) = \begin{cases} 1 & \text{if } t_j \leqslant t < t_{j+1} \\ 0 & \text{elsewhere} \end{cases}.$$

The function $\phi_j^p(t)$ is identically zero outside the interval $t_j < t < t_{j+p}$ and its supporting interval is $t_j < t < t_{j+1}$. Order p B-splines are linearly independent and the signal $x(t)$ can be modelled as

$$\hat{x}(t) = \sum_{k=0}^{N-1} c_j \phi_j^p(t).$$

The piecewise definition of B-splines and the possibility of selecting the position of the knots make the model highly flexible. They also have other interesting properties, including the fact that their interpolants rapidly converge to the $\mathrm{sinc}(\cdot)$ function, as the degree p increases, and they might degenerate into a Bézier spline. Finally, the local control property is also achieved since B-splines have compact support.

In our simulations, we subdivided the temporal interval where the P-wave was defined, into N identical segments. The knots at the extremes of the interval were repeated, so to have exactly $N-1+p$ knots (*e.g.*, $\phi_{N-1}^p(t)$ was supported on $t_{N-1} < t < t_N = \cdots = t_{N-1+p}$).

3.5.1.2 SINUSOIDAL (TRIGONOMETRIC) FUNCTIONS

P-waves can be approximated also by a linear mixture of sinusoidal basis functions:

$$\hat{x}(t) = \sum_{k=0}^{N-1} c_k \cos(\omega_k t + \psi_k) \tag{3.30}$$

where c_k, f_k and ψ_k are respectively, the amplitude, frequency and phase of the k-th sinusoid, and $\omega_k = 2\pi f_k$. Comparing equation (3.30) with equation (3.26), $\phi_k(t)$ is equal to $\cos(\omega_k t + \psi_k)$ which depends on the two additional parameters ω_k and ψ_k.

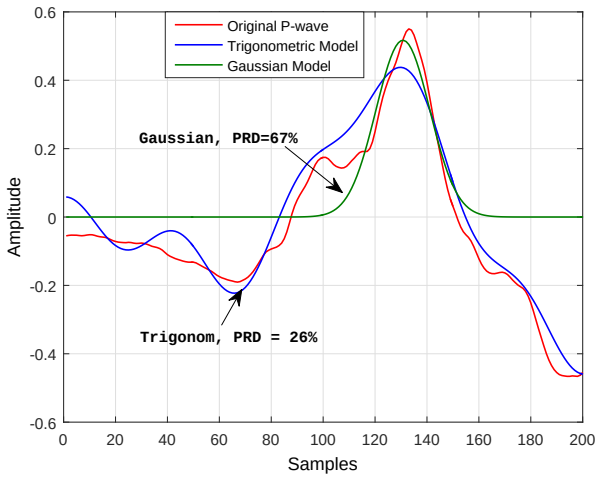

Figure 3.14: Trigonometric and Gaussian functions-based models (N = 3) for a real P-wave (subject `s0001_re`, lead 2).

3.5.1.3 GAUSSIAN BASIS FUNCTIONS

Each P wave can also be modeled by a superposition of Gaussian kernels with different amplitudes and widths, centered at specific points in time [4]. According to (3.26),

$$\hat{x}(t) = \sum_{k=0}^{N-1} c_k \phi_k(t) = \sum_{k=0}^{N-1} c_k \exp\left[-\frac{(t-t_k)^2}{2b_k^2}\right]. \tag{3.31}$$

However, each Gaussian kernel in (3.31) depends nonlinearly on two additional parameters: t_k and b_k. Unfortunately, there is no analytical formula to identify these parameters from observed data, as the problem is associated with the solution of an over-determined system of nonlinear equations. Levenberg-Marquardt nonlinear least squares were employed to minimize directly the cost function SMSSE$(x|c)$ and fitting the model in equation (3.31). The higher computational costs, due to the lack of a closed form solution, make the Gaussian expansion less practical for an automated fitting.

A comparison of trigonometric and Gaussian functions-based models for a P-wave obtained from a real ECG is shown in Fig. (3.14-3.19) at different model orders N.

3.5.2 IMPLEMENTATION AND RESULTS

The signals used in this study were taken from the PhysioNet PTB Diagnostic ECG Database [135] (sampling frequency: 1000 Hz; resolution: 16-bit). 561 ECG segments, each with duration of 10s, were selected from the twelve conventional leads, at the begining of each recording. After detecting QRS complexes, P waves were located in a 200 ms-long window starting 300 ms before the R waves. The percentage root-mean-

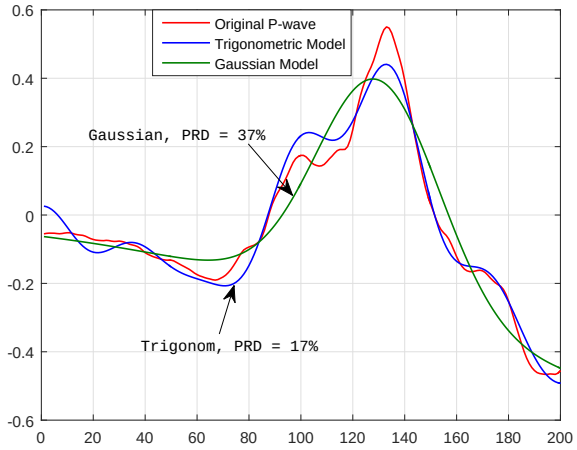

Figure 3.15: Trigonometric and Gaussian functions-based models (N = 6) for a real P-wave (subject `s0001_re`, lead 2).

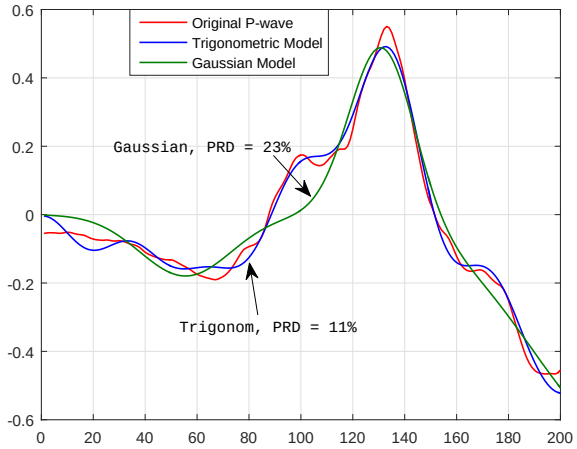

Figure 3.16: Trigonometric and Gaussian functions-based models (N = 9) for a real P-wave (subject `s0001_re`, lead 2).

square difference (PRD), a classical compression efficiency measure, was employed to compare the performances of the different models. PRD was calculated as:

$$\mathrm{PRD} = 100\sqrt{\frac{\sum_{i=1}^{N}(\hat{x}[t_i]-x[t_i])^2}{\sum_{i=1}^{N}x[t_i]^2}}, \tag{3.32}$$

where x and $\hat{x}$ are the original and modelled P wave. We term "compression ratio" the value: $r = N/n$.

The mean results are summarized in Fig. 3.20, for a number of free parameters N ranging from 3 to 21, and Table 3.1. As a reference, each original P-wave was 200 samples long, so r ranged from 1.5% to 10.5%. Trigonometric models displayed the minimum mean PRD. Together with B-spline models, they proved to be the most effective in following the details of the morphology (PRD: $0.51 \pm 0.62\%$ and $0.99 \pm 0.96\%$,

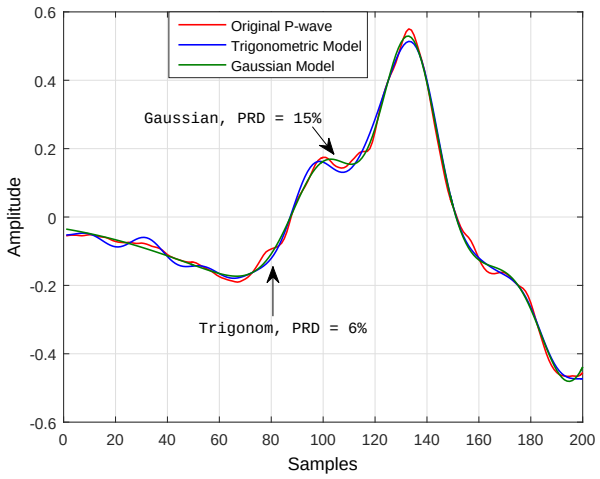

Figure 3.17: Trigonometric and Gaussian functions-based models (N = 12) for a real P-wave (subject `s0001_re`, lead 2).

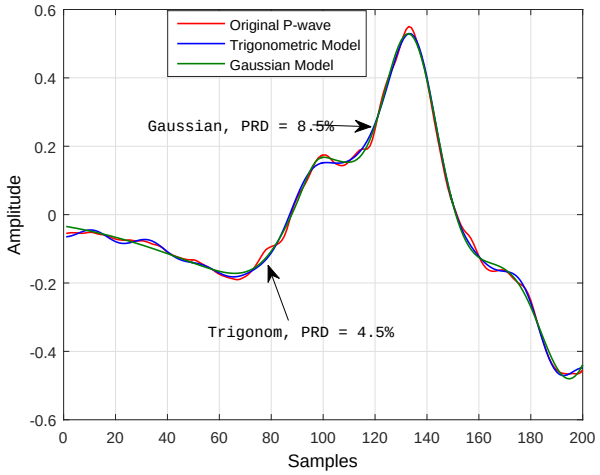

Figure 3.18: Trigonometric and Gaussian functions-based models (N = 15) for a real P-wave (subject `s0001_re`, lead 2).

respectively, on lead V1 at C=21), a possible explanation being that they form an orthogonal basis. This property is not shared by Bézier curves and Gaussian basis functions (PRD: $2.47 \pm 2.17\%$ and $3.57 \pm 6.83\%$). Correspondingly, the number of free parameters necessary to have a mean PRD $< 5\%$ in lead II, increased: C=10 for trigonometric, 11 for B-splines, 15 for Bézier polynomials and 18 for Gaussian functions.

3.6 SUMMARY

In this chapter, an extended nonlinear Bayesian filtering framework was proposed for analysis of atrial fibrillation from single channel ECG recordings. In the proposed method, ventricular activity (Q, R, S, and T waveforms), atrial activity and its fundamental frequency are directly utilized as hidden state variables, and simultaneously estimated

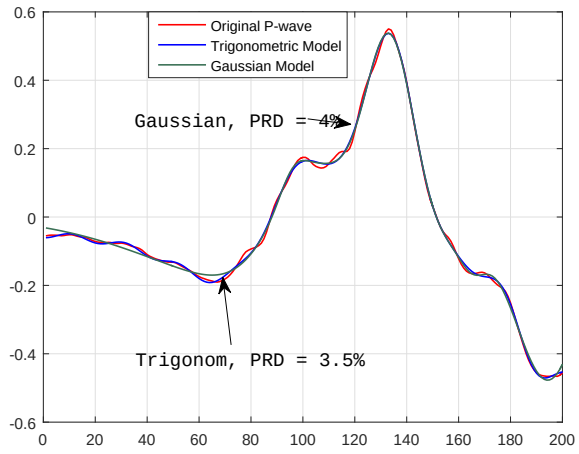

Figure 3.19: Trigonometric and Gaussian functions-based models (N = 18) for a real P-wave (subject `s0001_re`, lead 2).

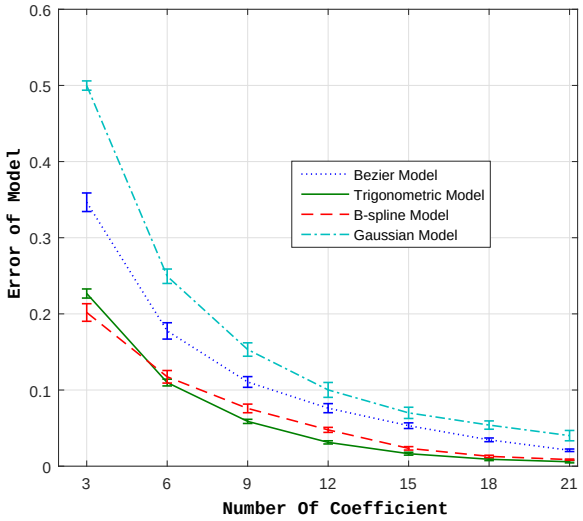

Figure 3.20: Mean PRD, averaged over any P-wave and lead, versus the order of the model.

as a time series through an EKS. Simultaneous frequency tracking of AF while separating the atrial and ventricular activity from single channel recordings is, to our knowledge, novel in this thesis. The proposed approach estimates the frequency of AF, while it separates atrial and ventricular activity, against other methods which analyze the AF frequency after QRS-T cancellation. The simulation results demonstrated that the framework has the capability of correctly tracking QRS-T and fibrillatory waves, on a beat-to-beat basis.

We compared the proposed filter with traditional method (ABS) for QRS-T cancellation and AF extraction. ABS can just be used for QRS-T cancellation, while the proposed method is also suited for Atrial activity signal and its frequency tracking. The quantitative results showed that the proposed filter is indeed more effective in

comparison with ABS for atrial and ventricular activity signal detection. The results demonstrated that the proposed framework is more robust to noise.

Although we have developed an algorithm for separating the atrial and ventricular activity signals, based on EKS, to be used on single-lead ECG channels, since atrial and ventricular signals have a corresponding term in the model, the proposed model can efficiently discriminate the signals even if desired and undesired atrial and ventricular signals overlap in time. The extension of this method to apply on Holter recordings (small number of channels, *e.g.*, up to 3 leads) is straightforward. The results indicated that the filter is accurate and robust to track the atrial frequency in case of constant frequency or gradually changing in time. However its performance was decreased in case of time-varying frequency. As a future work, we decide to extend the framework for AF detection and classification.

4

T-WAVE ALTERNANS ANALYSIS

Repolarization abnormalities produce periodic alternation of the T-wave morphology on the ECG. In 1908, macroscopic T-wave alternans (TWA) was described and seven decades after, microvolt TWA was discovered by Adam *et al.* [146] in 1981. After that, automatic detection and analysis of TWA was the subject of many studies and researches. From a methodological point of view, TWA analysis can be split in three main phases: signal processing, TWA detection, and TWA amplitude estimation [147]. The first stage is composed of preprocessing procedures such as QRS complex detection, baseline wander reduction, powerline noise cancellation and beats detection. In the stage of TWA detection, it is decided if there is a TWA in the signal or not. Finally in the last stage the amplitude of TWA is estimated. TWA analysis can be performed using single or multi-lead ECG recordings. This chapter deals with the TWA analysis using EKS.

4.1 TWA DETECTION AND ESTIMATION USING A BAYESIAN FRAMEWORK

There are several algorithms in the literature to automatically detect TWA [147], which are based on employing linear or nonlinear signal processing techniques. Recently, the Bayesian framework has been used for TWA detection [77, 78]. In this section, we aim to improve the model of cardiac signals, described in [77, 78] for TWA detection. The main advantages of new model are: i) the removal of the T amplitude dependency in the model, along the lines of what we proposed in [148]; ii) a decreased nonlinearity of the T wave model.

In [76], a general ECG Kalman filtering framework has been described for ECG interval analysis and TWA detection, which are reviewed in this chapter.

4.1.1 EKF17 DERIVED MODEL

Sayadi *et al.* modified the polar form of McSharry's model (EKF2), eq.2.3, while considering the parameters of Gaussian functions as a hidden state in the model. They proposed an AR model for each parameter. It is assumed that the Gaussian parameters can fluctuate very small in each beat. Please refer chapter 2 section 2.2.3.

4.1.2 EKF3 DERIVED MODEL

A different strategy has been proposed by Akhbari *et al.* to modify the EDM, eq.2.3 [77]. Considering the fact that the angular velocity changes in each ECG beat due to small changes of *PQRST* morphology, they considered the angular velocity as a state variable. Then the EKF3 was defined as follows:

Process equation:

$$\begin{cases} \theta_{k+1} = \theta_k + \omega_k \delta \\ z_{k+1} = z_k - \sum_{i=\in P,Q,R,S,T} \alpha_i \omega \frac{\theta_k - \theta_i}{b_i^2} \exp\left[-\frac{(\theta_k - \theta_i)^2}{2b_i^2}\right] + \eta_z \\ \omega_{k+1} = \omega_k + u_k \end{cases}, \tag{4.1}$$

Observation equation:

$$\begin{cases} \psi_k = \theta_k + v_{1,k} \\ s_k = z_k + v_{2,k} \\ \Omega_{k+1} = \beta\omega_k + v_{3,k} \end{cases}, \tag{4.2}$$

where u_k is a zero mean random noise and $\beta \approx 1$. Three observations are defined in the model. The angular velocity ω is simply estimated using $\omega = \frac{2\pi}{T_{RR}}$, where T_{RR} is the RR-peak period in each ECG cycle. The estimated ω value is considered almost constant for each R-R peak period.

4.1.3 EKF3-2 DERIVED MODEL

EKF3-2 is as the same as EKS3 but without considering the observation equation for angular velocity:

Process equation:

$$\begin{cases} \theta_{k+1} = \theta_k + \omega_k \delta \\ z_{k+1} = z_k - \sum_{i=\in P,Q,R,S,T} \alpha_i \omega \frac{\theta_k - \theta_i}{b_i^2} \exp\left[-\frac{(\theta_k - \theta_i)^2}{2b_i^2}\right] + \eta_z \\ \omega_{k+1} = \omega_k + u_k \end{cases}, \tag{4.3}$$

Observation equation:

$$\begin{cases} \psi_k = \theta_k + v_{1,k} \\ s_k = z_k + v_{2,k} \end{cases}, \tag{4.4}$$

4.1.4 EKF25 DERIVED MODEL

This model is a combination of EKF4, EKF3 and EKF17. The model consists of three state variables for ECG components (P, QRS and T wave) and a state variable for angular velocity. As mentioned before seven Gaussian kernels were used in EKF4 (two Gaussian kernels for each P and T waves). All the Gaussian parameters are also considered as hidden state variable. Hence the number of state variables is 25. The model is as follows:

Process equation:

$$\begin{cases} \theta_{k+1} = \theta_k + \omega_k \delta \\ P_{k+1} = P_k - \sum\limits_{i\in\{P^-,P^+\}} \alpha_i \omega \frac{\theta-\theta_i}{b_i^2} \exp\left[-\frac{(\theta-\theta_i)^2}{2b_i^2}\right] + \eta_P \\ C_{k+1} = C_k - \sum\limits_{i\in\{Q,R,S\}} \alpha_i \omega \frac{\theta-\theta_i}{b_i^2} \exp\left[-\frac{(\theta-\theta_i)^2}{2b_i^2}\right] + \eta_C \\ T_{k+1} = T_k - \sum\limits_{i\in\{T^-,T^+\}} \alpha_i \omega \frac{\theta-\theta_i}{b_i^2} \exp\left[-\frac{(\theta-\theta_i)^2}{2b_i^2}\right] + \eta_T \\ \omega_{k+1} = \omega_k + u_k \\ \alpha_{i,k+1} = \alpha_{i,k} + u_{j,k}, \qquad j \in \{1,2,3,4,5\} \\ b_{i,k+1} = b_{i,k} + u_{j,k}, \qquad j \in \{6,7,8,9,10\} \\ \theta_{i,k+1} = \theta_{i,k} + u_{j,k}, \qquad j \in \{11,12,13,14,15\} \end{cases}. \tag{4.5}$$

Observation equation:

$$\begin{cases} \psi_k = \theta_k + v_{1,k} \\ s_k = P_k + C_k + T_k + v_{2,k} \end{cases}, \tag{4.6}$$

Since the model has two observations and a linear model is considered for angular velocity, the model is called linear EKF25 with two observations. The main problem of the model is that it produces a baseline for each extracted ECG component. To overcome this problem they used four observation equations as follows:

Process equation:

$$\begin{cases} \theta_{k+1} = \theta_k + \omega_k \delta \\ P_{k+1} = P_k - \sum\limits_{i\in\{P^-,P^+\}} \alpha_i \omega \frac{\theta-\theta_i}{b_i^2} \exp\left[-\frac{(\theta-\theta_i)^2}{2b_i^2}\right] + \eta_P \\ C_{k+1} = C_k - \sum\limits_{i\in\{Q,R,S\}} \alpha_i \omega \frac{\theta-\theta_i}{b_i^2} \exp\left[-\frac{(\theta-\theta_i)^2}{2b_i^2}\right] + \eta_C \\ T_{k+1} = T_k - \sum\limits_{i\in\{T^-,T^+\}} \alpha_i \omega \frac{\theta-\theta_i}{b_i^2} \exp\left[-\frac{(\theta-\theta_i)^2}{2b_i^2}\right] + \eta_T \\ \omega_{k+1} = \omega_k + u_k \\ \alpha_{i,k+1} = \alpha_{i,k} + u_{j,k}, \qquad j \in \{1,2,3,4,5\} \\ b_{i,k+1} = b_{i,k} + u_{j,k}, \qquad j \in \{6,7,8,9,10\} \\ \theta_{i,k+1} = \theta_{i,k} + u_{j,k}, \qquad j \in \{11,12,13,14,15\} \end{cases}, \tag{4.7}$$

Observation equation:

$$\begin{cases} \psi_k = \theta_k + \nu_{1,k} \\ PP_k = P_k + \nu_{2,k} \\ CC_k = C_k + \nu_{3,k} \\ TT_k = T_k + \nu_{4,k} \end{cases}, \tag{4.8}$$

Hence the model is called linear EKF25 with four observations (EKF25-4obs).

4.1.5 EKF6 DERIVED MODEL

Recently Akhbari *et al.* proposed a modified EDM for T-wave alternance detection [77]. They considered separate states for PQRS and T waves and also considered an autoregressive (AR) model for each parameter of the Gaussian kernel of the T wave model. The discrete model is as follows:

$$\begin{cases} \theta_{k+1} = \theta_k + \omega\delta \\ PC_{k+1} = PC_k + \eta_{PC_k} \\ \qquad\qquad - \sum\limits_{i\in\{P,\,Q,\,R,\,S\}} \alpha_i \omega \frac{\theta_k-\theta_i}{b_i^2} \exp\left[-\frac{(\theta_k-\theta_i)^2}{2b_i^2}\right] \\ T_{k+1} = T_k + \eta_T - \alpha_T \omega \frac{\theta_k-\theta_T}{b_T^2} \exp\left[-\frac{(\theta_k-\theta_T)^2}{2b_T^2}\right] \\ \alpha_{T,k+1} = \alpha_{T,k} + \eta_{\alpha_{T,k}} \\ b_{T,k+1} = b_{T,k} + \eta_{b_{T,k}} \\ \theta_{T,k+1} = \theta_{T,k} + \eta_{\theta_{T,k}} \\ z_k = PC_k + T_k \end{cases}, \tag{4.9}$$

where θ_k was previously defined. PC_k and T_k are the state variables describing PQRS and T waves, respectively, while $\alpha_{T,k}$, $b_{T,k}$ and $\theta_{T,k}$ are the parameters of the T wave Gaussian function, evolved with first order AR dynamics. Being the number of state variables six and the number of observation equations four, the method was termed EKS6-4obs.

There are several disadvantages when applying EKS6-4obs: i) the dynamic model for T wave is strongly nonlinear and it also depends on T amplitude directly; ii) PQRS and T waves are sometimes mixed up; iii) it might produce a baseline drift. Although the authors proposed AR models for T wave Gaussian function parameters as a solution to these issues, EKS6-4obs is still not able to detect T wave amplitude when sudden changes happen in T-wave amplitude. To support our claim and explain the issue, consider the synthetic ECG in Fig. 4.1a. It displays an episode of macroscopic TWA, which is inspired by figure 2 in [97] and figure 1 in chapter (II). Such alterations often precede torsade de pointes and sudden cardiac death. So their detection is clearly relevant. The values of the initial parameters of the Gaussian kernel modelling the T-wave is very crucial when applying EKS6-4obs, since they are state variables in (4.9). In fact, T wave amplitude changes in time, (as shown in Fig. 4.1a), affect the value of the average template, which is in turn used to estimate the initial values of $\alpha_{T,k}$, $b_{T,k}$ and $\theta_{T,k}$. For example, consider the template in Fig. 4.1b, which is obtained by averaging the signal in Fig. 4.1a. This results in large errors on the updating state variables and low accuracy in T-wave amplitude detection. As discussed before, the main reason of poor T amplitude detection of EKS6-4obs is the dependency of the model on T Gaussian amplitude. For this reason, in section 4.1.6, we will introduce a new EDM, which no longer depends on the amplitude of the T Gaussian kernel.

4.1.6 A NEW SIGNAL DECOMPOSITION MODEL FOR T-WAVE ALTERNANS DETECTION

To remove the EDM dependency on T wave amplitude, present in other models [77, 78], we followed the approached we proposed in chapter (II). Let's define $\phi_T \equiv \alpha_T \exp[-(\theta - \theta_T)^2/(2b_T^2)]$, a new model can be derived as follows

$$\begin{cases} \dot{\theta} = \omega \\ \phi_{PC} = \sum_{i=\in P,Q,R,S} \alpha_i \omega \dfrac{\theta - \theta_i}{b_i^2} \exp\left[-\dfrac{(\theta-\theta_i)^2}{2b_i^2}\right] \\ \phi_T = \alpha_T \exp\left[-\dfrac{(\theta-\theta_T)^2}{2b_T^2}\right] \\ z = \phi_{PC} + \phi_T \end{cases}.$$

Table 4.1: TWA amplitude (mean ± standard deviation), as obtained by different approaches.

EDM	**TWA** (μV)						
	twa01	twa70	twa97	twa10	twa93	twa52	twa81
EKS6-4obs	10.7±1.7	8.1±3.2	13.2±4.2	8± 8.8	48.3±76.7	0.73±4.8	0.17± 2.4
EKS25-4obs	13.2±3.4	7.2±3.7	16.4±9.8	5.6± 13.2	62.8±82.3	1.26±8.6	-0.05± 2.4
EKF3	8.4±1.5	7.8±3.8	13.7±3.6	3.7± 0.2	48±35	0.75±1.3	2.6± 0.3
Artificial TWA	45	8	17	real ECG	real ECG	0	0 + noise

Taking the derivative of PC and ϕ_T, the new EDM becomes

$$\begin{cases} \dot{\theta} = \omega \\ \dot{\phi}_{PC} = -\sum_{i=\in P,Q,R,S} \alpha_i \omega \frac{\theta - \theta_i}{b_i^2} \exp\left[-\frac{(\theta-\theta_i)^2}{2b_i^2}\right] \\ \dot{\phi}_T = -\omega \left(\frac{\theta - \theta_T}{b_T^2}\right) \phi_T \\ z = \phi_{PC} + \phi_T \end{cases}. \tag{4.10}$$

It no longer depends on α_T, which is absorbed completely into the state ϕ_T. Since the number of states is 3, in the followings, we will term it EKS3.

4.2 RESULTS

As preliminary example, Fig. 4.1d shows the result of applying EKS3 to the synthetic ECG displaying macro alternation of T-wave forms, as discussed in the previous section. The T wave component follows more precisely, when compared to EKS6-4obs in Fig. 4.1c, the ECG morphology, due to the independence of the model from the T amplitude. For validation of our method, we used seven records obtained from the 2008 Physionet TWA challenge dataset [149]. Overall, it contains 100 multichannel ECG records sampled at 500 Hz. The decompositions for a specific case (record twa93), using both EKS3 and EKS6-4obs, are reported in Fig. 4.2. EKS6-4obs follows less precisely the T wave, producing a slight distortion. To quantify the performances, after detecting the T waves using EKS, we then separated odd and even T-peaks. The average difference between the T-amplitude of odd and even beats was directly employed as an estimate of TWA. These mean TWA values (along with their standard deviation) are given in table 4.1. The results show that for records: twa01, twa70 and twa97, which are known to be synthetic ECG with TWA added by construction (45 μV, 8 μV and 17 μV, respectively), the results of EKF3 are as good as other methods. However EKF3 displays a smaller variance, which is a key-point for adjudicating the presence of TWA in a real ECG record. Please notice that the large discrepancy between the expected and estimated TWA for record twa01, was a known issue also in the 2008 competition [149] (it was built using model "C", where artificial TWA was underestimated by

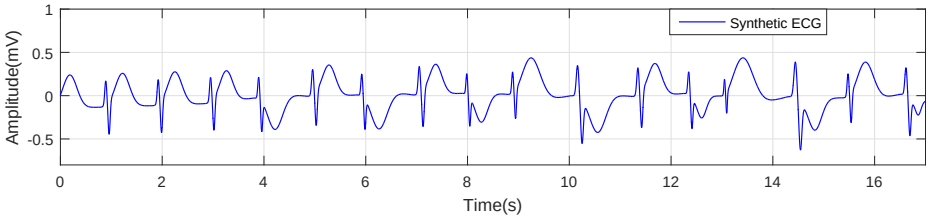

(a) Synthetic ECG

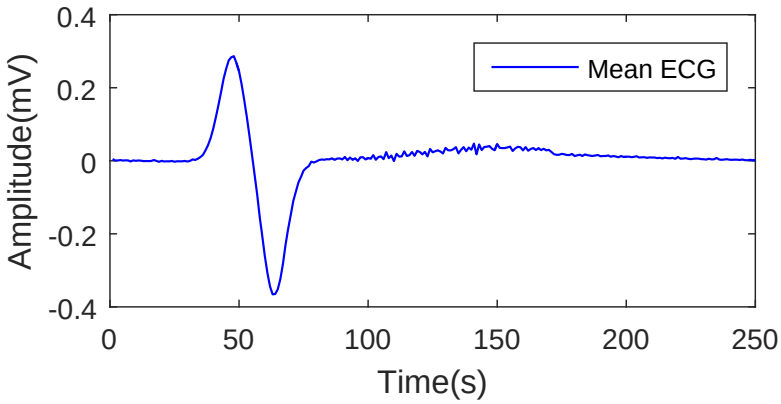

(b) Mean ECG pattern

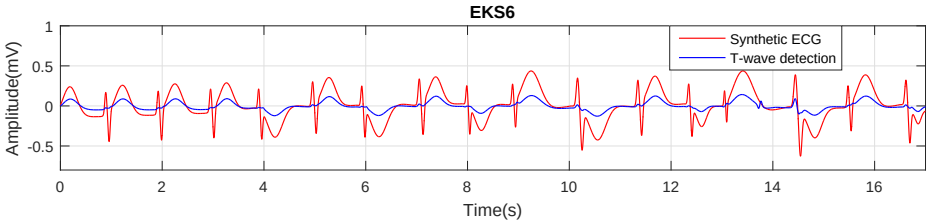

(c) T wave extraction provided by EKS6-40bs

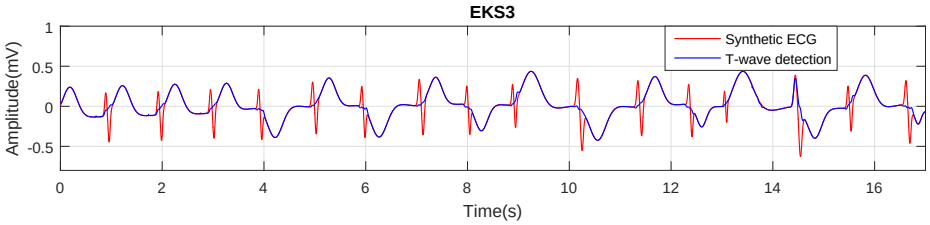

(d) T wave extraction provided by EKS3

Figure 4.1: T-wave estimates provided by EKS3 and EKS6-40bs, when applied to a synthetic signal.

many participants, likely due to the smaller projection of the T alternations in the ECG leads at disposal). Records twa10 and twa93 are instead in normal sinus rhythm. All the methods, except EKS3, displayed a large standard deviation of the T-peak values, which is larger than the TWA estimates. Finally, records twa52 and twa81 are synthetic ECG without additional TWA (in the second additional broadband noise was added). For these, all the methods provided small TWA estimates, but, again, EKS3 proved to provide the smallest standard deviation.

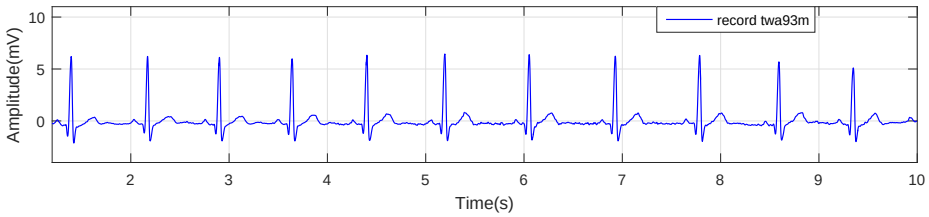

(a) ECG recordtwa93m.

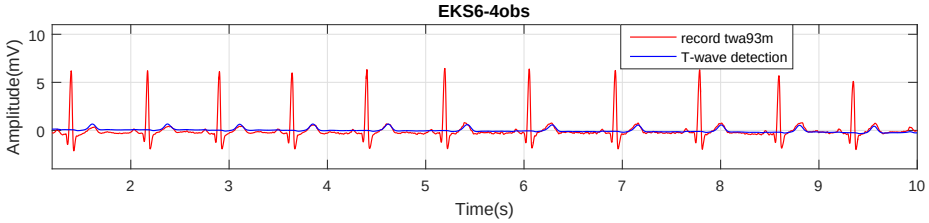

(b) T wave extraction provided by EKS6-4obs

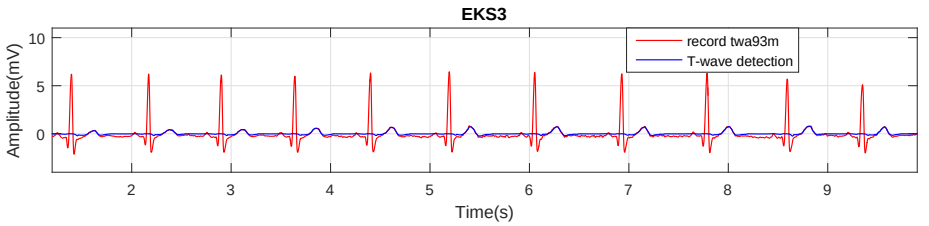

(c) T wave extraction provided by EKS3

Figure 4.2: T-wave detection provided by EKS6-4obs and EKS3, for record twa93 from the 2008 Physionet TWA challenge dataset.

4.3 T/QRS RATIO ESTIMATION AS A PROOF OF CONCEPT

Abnormality of ventricular repolarization in the ECG (like ST depression, T wave inversion and QT prolongation) have been shown to be related to cardiovascular mortality. A possible marker of ventricular repolarization is the ratio of T amplitude to QRS amplitude, also known as the T/QRS ratio. The T/QRS ratio has been shown important in distinguishing acute myocardial infraction (AMI) from left ventricular aneurysm (LVA) [150] or very relevant in fetal surveillance [151, 152]. However, the automatic and accurate calculation of this index in noisy scenarios can be very challenging given the possible errors in the location of the fiducial points. EKS3 can improve the estimated T/QRS ratio calculating it from the estimated components, hence reducing the impact of noise.

We tested the approach over the PhysioNet PTB Diagnostic ECG Database [124]. The database contains 549 records from 290 subjects. Each record consists of twelve conventional ECG leads plus the three Frank's ones, sampled at 1kHz with 16-bit resolution. The feasibility study was limited to 288 ECG segments, of 10s each, obtained from the beginning of selected records (about one for each subject; we considered the twelve standard leads only). The T/QRS ratio computation was repeated three times. First, it was performed directly on the original ECG data. Then, white Gaussian noise

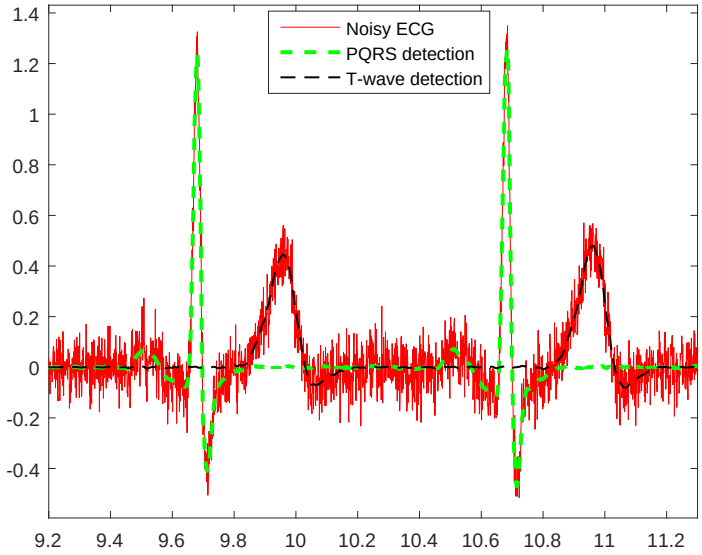

(a)

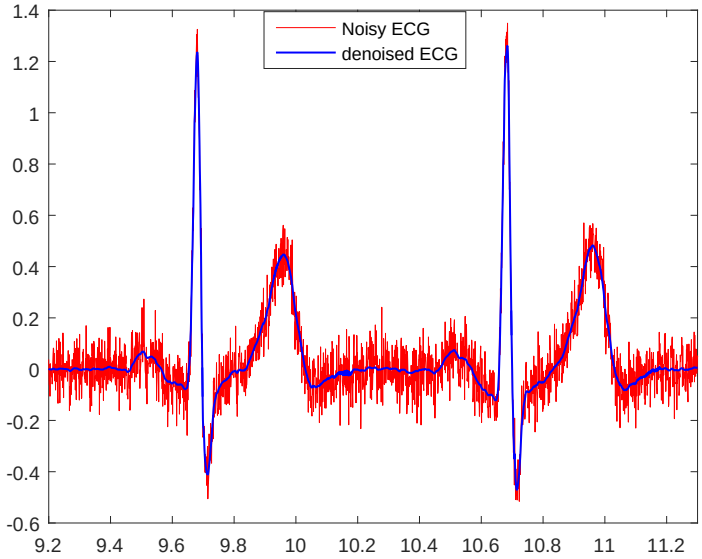

(b) The same noisy ECG overlaid with its de-noised version (the superposition of components produced by EKS3).

Figure 4.3: ECG denoising using EKS3.

with a signal-to-noise ratio of 10 dB was added to the ECG signal ("noisy ECG") and the T/QRS ratio was recomputed. Finally, T-wave and QRS-wave were automatically separated by EKS3, starting from the noisy ECG signal, and the T/QRS ratio was computed a third time employing the amplitudes of the components. In every case, the QRS and T peaks were located as the maximum values in the two windows of length 200ms and 250ms, starting from the Q onset and 100ms after the R-peak, respectively.

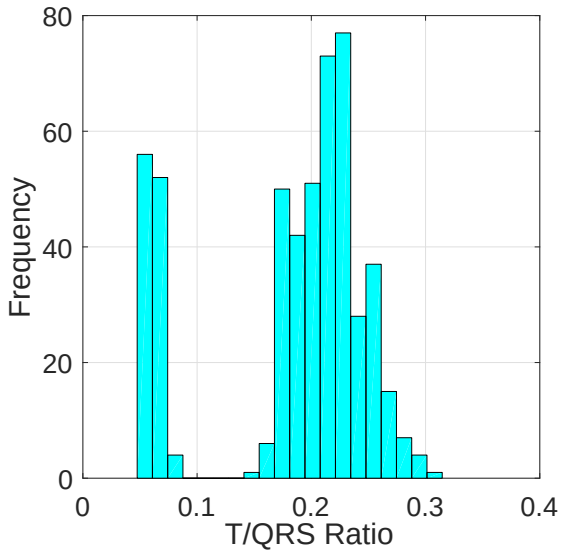

Figure 4.4: Histogram of T/QRS ratio values for ECG signals from the PhysioNet PTB Diagnostic ECG Database. After contaminating the ECG signal with broadband noise (SNR=10 dB).

Beat annotations contained into the database were employed. A Butterworth 3rd order bandpass filter (0.5 to 40 Hz) was employed as preprocessing step when EKS3 was not used. In Fig. 4.3(a), a couple of noisy ECG beats and the EKS3 outputs are shown. The amplitudes of T and QRS components, as obtained by EKS3, are close to the original ECG. Then, in Fig. 4.3(b) the ECG, as reconstructed by adding the components, is compared with the original noisy signal. Finally, in Fig. 4.5 and Fig. 4.6, scatter plots of the T/QRS ratios are compared for the original and noisy ECG. The scatter plots show the alignment of the actual and estimated T/QRS ratio using bandpass and the proposed model. When using EKS3, the results are better aligned along a straight line, which indicates that the model rendered the results more resilient to noise.

4.4 SUMMARY

In this chapter, a signal decomposition model-based Bayesian filtering method (EKS3) has been introduced for TWA estimation. Separate states for PQRS and T-wave were considered and simultaneously estimated as a time series through an EKS. Also, the amplitude of the Gaussian component representing the T-wave was embedded into the state itself (amplitude-free). The simulation results demonstrated that EKS3 has the capability of correctly tracking T wave amplitude, on a beat-to-beat basis.

There are some theoretical advantages that EKS3 has over other recent works in this context. It is able to track the T wave amplitude, even when abrupt changes happens in the T wave and it reduces the nonlinearity of the T-wave state. From a practical point of view, EKS3 outperformed EKS6-40bs and EKS25-40bs in the tests we performed. For example, components were sometimes mixed up by EKS6-40bs but not by EKS3, as shown for T wave in Fig. 4.1.

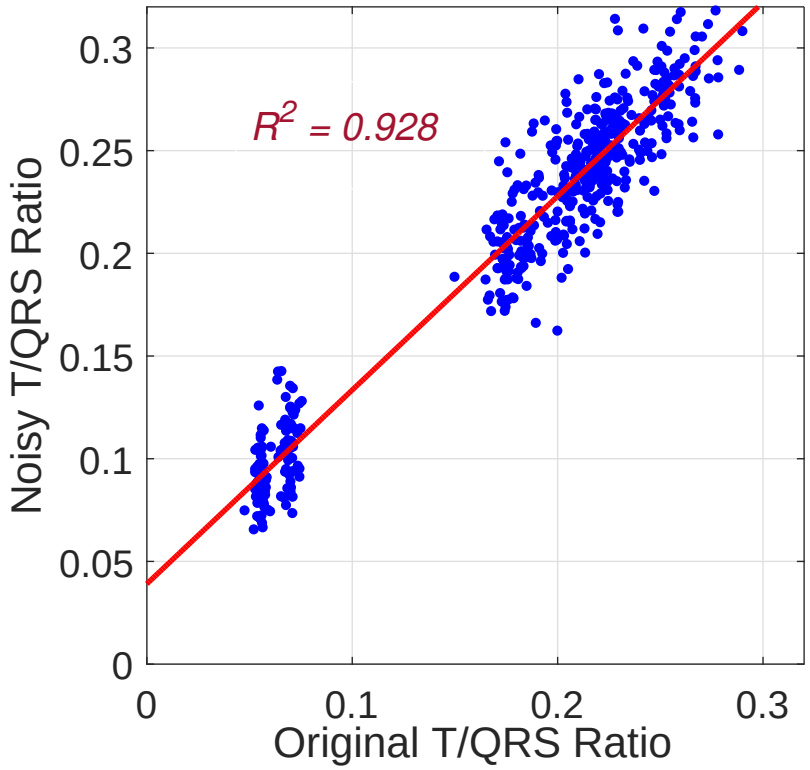

Figure 4.5: Histogram of T/QRS ratio values recalculated after bandpass (0.5 to 40 Hz) filtering. Notice the actual and estimated T/QRS ratio using bandpass (RMSE=0.7)

As compared with our previous EKS (EKS6), which is more general and proposed for ECG components separation, the performance of both methods for TWA detection was similar, but EKS3 has fewer state variables, Being tailored to this specific application, it results in a significant decrease in complexity.

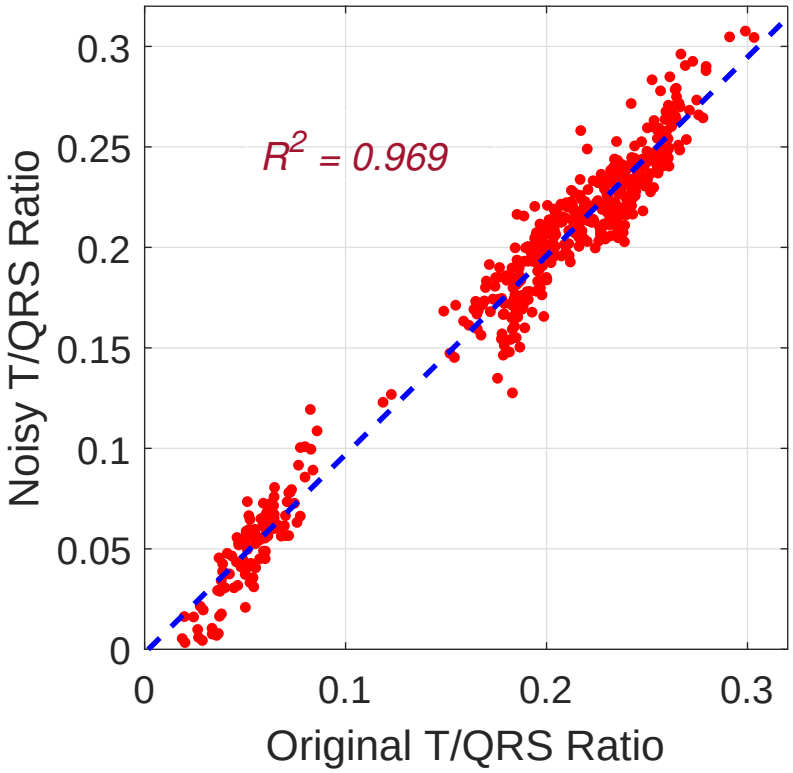

Figure 4.6: Histogram of T/QRS ratio values recalculated after EKS3. Notice the actual and estimated T/QRS ratio using the proposed model (RMSE=0.025)

5

BIOPHYSICAL MODEL-BASED ECG FEATURE EXTRACTION: $\mathcal{V}$-INDEX COMPUTATION

Spatial dispersion of ventricular repolarization (SHVR) is a property of the human heart which is responsible for the genesis of T wave on the ECG. Recently a new direct metric for quantifying SHVR has been introduced by Sassi and Mainardi, termed as $\mathcal{V}$-index [153]. It is derived from the analysis of a biophysical model of the ECG which is able to estimate the standard deviation of ventricular repolarization times (RTs). $\mathcal{V}$-index computation needs to solve an inverse problem. This chapter has a microscopic (action potential level) approach to repolarization modeling. Comparing to previous chapters where deal with macroscopic (morphologic level) approach, we apply sinusoidal signal modelling for improving the computation of $\mathcal{V}$-index. The model is useful for improving the estimation of standard deviation of ventricular ripolarization times. The rest of the chapter is organized as follows. In Section 5.1, the relevant background on bidomain model and *dominant T-wave* formalism is reviewed. Section 5.2 presents the original model-based sinusoidal functions for $\mathcal{V}$-index computation. General remarks and a discussion are given in the final section.

5.1 THE SURFACE SOURCE MODEL AND THE DOMINANT T-WAVE

It has been shown that the shapes of all ECG leads on the thorax during repolarization can be represented as a linear combination of a single waveform, termed as *dominant T-wave* (DTW), and its derivatives. The idea has been introduced by van Oostrom [154, 155]. The basic idea behind the model is that the shapes of T-waves across leads are similar. Thus they can be modeled as a scaled version of a DTW [156]. Let us consider

T waves samples $\{\psi_l(t_i)\}_{l=1}^{L}$ from L leads, collected in the $(L \times T)$ vector Ψ. Firstly the heart surface is divided into M contiguous regions (nodes):

$$\Psi = AD = A \begin{pmatrix} D_1(t_i) \\ \vdots \\ D_M(t_i) \end{pmatrix} \tag{5.1}$$

where A $[L \times M]$ is a transfer matrix which is fixed for a given subject. D $[M \times T]$ describes the repolarization phase of transmembrane potentials (TMPs). Then for the surface strength at node n

$$\begin{aligned} &D_n(t_i) = D(t_i, \rho_n) = D(t_i - \rho_n) \\ &n = 1, ..., M \end{aligned} \tag{5.2}$$

where ρ_n is repolarization time (RT). The RT in each node can be expressed as

$$\rho_n = \overline{\rho} + \Delta\rho_n, \tag{5.3}$$

where $\overline{\rho}$ is mean value of RTs.

When $\Delta\rho_n << \overline{\rho}$, by taking a Taylor expansion of (5.2) around a fixed point $\overline{\rho}$, (5.1) can be written as

$$\Psi \approx \sum_{k=1}^{N} (-1)^k A \frac{\Delta\rho^k}{k!} D^k(t_i - \overline{\rho}). \tag{5.4}$$

It is more common to express (5.4) as:

$$\Psi \approx \sum_{k=1}^{N} w_k T_d^{(k-1)}(t_i) \tag{5.5}$$

where $T_d = D'(t_i - \rho_n)$, $w_k = (-1)^k A \frac{\Delta\rho^k}{k!}$ is the lead factors and N is the number of dominant T-wave and its derivatives used to model the potentials. It can be shown that the DTW is equivalent to the time derivative of the transmembrane potential. In [153], the detailed description of $\mathcal{V}$-index for estimating the dispersion of repolarization times is presented. To compute the index, DTW and lead factors (scalar values) are estimated solving an inverse problem. In Appendix of [153], two numerical methods were discussed for estimating the DTW and lead factors. They consider upto three terms in (5.5). However in theory, more terms in Taylor expansion are needed for better approximation of the potentials and lead factors when the dispersion of the RTs increases. Considering the fact that the recorded ECG signals can be rather noisy, numerical methods are failed due to the effect of noise on the shape of DTW and specially its derivatives. For this reason, some parametric methods have been introduced based on analytic definitions of the DTW, to allow analytical computation of its derivatives. Three analytic forms, based on the combination of sigmoidal (S), Gaussian (G) or exponentials (E) functions, have been studied in [157].

In the following section, an analytical model is introduced for the DTW, based on trigonometric functions, which is a functional set closed under the operation of derivation. Therefore, the nonlinear iterative optimization required by previous methods is no longer necessary. Then, an iterative matrix factorization method (based on the solution of linear problems) is proposed, which respects the ranks of the matrixes involved. The approach allows to include higher order derivatives with ease, even in the presence of noise, leading to more accurate estimates of the $\mathcal{V}$-index. Such estimates of higher accuracy are potentially of clinical value, as they could help discriminating changes in SHVR, as induced, *e.g.*, by drugs in thorough QT studies.

5.2 FUNCTIONAL MODEL FOR DOMINANT T-WAVE

Let us consider the observation samples $x(t_i)$, collected in the $(1 \times T)$ vector x. It can be approximated with $\hat{x}(t_i)$, produced by a linear combination of basis functions $\phi_k(t)$, that is

$$\hat{x}(t_i) = \sum_{n=0}^{B-1} \alpha_n \phi_n(t_i) \quad \text{or} \quad \hat{x} = \alpha^T \Phi, \tag{5.6}$$

where

- B is the number of basis functions in the expansion.
- $\{\phi_n(t_i)\}_{n=0}^{B-1}$ are the basis functions.
- α_n is the corresponding coefficient of the n-th basis function.
- $\hat{x}$ designs an "acceptable" model for x.

The unknown parameters α_n are obtained as [158]

$$\alpha = \Phi(\Phi^T\Phi)^{-1}x^T. \tag{5.7}$$

5.2.1 SINUSOIDAL FUNCTION BASED INDEX COMPUTATION

As mentioned before, in theory for better approximation of potentials and lead factors more terms in the Taylor expansion (5.5) are needed, which is what we tackle in this research.

Let's define the following 2B-dimensional vector as sinusoidal basis waveforms

$$\Phi(t_i) \doteq [\phi_{c,0}(t_i), ..., \phi_{c,B-1}(t_i), \phi_{s,0}(t_i), ..., \phi_{s,B-1}(t_i)]^T$$

where

$$\phi_{c,n}(t_i) \doteq \cos(\lambda_n t_i) \qquad \text{and} \qquad \phi_{s,n}(t_i) \doteq \sin(\lambda_n t_i)$$

$\lambda_n = 2\pi f_n$ and f_n is the frequency of the sinusoid waves.

Then:

$$\begin{aligned} \hat{x}(t_i) &= \sum_{n=0}^{B-1} [\alpha_{c,n}\phi_{c,n}(t_i) + \alpha_{s,n}\phi_{s,n}(t_i)] \\ \text{or} \quad \hat{x} &= \alpha_c^T \Phi_c + \alpha_s^T \Phi_s, \end{aligned} \tag{5.8}$$

where $\hat{x}$ is the observation signal (*e.g.*, potentials and DTW), Φ_c and Φ_s are the cosine and sine parts of the model:

$$\begin{aligned} \Phi_c &= [\phi_{c,0}(t_i), \phi_{c,1}(t_i), ..., \phi_{c,B-1}(t_i)]^T \\ \Phi_s &= [\phi_{s,0}(t_i), \phi_{s,1}(t_i), ..., \phi_{s,B-1}(t_i)]^T \end{aligned} \tag{5.9}$$

As recalled earlier, sinusoidal basis waveforms have two nice properties: i) orthogonality; ii) they are a functional set closed under the operation of differentiation. In fact,

$$\frac{d^k}{dt^k}\phi_{c,n}(t_i) = \begin{cases} (-1)^{\frac{k}{2}}\lambda_n^k \phi_{c,n}(t_i), & k \text{ is even} \\ (-1)^{\frac{k+1}{2}}\lambda_n^k \phi_{s,n}(t_i), & k \text{ is odd} \end{cases} \tag{5.10}$$

and

$$\frac{d^k}{dt^k}\phi_{s,n}(t_i) = \begin{cases} (-1)^{\frac{k}{2}}\lambda_n^k \phi_{s,n}(t_i), & k \text{ is even} \\ (-1)^{\frac{k-1}{2}}\lambda_n^k \phi_{c,n}(t_i), & k \text{ is odd} \end{cases} \tag{5.11}$$

This is the main reason for choosing here these waveforms as basis functions for T_d. Using eq. (5.8) the potentials Ψ can be modeled with:

$$\hat{\Psi} = Q_c \Phi_c + Q_s \Phi_s \tag{5.12}$$

where Φ_c and Φ_s were previously defined in (5.9), Q_c and Q_s are $L \times B$ matrices containing the complete set of transform coefficients which are computed using eq. (5.7).

The first estimate of T_d is computed using SVD as discussed in [153]. Further we represent it using eq. (5.8):

$$T_d = p_c^T \Phi_c + p_s^T \Phi_s, \tag{5.13}$$

where p_c, p_s are the coefficients related to T_d. The basis waveforms are sinusoid, then p_c and p_s are the vector of Fourier coefficients.

Then by substituting (5.13) in (5.5) the potentials can be approximated as

$$\hat{\Psi} = W(H_c \Phi_c + H_s \Phi_s) \tag{5.14}$$

where W is $L \times N$ the complete set of lead factors, H_c and H_s are the $(N \times B)$ dimension matrix which their elements are:

$$h_c(k,n) = \begin{cases} (-1)^{\frac{k}{2}} \lambda_n^k p_{c,n}, & k \text{ is even} \\ (-1)^{\frac{k-1}{2}} \lambda_n^k p_{s,n}, & k \text{ is odd} \end{cases} \tag{5.15}$$

and

$$h_s(k,n) = \begin{cases} (-1)^{\frac{k}{2}} \lambda_n^k p_{s,n}, & k \text{ is even} \\ (-1)^{\frac{k+1}{2}} \lambda_n^k p_{c,n}, & k \text{ is odd} \end{cases} \tag{5.16}$$

Now from (5.12) and (5.14) we have

$$Q \approx WH \tag{5.17}$$

where $Q = [Q_c \; Q_s]$ and $H = [H_c \; H_s]$. So the problem is changed to find W and H, so that the error function $e = |Q - WH|_F$ is minimized. Considering the fact that W and H are unknown, finding the optimal value of W and H is difficult. However in the following we present an iterative procedure for estimating them.

As mentioned before we initially estimate T_d using SVD and further represented as (5.13). Having the coefficients p_c and p_s, the initial value of H_c and H_s can be computed using (5.15 and 5.16). Hence the only unknown in eq. (5.17) is W. The lead factors W can be computed via $W = (H^T H)^{-1} H Q^T$. The next step is to update T_d. For this reason having Q_c, Q_s and the previous estimated value of lead factors (W), we update the coefficients vector p_c and p_s to update T_d.

Considering that each elements of Q_c, Q_s can be expressed as:

$$\begin{aligned} q_c(m,n) &= \sum_{k=1}^{N} W_{m,k} h_c(k,n) \\ &= \sum_{k=1}^{N} W_{m,k} (-1)^{\frac{k}{2}} \lambda_n^k p_{c,n} + \sum_{k=1}^{N} W_{m,k} (-1)^{\frac{k-1}{2}} \lambda_n^k p_{s,n}, \\ q_s(m,n) &= \sum_{k=1}^{N} W_{m,k} h_s(k,n) \\ &= \sum_{k=1}^{N} W_{m,k} (-1)^{\frac{k+1}{2}} \lambda_n^k p_{c,n} + \sum_{k=1}^{N} W_{m,k} (-1)^{\frac{k}{2}} \lambda_n^k p_{s,n}. \end{aligned}$$

The previous equation can be rewritten as:

$$\begin{aligned} q_c(m,n) &= p_{c,n} z_1 - p_{s,n} z_2, \\ q_s(m,n) &= p_{c,n} z_2 + p_{s,n} z_1, \end{aligned} \tag{5.18}$$

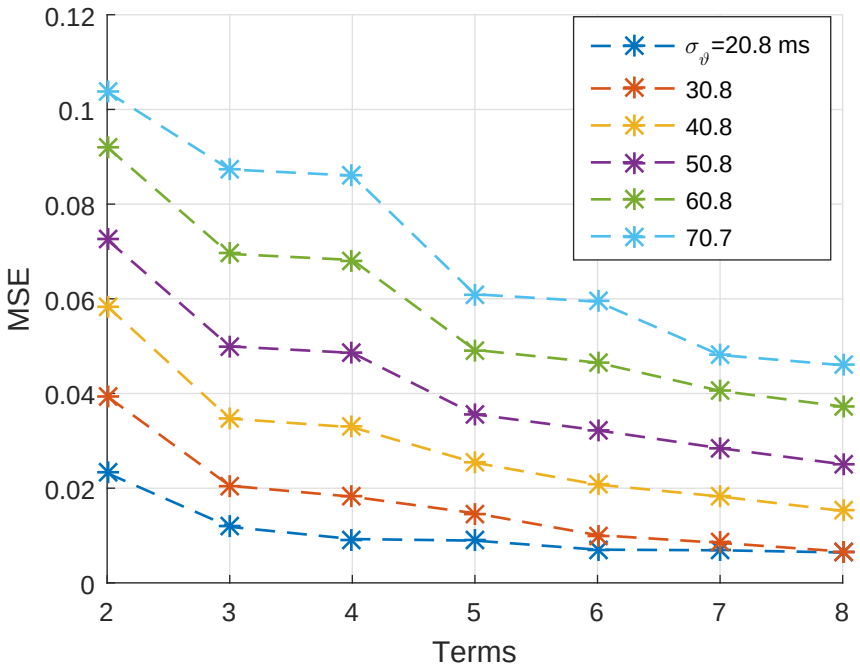

Figure 5.1: Comparison of the ability of Models for approximating the Potential with respect to number of terms in Taylor Expansion.

where

$$z_1 = \sum_{k=1}^{N} W_{m,k}(-1)^{\frac{k}{2}}\lambda_n^k,$$
$$z_2 = \sum_{k=1}^{N} W_{m,k}(-1)^{\frac{k+1}{2}}\lambda_n^k.$$

According to eq. (5.18) the coefficients $p_{c,n}$ and $p_{s,n}$ can be found as:

$$p_{c,n} = \frac{1}{2}\frac{\sum_{m=1}^{L}[q_c(m,n)z_1 + q_s(m,n)z_2]}{\sum_{m=1}^{L}[z_1z_1 + z_2z_2]}$$
$$p_{s,n} = \frac{1}{2}\frac{\sum_{m=1}^{L}[q_s(m,n)z_1 - q_s(m,n)z_2]}{\sum_{m=1}^{L}[z_1z_1 + z_2z_2]}$$

Having the new estimated value of coefficients p we can update T_d. The algorithm is repeated until satisfying acceptable error for (5.17).

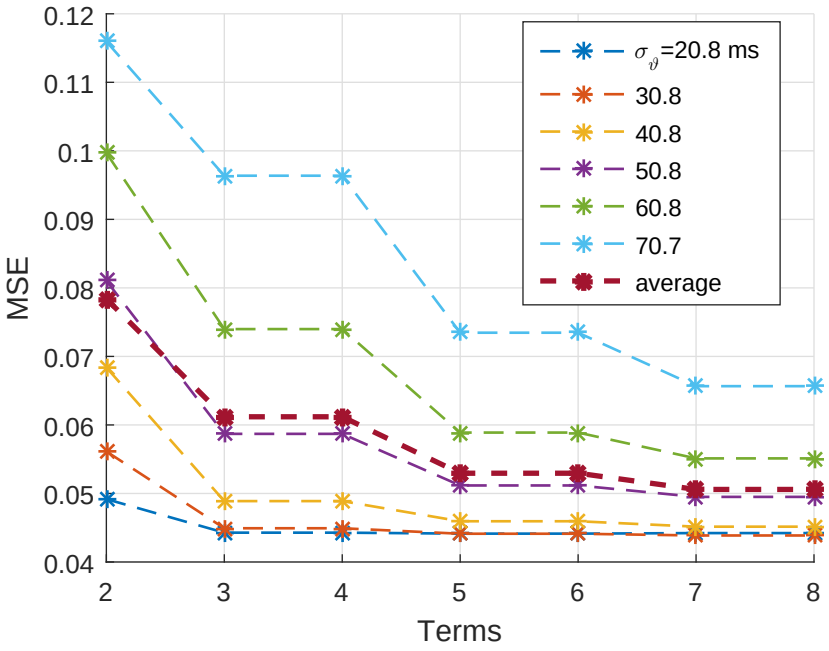

Figure 5.2: Comparison of the ability of Models for approximating w_1 with respect to number of terms in Taylor Expansion.

5.3 SIMULATIONS AND RESULTS

It is interesting to study how the number of terms in eq. (5.4) can affect on the approximating of potentials, as well as the lead factors. In this study we produced 40 synthetic ECGs, each ECG with 8 channels and 128 beats for different values of s_θ using a forward electrophysiological model (ECGSIM [155]). In particular, the values of s_θ was increased from the default values of (20.6, 30.5, 40.6, 50.6, 60.6 and 70.9) within ECGSIM. This choice permits a direct comparison with the results in [159].

The desired values of w were defined in eq. (5.5) and $\mathcal{V}$-index is defined as:

$$\mathcal{V}\text{-index} = \frac{\text{std}(w_2)}{\text{std}(w_1)}$$

Potentials and lead factors were computed using sinusoidal modelling changing the number of terms in (5.4). To quantify the performances of the algorithm, we employed the root mean square error (RMSE) defined as:

$$\text{RMSE} = \frac{|y - \hat{y}|_F}{|y|_F}$$

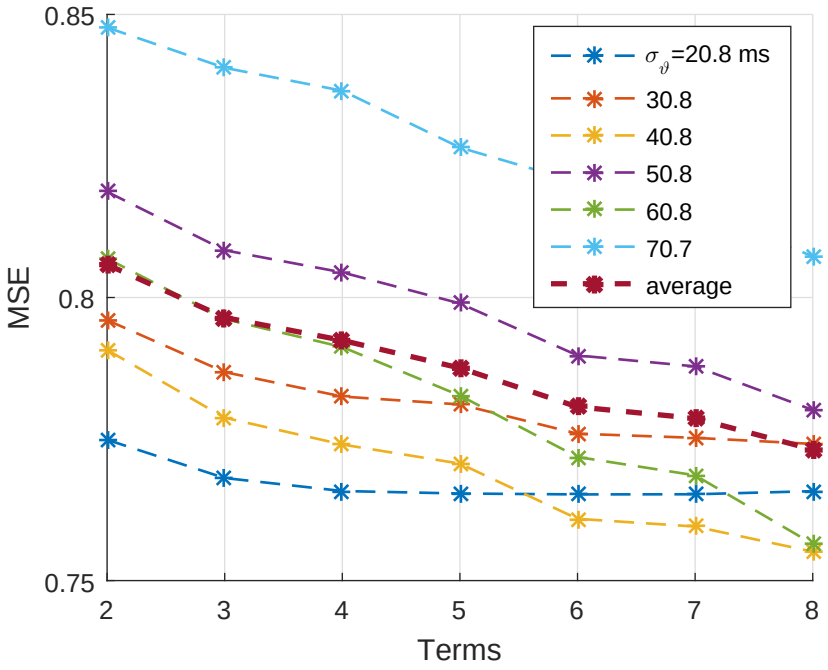

Figure 5.3: Comparison of the ability of Models for approximating w_2 with respect to number of terms in Taylor Expansion.

where y is the real value and $\hat{y}$ is the estimated value. Fig. 5.1 shows the results for approximating potentials. The result shows that the error of approximation is decreased when the number of terms is increased. However the approximation error is worse when the value of s_θ is larger. That means increasing the number of Taylor terms has high impact on estimating the potentials when s_θ is large. Fig. 5.2 and 5.3 illustrate that the estimation of the lead factors is improved when the number of terms in Taylor expansion is increased. Since the values of standard deviation of lead factors are required for computing $\mathcal{V}$-index, we reported the results for estimating the values of standard deviation of w_1 and w_2 also. Fig. 5.4 and 5.5 shows the results. It is shown that the approximation error of lead factors is decreased by increasing the number of Taylor terms. Average errors in $\mathcal{V}$-index estimates are summarized in Fig. 5.6, for different number of terms N ranging from 2 to 8, and in Table B.2. The number of basis functions was set to $B = 16$ in this study. Since DTW is a slowly varying signal, increasing B beyond 16 does not lead to a substantial improve, as shown in Fig. 5.7, while the computational costs rise significantly.

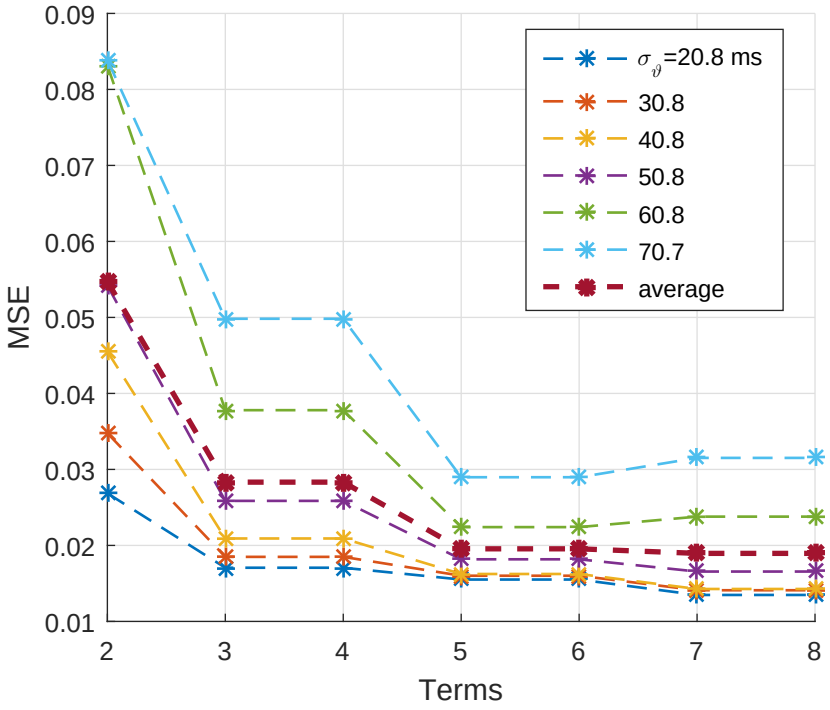

Figure 5.4: Comparison of the ability of Models for approximating the Standard deviation of w_1 with respect to number of terms in Taylor Expansion.

Table 5.1: Average values of RMSE for $\mathcal{V}$-index estimates, at each level of repolarization heterogeneity and number of model's terms.

σ_ϑ (ms)	N						
	2	3	4	5	6	7	8
20.8	0.273±0.09	0.269±0.09	0.263±0.09	0.262± 0.09	0.262±0.10	0.261±0.10	0.261±0.10
30.8	0.293±0.09	0.285±0.08	0.284±0.09	0.282± 0.09	0.291±0.10	0.290±0.10	0.297±0.11
40.8	0.296±0.10	0.287±0.08	0.283±0.08	0.279± 0.08	0.277±0.09	0.275±0.09	0.277±0.10
50.8	0.307±0.01	0.300±0.09	0.296±0.09	0.290± 0.09	0.286±0.09	0.284±0.09	0.287±0.10
60.8	0.295±0.11	0.295±0.10	0.290±0.10	0.287±0.01	0.280±0.10	0.280±0.10	0.276±0.10
70.7	0.302±0.06	0.305±0.06	0.296±0.07	0.297± 0.06	0.287±0.06	0.288±0.06	0.278±0.06

5.4 SUMMARY

In this chapter, an iterative algorithm has been introduced for estimating ECG potentials and lead factors, as well as $\mathcal{V}$-index, using sinusoidal basis functions. The proposed method allowed us to include higher order terms in Taylor expansion. We tested the method on simulated data generated with a forward electrophysiological model for increasing values of heterogeneity of ventricular repolarization, s_θ. It was shown

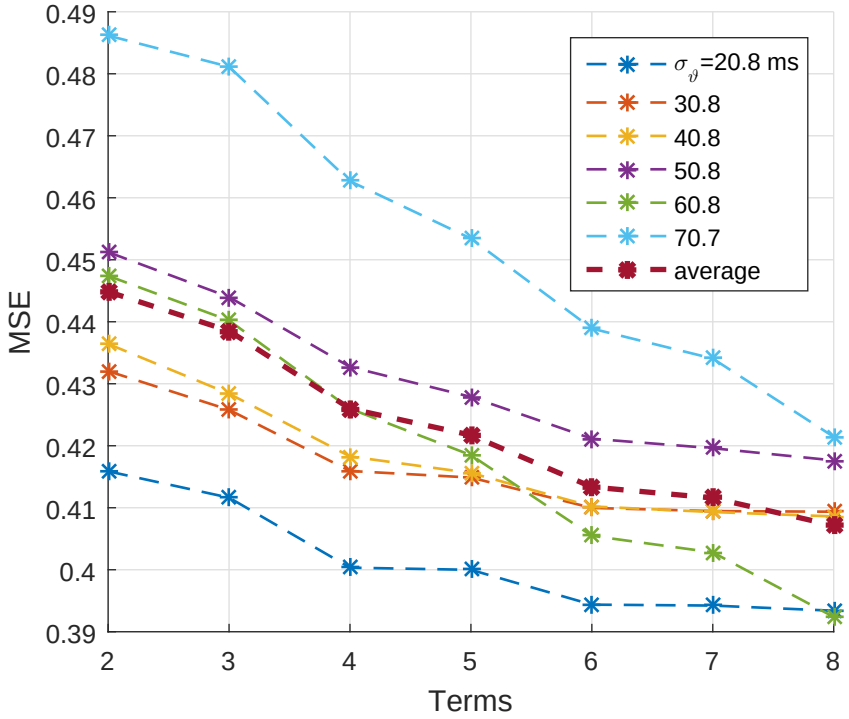

Figure 5.5: Comparison of the ability of Models for approximating the Standard deviation of w_2 with respect to number of terms in Taylor Expansion.

that the error of approximation for potentials, lead factors and standard deviation of the lead factors is decreased when the number of Taylor terms is increased. However the approximation error is worse when the value of s_θ is larger. When s_θ is small, the less Taylor terms are needed to approximate potentials as well as lead factors.

In future works, the increased accuracy in estimating the $\mathcal{V}$-index will be exploited in the analysis of real ECG data.

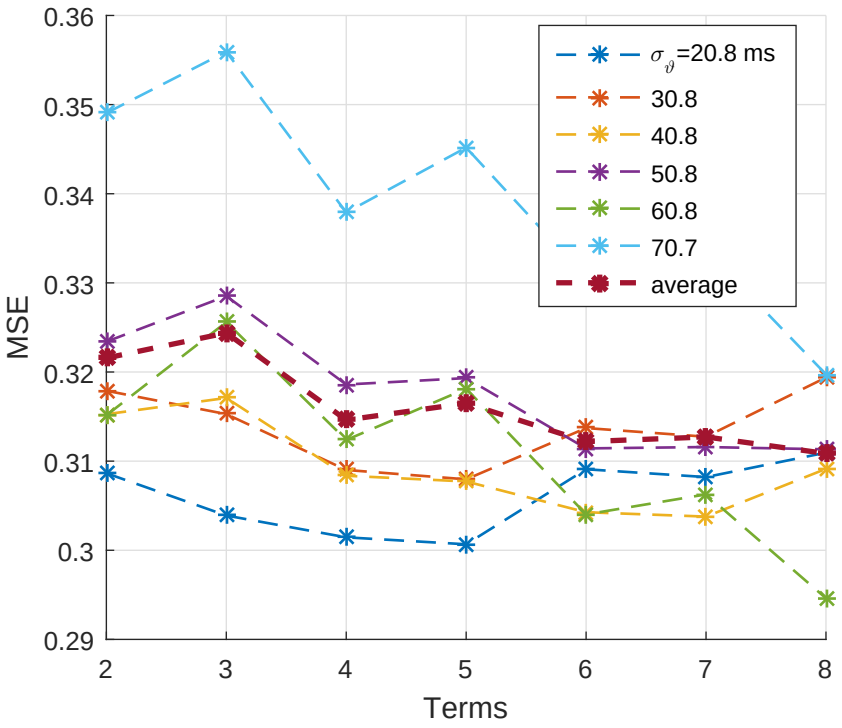

Figure 5.6: Comparison of the ability of Models for approximating the $\mathcal{V}$-index with respect to number of terms in Taylor Expansion.

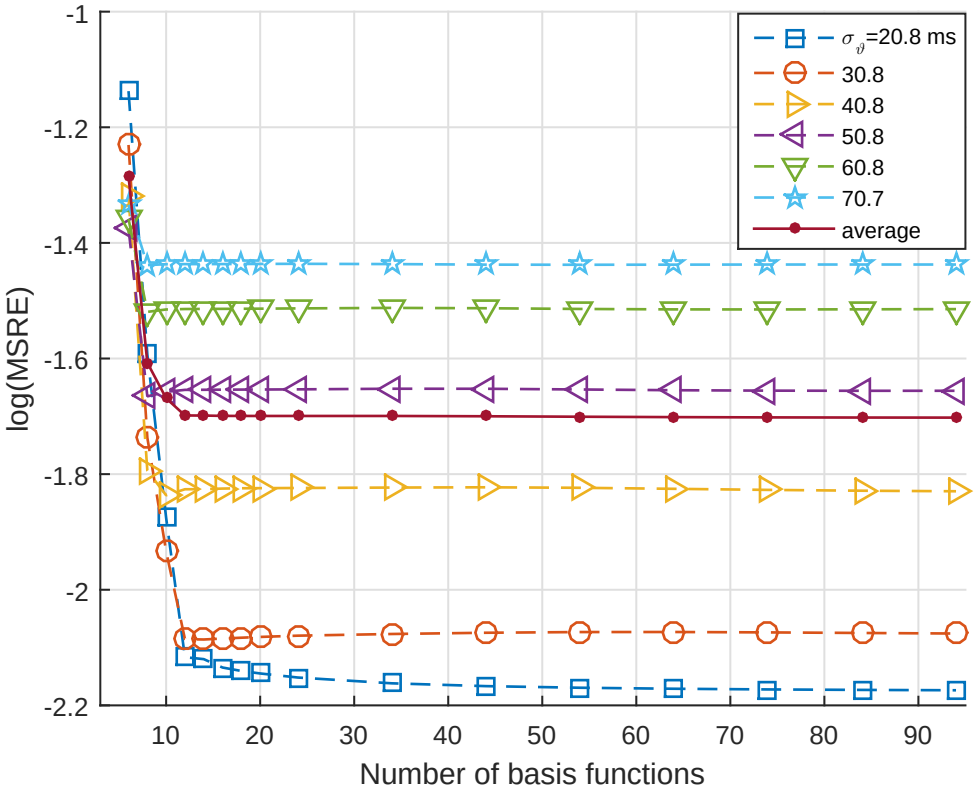

Figure 5.7: Ability of the model in approximating the ECG Ψ versus the number of sinusoidal basis functions B at $N = 4$.

6

CONCLUSIONS AND FUTURE WORKS

6.1 CONCLUSIONS

In this research, the problem of cardiac signals analysis and feature extraction was studied using adaptive signal modelling. Different ECG models based Bayesian estimation were proposed to improve the signal processing aspect of cardiac signal and its waveform components estimation. More specifically, in chapter 2, a signal decomposition model-based Bayesian filtering framework was proposed for ECG signal processing (EKS6). The framework is generic and can be used for multiple purposes like ECG denoising, feature extraction, beat segmentation and classification. The proposed model has several advantages when compared with previous ECG models:

- The non-linearity of the model has been decreased with respect to previous models. In fact EKF/EKS linearizes the dynamical model at an operating point by approximating the state model through a first order Taylor series approximation. However for most non-linear models the truncation of the Taylor series is a poor approximation. The accuracy of the linearization depends on the amount of local non-linearity in the functions being approximated. Then, the posterior mean and covariance estimations become suboptimal and model errors are introduced. This can lead to instability, particularly when the system dynamics are strongly nonlinear. Hence the proposed model was derived to reduce the non-linearity of the state model with respect to previous solutions.

- The model no longer depends on the amplitude of the Gaussian kernels. ECG is a non-stationary signal and its morphology can change over time. One of the parameters which can be affected by the non-stationary behavior of ECG is the amplitude of the Gaussian components of the model. Hence they were considered as process noise variable in the previous methods. Now with the new model it was shown that they need not to be considered as process noise variable.

- Components were sometimes mixed up by previous EKS (EKS4) but not by EKS6. EKS6 has two extra state variables with respect to EKS4 (a price to pay for removing amplitude from the model), and, in principle, a larger number of degrees of freedom surely helps EKS6 in better following the ECG components. However, this is not the main source of the performance improvement, but the improvement is due to the new EDM proposed in EKS6.

- A baseline drift is produced by EKS4 in ECG component waveforms extraction. The problem is solved by the new EDM proposed in EKS6.

In patients with atrial fibrillation, the dominant repetition rate of the atrial fibrillatory waves, or fibrillatory frequency plays an important role for non-invasive assessment of atrial electrical remodeling. It can be assessed from the ECG signals by signal processing tools such as power spectral analysis and short-time Fourier transform (STFT), after ventricular activity cancellation (or f-wave extraction). In this research we explored if it is possible to estimate the FF accurately, while ignoring the step of VA cancellation. Methods based on singular or independent component analysis of ECG signals were previously proposed for this task, but: (i) they requires multi-lead recordings (not available in mobile single-lead ECG devices); and (ii) the fibrillatory activity is inherently spread into multiple components. In chapter 3, a nonlinear Bayesian filtering framework was proposed for ECG analysis in Atrial fibrillation. The proposed method is novel and utilizes the temporal dynamics of cardiac signals within a Bayesian filtering framework for ECG based atrial fibrillation characterization. To the best of our knowledge, this method is the first approach to analyze the fibrillatory frequency, while ignoring the step of ventricular activity cancellation. This new model is able to track atrial activity, ventricular activity and fibrillatory frequency simultaneously, in long recordings.

In chapter 4, we described a signal decomposition model based Bayesian framework (EKS3) to improve the detection of a specific clinical research topic referred to as T wave alternans. There are some theoretical advantages that the proposed method has over other recent works in this context. It is able to track the T wave amplitude, even when abrupt changes happens in the T wave and it reduces the nonlinearity of the T-wave state. The method is a special case of the model presented in chapter 2 for ECG components separation, and the performance of both methods for TWA detection was similar, but EKS3 has fewer state variables. Being tailored to this specific application, it results in a significant decrease in complexity.

Noninvasive assessment of the SHVR is gaining acceptance as a tool for characterizing the heterogeneity of the ventricular repolarization. In such context, a metric known as $\mathcal{V}$-index can be used to estimate the standard deviation of ventricular myocytes' repolarization times. In chapter 5, we introduced a new algorithm based on trigonometric functions, which is a functional set closed under the operation of derivation for estimating the $\mathcal{V}$-index. Therefore, the nonlinear iterative optimization required by previous methods is no longer necessary. Then, we suggested an iterative matrix factorization method (based on the solution of linear problems), which respects the ranks of the matrixes involved. The approach allowed to include higher order derivatives with ease,

even in the presence of noise, leading to more accurate estimates of the $\mathcal{V}$-index. We obtained that a higher number of lead factors resulted in a more robust estimate of high values of SHVR, confirming the results reported in previous studies. Moreover, the analytical form, having more reliable estimate of DTW derivatives, obtained the lowest values of MSE between data and model.

We tested the method on simulated data generated with a forward electrophysiological model for increasing values of heterogeneity of ventricular repolarization, s_θ. It was shown that the error of approximation for potentials, lead factors and standard deviation of the lead factors is decreased when the number of Taylor terms is increased. However the approximation error is worse when the value of s_θ is larger. When s_θ is small, the less Taylor terms is needed to approximate potentials as well as lead factors. The procedure can be extended to another basis functions like polynomial basis.

We tested the method also on real data. On real data, the method was able to detect the effects of moxifloxacin [160].

6.2 FUTURE WORKS

Some of the possible future works are listed bellow:

- The proposed model in chapter 2, (EKS6) can be extended to other applications such as extracting fetal ECG from the maternal abdomen ECG recordings as the merit of the proposed approach with respect to other models was discussed. Therefore, it is possible to increase the accuracy of fetal ECG extraction as well as fetal ECG components separation.

- As a real application, EKS6 was employed for T/QRS ratio calculation. The method can be used for many other applications such as robust extraction of other ECG fiducial point markers, including ST-level, QT and PR-intervals.

- In the research we only considered 10s ECG recordings for testing the performance of the proposed method. However, the approach should be tested on longer recordings and we plan to do it in the future.

- The new EDM in EKS6 has many advantages as discussed before. However, it depends on the initial condition which can be considered as disadvantage of the model, as it makes it highly susceptible to initial conditions. It is undesirable for a stable system. The stability and observability of the steady state space of the proposed framework (EKS6) needs to be studied in the future.

- The feasibility of using ECG based human identification has been investigated by other researchers and ECG known as one of the most accurate biometrics [161, 162]. Wavelet and Fourier coefficients of the ECG have been used as features for ECG based biometric systems. However, the number of features extracted from DWT and DFT coefficients is too much. The ECG features extracted by EKS6 can be used for ECG classification and human identification in the future.

- The results of chapter 3 showed that an accurate FF estimation is possible using EKF/EKS, while avoiding a preliminar step for VA cancellation. The technique effectively estimated also the AA itself. In the future the proposed method will be employed for FF tracking in holter ECGs in AF patients.
- A sum of Gaussian functions has been used for ECG modelling. Since ECG is a non-stationary signal, Kalman filter was used to update the parameters of the model on a beat to beat basis. Kalman filter can be avoided if we can derive a linear method to estimate the parameters of the sum of Gaussian model.
- The dynamical model which was introduced for warping functions can be combined within a Kalman filter structure to improve the estimation of warping functions. The method can also be extended to high-dimensional curves for image alignment.

REFERENCES

[1] L. E. Hinkle, S. T. Carver, and D. C. Argyros, "The prognostic significance of ventricular premature contractions in healthy people and in people with coronary heart disease," *Acta Cardiol.*, vol. Suppl 18, pp. 5–32, 1974. *(Cited on page 1)*

[2] K. Rosén, A. Dagbjartsson, B. Henriksson, H. Lagercrantz, and I. Kjellmer, "The relationship between circulating catecholamines and ST waveform in the fetal lamb electrocardiogram during hypoxia," *Am. J. Obstet. Gynecol.*, vol. 149, pp. 190–195, 1984. *(Cited on page 2)*

[3] J. H. Becker, L. Bax, I. Amer-Wåhlin, K. Ojala, C. Vayssière, M. E. Westerhuis, B.-W. Mol, G. H. Visser, K. Maršál, A. Kwee, and K. G. M. Moons, "ST analysis of the fetal electrocardiogram in intrapartum fetal monitoring: a meta-analysis," *Obstet. Gynecol.*, vol. 119, pp. 145–154, 2012. *(Cited on page 2)*

[4] F. Censi, G. Calcagnini, C. Ricci, R. Ricci, M. Santini, A. Grammatico, and P. Bartolini, "P-wave morphology assessment by a Gaussian functions-based model in atrial fibrillation patients," *IEEE Trans. Biomed. Eng.*, vol. 54, pp. 663–672, 2007. *(Cited on pages 2, 53, and 57)*

[5] M. A. Colman, O. V. Aslanidi, J. Stott, V. Holden, and H. Zhang, "Correlation between P-wave morphology and origin of atrial focal tachycardia - insights from realistic models of the human atria and torso," *IEEE Trans. Biomed. Eng.*, vol. 58, pp. 2952–2955, 2011. *(Cited on page 2)*

[6] P. Kligfield, K. G. Lax, and P. M. Okin, "QT interval-heart rate relation during exercise in normal men and women: Definition by linear regression analysis," *JACC*, vol. 28, pp. 1547–1555, 1996. *(Cited on pages 2 and 17)*

[7] M. Malik, P. Färbom, V. Batchvarov, K. Hnatkova, and A. J. Camm, "Relation between QT and RR intervals is highly individual among healthy subjects: implications for heart rate correction of the QT interval," *Heart*, vol. 87, no. 3, pp. 220–228, 2002. *(Cited on page 2)*

[8] R. L. Verrier, T. Klingenheben, M. Malik, N. El-Sherif, D. V. Exner, S. H. Hohnloser, T. Ikeda, J. P. Martínez, S. M. Narayan, T. Nieminen, and D. S. Rosenbaum, "Microvolt T-wave alternans: Physiological basis, methods of measurement, and clinical utility-consensus guideline by ISHNE," *J. Am. Coll. Cardiol.*, vol. 58, pp. 1309–1324, 2011. *(Cited on page 2)*

[9] J. Pan and W. J. Tompkins, "A real-time qrs detection algorithm," *IEEE Transactions on Biomedical Engineering*, vol. BME-32, no. 3, pp. 230–236, 1985. *(Cited on pages 3 and 24)*

[10] M. Okada, "A digital filter for the qrs complex detection," *IEEE Transactions on Biomedical Engineering*, no. 12, pp. 700–703, 1979. *(Cited on page 3)*

[11] Y. Sun, S. Suppappola, and T. A. Wrublewski, "Microcontroller-based real-time qrs detection." *Biomed Instrum Technol*, vol. 26, no. 6, pp. 477–84, 1992. *(Cited on page 3)*

[12] S. Suppappola and Y. Sun, "Nonlinear transforms of ecg signals for digital qrs detection: a quantitative analysis," *IEEE Transactions on Biomedical Engineering*, vol. 41, no. 4, pp. 397–400, 1994. *(Cited on page 3)*

[13] Z. Dokur, T. Olmez, E. Yazgan, and O. K. Ersoy, "Detection of {ECG} waveforms by neural networks," *Med Eng Phys*, vol. 19, no. 8, pp. 738 – 741, 1997. *(Cited on page 3)*

[14] G. Vijaya, V. Kumar, and H. K. Verma, "Ann-based qrs-complex analysis of ecg," *J Med Eng Technol*, vol. 22, no. 4, pp. 160–167, 1998. *(Cited on page 3)*

[15] O. Meste, H. Rix, P. Caminal, and N. V. Thakor, "Ventricular late potentials characterization in time-frequency domain by means of a wavelet transform," *Biomedical Engineering, IEEE Transactions on*, vol. 41, no. 7, pp. 625–634, 1994. *(Cited on page 3)*

[16] L. Senhadji, G. Carrault, J. J. Bellanger, and G. Passariello, "Comparing wavelet transforms for recognizing cardiac patterns," *Engineering in Medicine and Biology Magazine, IEEE*, vol. 14, no. 2, pp. 167–173, 1995. *(Cited on page 3)*

[17] K. Sternickel, "Automatic pattern recognition in ECG time series," *Computer Methods and Programs in Biomedicine*, vol. 68, no. 2, pp. 109–115, May 2002. *(Cited on page 3)*

[18] J. S. Sahambi, S. N. Tandon, and R. K. P. Bhatt, "Using wavelet transforms for ECG characterization. An on-line digital signal processing system," *Engineering in Medicine and Biology Magazine, IEEE*, vol. 16, no. 1, pp. 77–83, 1997. *(Cited on page 3)*

[19] ——, "Wavelet based ST-segment analysis," *Medical and Biological Engineering and Computing*, vol. 36, no. 5, pp. 568–572, 1998. *(Cited on page 3)*

[20] C. Li, C. Zheng, and C. Tai, "Detection of ECG characteristic points using wavelet transforms," *Biomedical Engineering, IEEE Transactions on*, vol. 42, no. 1, pp. 21–28, 1995. *(Cited on page 3)*

[21] J. Martinez, R. Almeida, S. Olmos, A. Rocha, and P. Laguna, "A Wavelet-Based ECG Delineator: Evaluation on Standard Databases," *IEEE Transactions on Biomedical Engineering*, vol. 51, no. 4, pp. 570–581, Apr. 2004. *(Cited on page 3)*

[22] S. Mallat and S. Zhong, "Characterization of signals from multiscale edges," *Pattern Analysis and Machine Intelligence, IEEE Transactions on*, vol. 14, no. 7, pp. 710–732, 1992. *(Cited on page 3)*

[23] E. Soria-Olivas, M. Martinez-Sober, J. Calpe-Maravilla, J. F. Guerrero-Martinez, J. Chorro-Gasco, and J. Espi-Lopez, "Application of adaptive signal processing for determining the limits of p and t waves in an ecg," *IEEE Transactions on Biomedical Engineering*, vol. 45, no. 8, pp. 1077–1080, 1998. *(Cited on page 4)*

[24] S. Graja and J. M. Boucher, "Hidden markov tree model applied to ecg delineation," *IEEE Transactions on Instrumentation and Measurement*, vol. 54, no. 6, pp. 2163–2168, 2005. *(Cited on page 4)*

[25] A. Koski, "Modelling ecg signals with hidden markov models," *Artificial Intelligence in Medicine*, vol. 8, no. 5, pp. 453 – 471, 1996. *(Cited on page 4)*

[26] N. P. Hughes, L. Tarassenko, and S. J. Roberts, "Markov models for automated ecg interval analysis." in *NIPS*, S. Thrun, L. K. Saul, and B. Sch olkopf, Eds. MIT Press, 2003, pp. 611–618. *(Cited on page 4)*

[27] B. Kohler, C. Hennig, and R. Orglmeister, "QRS detection using zero crossing counts," *Appl. Genomics Proteomics*, vol. 2, no. 2, pp. 138–145, 2003. *(Cited on page 4)*

[28] M. Akhbari, M. B. Shamsollahi, C. Jutten, A. A. Armoundas, and O. Sayadi, "Ecg denoising and fiducial point extraction using an extended kalman filtering framework with linear and nonlinear phase observations," *Physiological Measurement*, vol. 37, no. 2, p. 203, 2016. [Online]. Available: http://stacks.iop.org/0967-3334/37/i=2/a=203 *(Cited on page 4)*

[29] O. Sayadi and M. B. Shamsollahi, "A model-based Bayesian framework for ECG beat segmentation," *Physiol. Meas.*, vol. 30, pp. 335–352, 2009. *(Cited on pages 4, 6, and 13)*

[30] H. J. L. M. Vullings, M. H. G. Verhaegen, and H. B. Verbruggen, "Automated ecg segmentation with dynamic time warping," in *Engineering in Medicine and Biology Society, 1998. Proceedings of the 20th Annual International Conference of the IEEE*, 1998, pp. 163–166 vol.1. *(Cited on page 4)*

[31] ——, *ECG segmentation using time-warping*. Berlin, Heidelberg: Springer Berlin Heidelberg, 1997, pp. 275–285. *(Cited on page 4)*

[32] Z. Zidelmal, A. Amirou, D. Ould-Abdeslam, and J. Merckle, "{ECG} beat classification using a cost sensitive classifier," *Computer Methods and Programs in Biomedicine*, vol. 111, no. 3, pp. 570 – 577, 2013. *(Cited on page 4)*

[33] C. Lin, A. Giremus, C. Mailhes, and J.-Y. Tourneret, "Beat-to-beat p and t wave delineation in ecg signals using a marginalized particle filter," in *Signal Processing Conference (EUSIPCO), 2012 Proceedings of the 20th European*. IEEE, 2012, pp. 479–483. *(Cited on page 4)*

[34] M. Rakshit, D. Panigrahy, and P. Sahu, "Ekf with pso technique for delineation of p and t wave in electrocardiogram (ecg) signal," in *Signal Processing and Integrated Networks (SPIN), 2015 2nd International Conference on*. IEEE, 2015, pp. 696–701. *(Cited on page 4)*

[35] C. Lin, C. Mailhes, and J.-Y. Tourneret, "P-and t-wave delineation in ecg signals using a bayesian approach and a partially collapsed gibbs sampler," *IEEE transactions on biomedical engineering*, vol. 57, no. 12, pp. 2840–2849, 2010. *(Cited on page 4)*

[36] C. Lin, G. Kail, A. Giremus, C. Mailhes, J.-Y. Tourneret, and F. Hlawatsch, "Sequential beat-to-beat p and t wave delineation and waveform estimation in ecg signals: Block gibbs sampler and marginalized particle filter," *Signal Processing*, vol. 104, pp. 174–187, 2014. *(Cited on page 4)*

[37] C. Members, V. Fuster, L. E. Rydén, R. W. Asinger, D. S. Cannom, H. J. Crijns, R. L. Frye, J. L. Halperin, G. N. Kay, W. W. Klein, S. Lévy, R. L. McNamara, E. N. Prystowsky, L. S. Wann, D. G. Wyse, R. J. Gibbons, E. M. Antman, J. S. Alpert, D. P. Faxon, V. Fuster, G. Gregoratos, L. F. Hiratzka, A. K. Jacobs, R. O. Russell, S. C. Smith, E. C. for Practice Guidelines & Policy Conferences Members, W. W. Klein, A. Alonso-Garcia, C. Blomström-Lundqvist, G. de Backer, M. Flather, J. Hradec, A. Oto, A. Parkhomenko, S. Silber, and A. Torbicki, "ACC/AHA/ESC Guidelines for the Management of Patients With Atrial Fibrillation: Executive Summary A Report of the American College of Cardiology/American Heart Association Task Force on Practice Guidelines and the European Society of Cardiology Committee for Practice Guidelines and Policy Conferences (Committee to Develop Guidelines for the Management of Patients With Atrial Fibrillation) Developed in Collaboration With the North American Society of Pacing and Electrophysiology," *Circulation*, vol. 104, pp. 2118–2150, 2001. *(Cited on page 4)*

[38] N. M. Wheeldon, "Atrial fibrillation and anticoagulant therapy," *European Heart Journal*, vol. 16, pp. 302–312, 1995. *(Cited on page 4)*

[39] S. T. Mathew, J. Patel, and S. Joseph, "Atrial fibrillation: Mechanistic insights and treatment options," *European Journal of Internal Medicine*, vol. 20, no. 7, pp. 672 – 681, 2009. *(Cited on page 4)*

[40] Y. Miyasaka, "Secular Trends in Incidence of Atrial Fibrillation in Olmsted County, Minnesota, 1980 to 2000, and Implications on the Projections for Future Prevalence," *Circulation*, vol. 114, no. 2, pp. 119–125, 2006. *(Cited on page 4)*

[41] A. S. Gami, "Association of Atrial Fibrillation and Obstructive Sleep Apnea," *Circulation*, vol. 110, no. 4, pp. 364–367, 2004. *(Cited on page 4)*

[42] K. J. Mukamal, "Alcohol Consumption and Risk of Atrial Fibrillation in Men and Women: The Copenhagen City Heart Study," *Circulation*, vol. 112, no. 12, pp. 1736–1742, 2005. *(Cited on page 4)*

[43] M. Stridh, L. Sörnmo, C. J. Meurling, and S. B. Olsson, "Characterization of atrial fibrillation using the surface ECG: time-dependent spectral properties," *IEEE Trans. Biomed. Eng.*, vol. 48, no. 1, pp. 19–27, 2001. *(Cited on page 4)*

[44] J. Rieta, F. Castells, C. Sanchez, V. Zarzoso, and J. Millet, "Atrial activity extraction for atrial fibrillation analysis using blind source separation," *IEEE Trans. Biomed. Eng.*, vol. 51, no. 7, pp. 1176–1186, 2004. *(Cited on page 4)*

[45] F. Castells, J. Rieta, J. Millet, and V. Zarzoso, "Spatiotemporal blind source separation approach to atrial activity estimation in atrial tachyarrhythmias," *IEEE Trans. Biomed. Eng.*, vol. 52, no. 2, pp. 258–267, 2005. *(Cited on page 4)*

[46] M. Lemay, J. Vesin, A. van Oosterom, V. Jacquemet, and L. Kappenberger, "Cancellation of Ventricular Activity in the ECG: Evaluation of Novel and Existing Methods," *IEEE Trans. Biomed. Eng.*, vol. 54, pp. 542–546, 2007. *(Cited on pages 4 and 5)*

[47] R. Sassi, V. Corino, and L. Mainardi, "Analysis of surface atrial signals: Time series with missing data?" *Annals of Biomedical Engineering*, vol. 37, pp. 2082–2092, 2009. *(Cited on page 4)*

[48] R. Alcaraz, F. Hornero, A. Martínez, and J. J. Rieta, "Short-time regularity assessment of fibrillatory waves from the surface ECG in atrial fibrillation," *Physiological Measurement*, vol. 33, no. 6, pp. 969–984, 2012-06-01. *(Cited on page 4)*

[49] R. Alcaraz and J. Rieta, "A review on sample entropy applications for the non-invasive analysis of atrial fibrillation electrocardiograms," *Biomedical Signal Processing and Control*, vol. 5, no. 1, pp. 1–14, 2010. *(Cited on page 4)*

[50] L. Sörnmo, M. Stridh, D. Husser, A. Bollmann, and S. B. Olsson, "Analysis of atrial fibrillation: from electrocardiogram signal processing to clinical management," *Philosophical Transactions of the Royal Society of London A: Mathematical, Physical and Engineering Sciences*, vol. 367, pp. 235–253, 2009. *(Cited on page 4)*

[51] V. D. Corino, R. Sassi, L. T. Mainardi, and S. Cerutti, "Signal processing methods for information enhancement in atrial fibrillation: Spectral analysis and non-linear parameters," *Biomedical Signal Processing and Control*, vol. 1, pp. 271 – 281, 2006. *(Cited on pages 4 and 49)*

[52] J. Slocum, A. Sahakian, and S. Swiryn, "Diagnosis of atrial fibrillation from surface electrocardiograms based on computer-detected atrial activity," *J. Electrocardiol.*, vol. 25, pp. 1–8, 1992. *(Cited on page 4)*

[53] J. J. Rieta and F. Hornero, "Comparative study of methods for ventricular activity cancellation in atrial electrograms of atrial fibrillation," *Physiological Measurement*, vol. 28, no. 8, p. 925, 2007. *(Cited on page 4)*

[54] M. Stridh, L. Sörnmo, C. Meurling, and S. Olsson, "Sequential Characterization of Atrial Tachyarrhythmias Based on ECG Time-Frequency Analysis," *IEEE Trans. Biomed. Eng.*, vol. 51, pp. 100–114, 2004. *(Cited on pages 4 and 5)*

[55] V. Corino, L. Mainardi, M. Stridh, and L. Sörnmo, "Improved time–frequency analysis of atrial fibrillation signals using spectral modeling," *IEEE Trans. Biomed. Eng.*, vol. 55, pp. 2723–2730, 2008. *(Cited on page 4)*

[56] D. Husser, M. Stridh, L. Sörnmo, C. Geller, H. U. Klein, B. Olsson, and A. Bollmann, "Time-frequency analysis of the surface electrocardiogram for monitoring antiarrhythmic drug effects in atrial fibrillation," *The American Journal of Cardiology*, vol. 95, no. 4, pp. 526–528, 2005. *(Cited on page 4)*

[57] P. Langley, J. Rieta, M. Stridh, J. Millet, L. Sörnmo, and A. Murray, "Comparison of atrial signal extraction algorithms in 12-lead ecgs with atrial fibrillation," *IEEE Trans. Biomed. Eng.*, vol. 53, pp. 343–346, 2006. *(Cited on page 4)*

[58] M. Stridh and L. Sörnmo, "Spatiotemporal QRST cancellation techniques for analysis of atrial fibrillation." *IEEE Trans. Biomed. Eng.*, vol. 48, pp. 105–111, 2001. *(Cited on pages 4, 5, and 43)*

[59] D. Raine, P. Langley, A. Murray, S. S. Furniss, and J. P. Bourke, "Surface atrial frequency analysis in patients with atrial fibrillation: Assessing the effects of linear left atrial ablation," *Journal of Cardiovascular Electrophysiology*, vol. 16, no. 8, 2005. *(Cited on page 4)*

[60] A. Petrenas, V. Marozas, L. Sörnmo, and A. Lukosevicius, "An Echo State Neural Network for QRST Cancellation During Atrial Fibrillation." *IEEE Trans. Biomed. Eng.*, vol. 59, pp. 2950–2957, 2012. *(Cited on pages 4 and 43)*

[61] I. A. Dotsinsky and T. V. Stoyanov, "Ventricular beat detection in single channel electrocardiograms," *BioMedical Engineering OnLine*, vol. 3, no. 3, p. 9, 2004. *(Cited on page 5)*

[62] M. Lemay, V. Jacquemet, A. Forclaz, J. Vesin, and L. Kappenberger, "Spatiotemporal QRST cancellation method using separate QRS and T-waves templates," in *Computers in Cardiology*, 2005, pp. 611–614. *(Cited on page 5)*

[63] R. Alcaraz and J. J. Rieta, "Adaptive singular value cancelation of ventricular activity in single-lead atrial fibrillation electrocardiograms," *Physiol. Meas.*, vol. 29, pp. 1351–1369, 2008. *(Cited on page 5)*

[64] R. Alcaraz and J. Rieta, "Adaptive singular value QRST cancellation for the analysis of short single lead atrial fibrillation electrocardiograms," in *Computers in Cardiology*, 2007, pp. 513–516. *(Cited on page 5)*

[65] C. Sanchez, J. Millet, J. J. Rieta, F. Castells, J. Rodenas, R. Ruiz-Granell, and V. Ruiz, "Packet wavelet decomposition: An approach for atrial activity extraction," in *Computers in Cardiology, 2002*, 2002, pp. 33–36. *(Cited on page 5)*

[66] J. Lee, J. h. Lee, J. w. Park, M. h. Song, and K. j. Lee, "A ventricular activity cancellation algorithm based on event synchronous adaptive filter for single-lead electrocardiograms," in *2012 Annual International Conference of the IEEE Engineering in Medicine and Biology Society*, 2012, pp. 5226–5229. *(Cited on page 5)*

[67] H. Dai, S. Jiang, and Y. Li, "Atrial activity extraction from single lead ECG recordings: Evaluation of two novel methods," *Comput. Biol. Med.*, vol. 43, no. 3, pp. 176–183, 2013. *(Cited on page 5)*

[68] F. Nilsson, M. Stridh, A. Bollmann, and L. Sörnmo, "Predicting spontaneous termination of atrial fibrillation using the surface ECG," *Medical Engineering and Physics*, vol. 28, no. 8, pp. 802 – 808, 2006. *(Cited on page 5)*

[69] F. Sandberg, M. Stridh, and L. Sörnmo, "Frequency Tracking of Atrial Fibrillation Using Hidden Markov Models," *IEEE Trans. Biomed. Eng.*, vol. 55, pp. 502–511, 2008. *(Cited on page 5)*

[70] G.-X. Yan, R. S. Lankipalli, J. F. Burke, S. Musco, and P. R. Kowey, "Ventricular repolarization components on the electrocardiogramcellular basis and clinical significance," *Journal of the American College of Cardiology*, vol. 42, no. 3, pp. 401–409, 2003. *(Cited on page 5)*

[71] D. M. Bloomfield, J. T. Bigger, R. C. Steinman, P. B. Namerow, M. K. Parides, A. B. Curtis, E. S. Kaufman, J. M. Davidenko, T. S. Shinn, and J. M. Fontaine, "Microvolt T-wave alternans and the risk of death or sustained ventricular arrhythmias in patients with left ventricular dysfunction," *J Am Coll Cardiol*, vol. 47, pp. 456–463, 2006. *(Cited on page 6)*

[72] M. L. Walker and D. S. Rosenbaum, "Repolarization alternans: implications for the mechanism and prevention of sudden cardiac death," *Cardiovasc Res*, vol. 57, pp. 599–614, 2003. *(Cited on page 6)*

[73] P. E. McSharry, G. D. Clifford, L. Tarassenko, and L. A. Smith, "A Dynamic Model for Generating Synthetic Electrocardiogram Signals," *IEEE Trans. Biomed. Eng.*, vol. 50, pp. 289–294, 2003. *(Cited on pages 6, 11, 16, and 21)*

[74] R. Sameni, M. B. Shamsollahi, C. Jutten, and G. D. Clifford, "A nonlinear Bayesian filtering framework for ECG denoising," *IEEE Trans. Biomed. Eng.*, vol. 54, pp. 2172–2185, 2007. *(Cited on pages 6, 11, 12, 14, 24, and 40)*

[75] G. D. Clifford, S. Nemati, and R. Sameni, "An artificial vector model for generating abnormal electrocardiographic rhythms," *Physiol. Meas.*, vol. 31, pp. 595–609, 2010. *(Cited on pages 6 and 12)*

[76] M. Akhbari, "Inter-beat and Intra-beat ECG Interval Analysis Based on State Space and Hidden Markov Models," Ph.D. dissertation, Institut National Polytechnique de Grenoble - INPG ; Sharif University of Technology (SUT), 2016, joint PhD thesis between INPG, Grenoble, France and Sharif University of Technology, Tehran, Iran. *(Cited on pages 6 and 63)*

[77] M. Akhbari, M. Shamsollahi, and C. Jutten, "T wave alternans detection in ECG using extended Kalman filter and dualrate EKF," in *Proc. 22nd European Signal Processing Conf. (EUSIPCO)*, 2014, pp. 2500–2504. *(Cited on pages 6, 63, 64, 66, and 67)*

[78] ——, "ECG fiducial points extraction by extended Kalman filtering," in *Proc. 36th International Conf. on Telecommunications and Signal Processing (TSP)*, 2013, pp. 628–632. *(Cited on pages 6, 63, and 67)*

[79] E. Steyerberg, *Clinical Prediction Models: A Practical Approach to Development, Validation, and Updating*. Springer Science & Business Media: Springer Science & Business Media, 2008. *(Cited on page 10)*

[80] J. Jeon and J. W. Taylor, "Short-term density forecasting of wave energy using arma-garch models and kernel density estimation," *International Journal of Forecasting*, vol. 32, no. 3, pp. 991 – 1004, 2016. *(Cited on page 10)*

[81] P. R. Junior, F. L. R. Salomon, E. de Oliveira Pamplona *et al.*, "Arima: An applied time series forecasting model for the bovespa stock index," *Applied Mathematics*, vol. 5, no. 21, pp. 33–83, 2014. *(Cited on page 10)*

[82] H. Li and O. Chutatape, "Automated feature extraction in color retinal images by a model based approach," *IEEE Transactions on Biomedical Engineering*, vol. 51, no. 2, pp. 246–254, 2004. *(Cited on page 11)*

[83] D. P. Burke, S. P. Kelly, P. de Chazal, R. B. Reilly, and C. Finucane, "A parametric feature extraction and classification strategy for brain-computer interfacing," *IEEE Transactions on Neural Systems and Rehabilitation Engineering*, vol. 13, no. 1, pp. 12–17, 2005. *(Cited on page 11)*

[84] L. Deng, J. Droppo, and A. Acero, "Exploiting variances in robust feature extraction based on a parametric model of speech distortion." in *INTERSPEECH*, 2002. *(Cited on page 11)*

[85] G. Lamarque, P. Ravier, and C. Dumez-Viou, "A new concept of virtual patient for real-time ecg analyzers," *Instrumentation and Measurement, IEEE Transactions on*, vol. 60, no. 3, pp. 939 –946, 2011. *(Cited on page 11)*

[86] P. Ravier, F. Leclerc, C. Dumez-Viou, and G. Lamarque, "Redefining Performance Evaluation Tools for Real-Time QRS Complex Classification Systems," *Biomedical Engineering, IEEE Transactions on*, vol. 54, no. 9, pp. 1706 –1710, 2007. *(Cited on page 11)*

[87] O. Sayadi and M. B. Shamsollahi, "ECG denoising and compression using a modified extended Kalman filter structure," *IEEE Trans. Biomed. Eng.*, vol. 55, pp. 2240–2248, 2008. *(Cited on pages 11, 12, 13, and 24)*

[88] R. Sameni, G. D. Clifford, C. Jutten, and M. B. Shamsollahi, "Multichannel ECG and noise modeling: Application to maternal and fetal ECG signals," *EURASIP J. Adv. Signal Process.*, pp. 043 407:1–14, 2007. *(Cited on pages 11, 12, 16, and 37)*

[89] G. D. Clifford, A. Shoeb, P. E. McSharry, and B. A. Janz, "Model-based filtering, compression and classification of the ECG," *Int. J. Bioelectromagn.*, vol. 7, pp. 158–161, 2005. *(Cited on page 12)*

[90] R. Sameni, M. Shamsollahi, and C. Jutten, "Filtering electrocardiogram signals using the extended kalman filter," in *27th Annual International Conference of the IEEE Engineering in Medicine and Biology Society (EMBS)*, 2006, pp. 5639–5642. *(Cited on page 12)*

[91] R. Sameni, M. Shamsollahi, C. Jutten, and M. Babaie-Zadeh, "Filtering noisy ecg signals using the extended kalman filter based on a modified dynamic ecg model," in *Computers in Cardiology, 2005*. Ieee, 2005, pp. 1017–1020. *(Cited on page 12)*

[92] R. Sameni, M. B. Shamsollahi, and C. Jutten, "Model-based Bayesian filtering of cardiac contaminants from biomedical recordings," *Physiol. Meas.*, vol. 29, pp. 595–613, 2008. *(Cited on page 12)*

[93] G. Clifford, S. Nemati, and R. Sameni, "An Artificial Multi-Channel Model for Generating Abnormal Electrocardiographic Rhythms," in *Computers in Cardiology, 2008*, 2008, pp. 773–776. *(Cited on page 12)*

[94] O. Sayadi, M. B. Shamsollahi, and G. D. Clifford, "Robust detection of premature ventricular contractions using a wave-based Bayesian framework," *IEEE Trans. Biomed. Eng.*, vol. 57, pp. 353–362, 2010. *(Cited on pages 13 and 24)*

[95] ——, "Synthetic ECG generation and Bayesian filtering using a Gaussian wave-based dynamical model," *Physiol. Meas.*, vol. 31, pp. 1309–1329, 2010. *(Cited on pages 13, 20, and 26)*

[96] E. Kheirati Roonizi, "A new algorithm for fitting a gaussian function riding on the polynomial background," *Signal Processing Letters, IEEE*, vol. 20, no. 11, pp. 1062–1065, 2013. *(Cited on page 14)*

[97] E. A. Raeder, D. S. Rosenbaum, R. Bhasin, and R. J. Cohen, "Alternating morphology of the QRST complex preceding sudden death," *N. Engl. J. Med.*, vol. 326, pp. 271–272, 1992. *(Cited on pages 14 and 67)*

[98] L. TABACK, E. MARDEN, H. L. MASON, and H. V. PIPBERGER, "Digital recording of electrocardiographic data for analysis by digital computer." *IRE Transactions on Medical Electronics*, pp. 6–167, 1959. *(Cited on page 15)*

[99] F. W. STALLMANN and H. V. PIPBERGER, "Automatic recognition of electrocardiographic waves by digital computer," *Circulation Research*, vol. 9, no. 6, pp. 1138–1143, 1961. [Online]. Available: http://circres.ahajournals.org/content/9/6/1138 *(Cited on page 15)*

[100] P. HV, S. FW, and B. AS, "Automatic analysis of the p-qrs-t complex of the electrocardiogram by digital computer," *Annals of Internal Medicine*, vol. 57, no. 5, pp. 776–787, 1962. [Online]. Available: +http://dx.doi.org/10.7326/0003-4819-57-5-776 *(Cited on page 15)*

[101] J. Richardson, L. Haywood, V. Murthy, and G. Harvey, "A mathematical model for ecg wave forms and power spectra," *Mathematical Biosciences*, vol. 12, no. 3, pp. 321 – 328, 1971. [Online]. Available: http://www.sciencedirect.com/science/article/pii/0025556471900265 *(Cited on page 15)*

[102] M. E. Nygards and J. Hulting, "Homomorphic analysis and modeling of ecg signals," *Computers and Biomedical Research*, vol. 12, no. 2, pp. 181–202, 1979. *(Cited on page 15)*

[103] T. Y. Young and W. H. Huggins, "On the representation of electrocardiograms," *Bio-medical Electronics, IEEE Transactions on*, vol. 10, no. 3, pp. 86 –95, 1963. *(Cited on page 15)*

[104] I. Murthy, M. Rangaraj, K. Udupa, and A. Goyal, "Homomorphic analysis and modeling of ecg signals," *IEEE Transactions on Biomedical Engineering*, vol. BME-26, no. 6, pp. 330–44, 1979. *(Cited on page 15)*

[105] L. Sörnmo, P. O. BSörnmorjesson, M. E. Nygards, and O. Pahlm, "A method for evaluation of qrs shape features using a mathematical model for the ecg," *IEEE Transactions on Biomedical Engineering*, vol. BME-28, no. 10, pp. 713–717, 1981. *(Cited on page 15)*

[106] L. P., R. Janë, S. Olmos, N. Thakor, and P. Rix, H. Caminal, "Adaptive estimation of qrs complex wave features of ecg signal by the hermite model." *Med Biol Eng Comput.*, vol. 34, no. 1, pp. 58–68, 1996. *(Cited on page 15)*

[107] S. Suppappola, Y. Sun, and S. A. Chiaramida, "Gaussian pulse decomposition: An intuitive model of electrocardiogram waveforms," *Annals of Biomedical Engineering*, vol. 25, no. 2, pp. 252–260, 1997. *(Cited on page 16)*

[108] E. Kheirati Roonizi and R. Sameni, "Morphological modeling of cardiac signals based on signal decomposition," *Comput. Biol. Med.*, vol. 43, pp. 1453–1461, 2013. *(Cited on pages 16, 20, and 27)*

[109] R. Sameni, C. Jutten, and M. B. Shamsollahi, "Multichannel electrocardiogram decomposition using periodic component analysis," *IEEE Trans. Biomed. Eng.*, vol. 55, no. 8, pp. 1935–1940, 2008. *(Cited on page 16)*

[110] R. E. Kalman, "A new approach to linear filtering and prediction problems," *ASME Journal of Basic Engineering*, 1960. *(Cited on page 18)*

[111] S. M. Kay, *Fundamentals of Statistical Signal Processing: Estimation Theory*. Upper Saddle River, NJ, USA: Prentice-Hall, Inc., 1993. *(Cited on page 18)*

[112] Y. Wang and M. Papageorgiou, "Real-time freeway traffic state estimation based on extended kalman filter: a general approach," *Transportation Research Part B: Methodological*, vol. 39, no. 2, pp. 141 – 167, 2005. *(Cited on page 19)*

[113] J. Choi, A. C. de Castro Lima, and S. Haykin, "Kalman filter-trained recurrent neural equalizers for time-varying channels." *IEEE Trans. Communications*, vol. 53, no. 3, pp. 472–480, 2005. *(Cited on page 19)*

[114] S. Y. Chen, "Kalman filter for robot vision: A survey," *IEEE Transactions on Industrial Electronics*, vol. 59, no. 11, pp. 4409–4420, 2012. *(Cited on page 19)*

[115] Z. Dong, *Robust Kalman Filter with Application to State Estimation of a Nuclear Reactor*. INTECH Open Access Publisher, 2010. [Online]. Available: https://books.google.it/books?id=FuzYoAEACAAJ *(Cited on page 19)*

[116] J. Zhang, G. Welch, N. Ramakrishnan, and S. Rahman, "Kalman filters for dynamic and secure smart grid state estimation," *Intelligent Industrial Systems*, vol. 1, no. 1, pp. 29–36, 2015. *(Cited on page 19)*

[117] Y. Yang, W. Hu, and Y. Min, "Projected unscented kalman filter for dynamic state estimation and bad data detection in power system," *IET Conference Proceedings*, pp. 12.30–12.30(1), 2014. *(Cited on page 19)*

[118] G. Jo and H. S. Choi, "Velocity-aided underwater navigation system using receding horizon kalman filter," *IEEE Journal of Oceanic Engineering*, vol. 31, no. 3, pp. 565–573, 2006. *(Cited on page 19)*

[119] Y. Xincun, O. Yongzhong, S. Fuping, and F. Hui, "Kalman filter applied in underwater integrated navigation system," *Geodesy and Geodynamics*, vol. 4, no. 1, pp. 46 – 50, 2013. *(Cited on page 19)*

[120] G. Ligorio and A. M. Sabatini, "A novel kalman filter for human motion tracking with an inertial-based dynamic inclinometer," *IEEE Transactions on Biomedical Engineering*, vol. 62, no. 8, pp. 2033–2043, 2015. *(Cited on page 19)*

[121] D. Sauter, B. J. Martin, N. Di Renzo, and C. Vomscheid, "Analysis of eye tracking movements using innovations generated by a kalman filter," *Medical and Biological Engineering and Computing*, vol. 29, no. 1, pp. 63–69, 1991. *(Cited on page 19)*

[122] S. Jayaram, "A new fast converging kalman filter for sensor fault detection and isolation," *Sensor Review*, vol. 30, no. 3, pp. 219–224, 2010. *(Cited on page 19)*

[123] B. D. O. Anderson and J. B. Moore, *Optimal Filtering*. Dover Publications, Inc., 1979. *(Cited on page 19)*

[124] A. L. Goldberger, L. A. N. Amaral, L. Glass, J. M. Hausdorff, P. C. Ivanov, R. G. Mark, J. E. Mietus, G. B. Moody, C.-K. Peng, and H. E. Stanley, "Physiobank, Physiotoolkit, and Physionet: Components of a new research resource for complex physiologic signals," *Circulation*, vol. 101, pp. e215–e220, 2000. *(Cited on pages 27 and 70)*

[125] E. Kheirati Roonizi and M. Fatemi, "A modified Bayesian filtering framework for ECG beat segmentation," in *Proc. of the 22nd Iranian Conference on Electrical Engineering (ICEE)*, 2014, pp. 1868–1872. *(Cited on pages IX, 30, and 32)*

[126] P. Maybeck, *Stochastic Models, Estimation, and Control*. Mathematics in Science and Engineering. Elsevier Science, 1982. *(Cited on page 31)*

[127] J. Behar, J. Oster, and G. Clifford, "A Bayesian filtering framework for accurate extracting of the non invasive FECG morphology," in *Computing in Cardiology*, vol. 41, 2014, pp. 53–56. *(Cited on page 31)*

[128] M. Niknazar, B. Rivet, and C. Jutten, "Fetal ECG extraction by extended state Kalman filtering based on single-channel recordings." *IEEE Trans. Biomed. Eng.*, vol. 60, pp. 1345–1352, 2013. *(Cited on page 32)*

[129] J. Slocum, E. Byrom, L. McCarthy, A. Sahakian, and S. Swiryn, "Computer detection of atrioventricular dissociation from surface electrocardiograms during wide QRS complex tachycardias." *Circulation*, vol. 72, no. 5, pp. 1028–1036, 1985. *(Cited on page 35)*

[130] L. Sörnmo, "Vectorcardiographic loop alignment and morphologic beat-to-beat variability," *IEEE Transactions on Biomedical Engineering*, vol. 45, no. 12, pp. 1401–1413, 1998. *(Cited on page 36)*

[131] V. D. Corino, M. W. Rivolta, R. Sassi, F. Lombardi, and L. T. Mainardi, "Ventricular activity cancellation in electrograms during atrial fibrillation with constraints on residuals' power," *Medical Engineering & Physics*, vol. 35, no. 12, pp. 1770–1777, 2013. *(Cited on page 36)*

[132] A. Bollmann, D. Husser, L. Mainardi, F. Lombardi, P. Langley, A. Murray, J. J. Rieta, J. Millet, S. B. Olsson, M. Stridh, and L. Sörnmo, "Analysis of surface electrocardiograms in atrial fibrillation: techniques, research, and clinical applications," *Europace*, vol. 8, no. 11, pp. 911–926, 2006. *(Cited on page 37)*

[133] E. Roonizi and R. Sassi, "A Signal Decomposition Model-Based Bayesian Framework for ECG Components Separation," *IEEE Transactions on Signal Processing*, vol. 64, no. 3, pp. 665–674, 2016. *(Cited on pages 39, 40, 43, and 45)*

[134] C. Roads, *The Computer Music Tutorial*. Cambridge, MA, USA: MIT Press, 1996. *(Cited on page 40)*

[135] A. L. Goldberger, L. A. N. Amaral, L. Glass, J. M. Hausdorff, P. C. Ivanov, R. G. Mark, J. E. Mietus, G. B. Moody, C.-K. Peng, and H. E. Stanley, "PhysioBank, PhysioToolkit, and PhysioNet components of a new research resource for complex physiologic signals," *Circulation*, vol. 101, pp. e215–e220, 2000. *(Cited on pages 43 and 57)*

[136] G. Moody, "Spontaneous termination of atrial fibrillation: A challenge from physionet and computers in cardiology 2004," *Computers in Cardiology*, vol. 31, pp. 101–104, 2004. *(Cited on page 49)*

[137] A. Fujiki, R. Yoshioka, M. Sakabe, and S. Kusuzaki, "QT/RR relation during atrial fibrillation based on a single beat analysis in 24-h Holter ECG: The role of the second and further preceding RR intervals in QT modification ," *Journal of Cardiology*, vol. 57, no. 3, pp. 269 – 274, 2011. *(Cited on page 51)*

[138] F. Ehlert, J. Goldberger, J. Rosenthal, and A. Kadish, "Relation between QT and RR intervals during exercise testing in atrial fibrillation," *The American journal of cardiology*, vol. 70, no. 3, pp. 332–338, 1992. *(Cited on page 51)*

[139] A. Fujiki and M. Sakabe, "Comparison of QT/RR Relation Based on a 15-s Averaged ECG and a Single Beat ECG During Atrial Fibrillation," *Circulation Journal*, vol. 75, no. 2, pp. 274–279, 2011. *(Cited on page 51)*

[140] P. G. Platonov, "P-wave morphology: Underlying mechanisms and clinical implications," *Ann Noninvasive Electrocardiol*, vol. 17, pp. 161–169, 2012. *(Cited on page 52)*

[141] A. Herreros, E. B. Lázaro, R. Johansson, J. Carlson, J. R. Perán, and B. Olsson, "Analysis of changes in the beat-to-beat P-wave morphology using clustering techniques," *Biomed Signal Process Control*, vol. 4, pp. 309 – 316, 2009. *(Cited on page 52)*

[142] A. Michelucci, G. Bagliani, A. Colella, P. Pieragnoli, M. C. Porciani, G. Gensini, and L. Padeletti, "P-wave assessment: state of the art update," *Cardiac Electrophysiol. Rev.*, vol. 6, pp. 215–220, 2002. *(Cited on page 53)*

[143] J. Carlson, R. Johansson, and B. Olsson, "Classification of electrocardiographic P-wave morphology," *IEEE Trans. Biomed. Eng.*, vol. 48, pp. 401–405, 2001. *(Cited on page 53)*

[144] E. Cohen, R. F. Riesenfeld, and G. Elber, Eds., *Geometric Modeling with Splines: An Introduction*. A K Peters/CRC Press, Natick (MA), 2001. *(Cited on page 55)*

[145] P. Diercks, *Curve and surface fitting with splines*. Oxford: Oxford University Press, 1995. *(Cited on page 56)*

[146] D. R. Adam, S. Akselrod, and R. J. Cohen, "Estimation of ventricular vulnerability to fibrillation through t-wave time series analysis," in *Computing in Cardiology*, vol. 8, 1981, pp. 307–310. *(Cited on page 63)*

[147] J. P. Martinez and S. Olmos, "Methodological principles of t wave alternans analysis: a unified framework," *IEEE Transactions on Biomedical Engineering*, vol. 52, no. 4, pp. 599–613, 2005. *(Cited on page 63)*

[148] E. Kheirati Roonizi and R. Sassi, "A signal decomposition model-based bayesian framework for ECG components separation," *IEEE Trans Sig Process*, 2015, (accepted, in press). *(Cited on page 63)*

[149] G. B. Moody, "The Physionet / Computers in Cardiology challenge 2008: T-wave alternans," *Comput Cardiol*, vol. 35, pp. 505–508, 2008. *(Cited on page 68)*

[150] S. W. Smith, "T/QRS ratio best distinguishes ventricular aneurysm from anterior myocardial infarction," *Am. J. Emerg. Med.*, vol. 23, pp. 279–287, 2005. *(Cited on page 70)*

[151] K. G. Rosén, I. Amer-Wåhlin, R. Luzietti, and H. Norén, "Fetal ECG waveform analysis," *Best Pract. Res. Clin. Obstet. Gynaecol.*, vol. 18, pp. 485–514, 2004. *(Cited on page 70)*

[152] I. Amer-Wåhlin, S. Arulkumaran, H. Hagberg, K. Maršál, and G. Visser, "Fetal electrocardiogram: ST waveform analysis in intrapartum surveillance," *BJOG*, vol. 114, pp. 1191–1193, 2007. *(Cited on page 70)*

[153] R. Sassi and L. T. Mainardi, "An estimate of the dispersion of repolarization times based on a biophysical model of the ECG," *IEEE Trans Biomed Eng*, vol. 58, pp. 3396–3405, 2011. *(Cited on pages 75, 76, and 78)*

[154] A. van Oosterom, "Genesis of the T wave as based on an equivalent surface source model," *J Electrocardiol*, vol. 34, pp. 217–227, 2001. *(Cited on page 75)*

[155] ——, "The Dominant T Wave." *J Electrocardiol*, vol. 37, pp. 193–197, 2004. *(Cited on pages 75 and 81)*

[156] ——, "The dominant T wave and its significance." *J Cardiovasc Electrophysiol*, vol. 14, pp. 180–187, 2003. *(Cited on page 75)*

[157] L. Mainardi, D. Di Donato, D. Falcone, and R. Sassi, "Improved estimation of V-index based on analytic forms of Dominant T-Wave," in *Comput Cardiol*, vol. 40, 2013, pp. 467–470. *(Cited on page 76)*

[158] E. Kheirati Roonizi and R. Sassi, "A Signal Decomposition Approach to Morphological Modeling of P wave," *Comput Cardiol*, vol. 41, pp. 341–344, 2014. *(Cited on page 77)*

[159] B. H. Van Huysduynen, C. A. Swenne, H. H. Draisma, M. L. Antoni, H. Van De Vooren, E. E. Vand Der Wall, and M. J. Schalij, "Validation of ECG Indices of Ventricular Repolarization Heterogeneity: A Computer Simulation Study." *J Cardiovasc Electrophysiol*, vol. 16, pp. 1097–1103, 2005. *(Cited on page 81)*

[160] E. K. Roonizi, M. W. Rivolta, L. T. Mainardi, and R. Sassi, "A comparison of three methodologies for the computation of v-index," in *2015 Computing in Cardiology Conference (CinC)*, 2015, pp. 593–596. *(Cited on page 89)*

[161] S. A. Israel, J. M. Irvine, B. K. Wiederhold, and M. D. Wiederhold, *The Heartbeat: The Living Biometric*. John Wiley, Sons, Inc., 2009, pp. 429–459. *(Cited on page 89)*

[162] ——, "Ecg to identify individuals," *Pattern Recognition*, vol. 38, pp. 133–142, 2005. *(Cited on page 89)*

[163] T. Gasser and A. Kneip, "Searching for structure in curve samples," *Journal of the American Statistical Association*, pp. 1179–1188, 1995. *(Cited on page 109)*

[164] A. Kneip and J. Ramsay, "Combining registration and fitting for functional models," *Journal of the American Statistical Association*, pp. 1155–1165, 2008. *(Cited on page 109)*

[165] J. O. Ramsay and X. Li, "Curve registration," *Journal of the Royal Statistical Society - Series B*, pp. 351–363, 1998. *(Cited on page 109)*

[166] K. Wang and T. Gasser, "Alignment of curves by dynamic time warping," *The Annals of Statistics*, pp. 1251–1276, 1997. *(Cited on page 109)*

[167] J. Ramsay and B. Silverman, *Functional Data Analysis*. Springer, New York., 2005. *(Cited on pages 109 and 113)*

[168] J. O. Ramsay, "Estimating smooth monotone functions," *Journal of the Royal Statistical Society - Series B*, pp. 365–375, 1996. *(Cited on page 109)*

[169] R. Tang and H.-G. MÃŒller, "Pairwise curve synchronization for functional data," *Biometrika* , pp. 875–889, 2008. *(Cited on page 109)*

[170] A. Kneip, X. Li, K. B. MacGibbon, and J. O. Ramsay, "Curve registration by local regression," *The Canadian Journal of Statistics*, pp. 19–29, 2000. *(Cited on page 109)*

[171] G. M. James, "Curve alignment by moments," *The Annals of Applied Statistics*, pp. 480–501, 2007. *(Cited on page 109)*

[172] K. Wang and T. Gasser, "Synchronizing sample curves nonparametrically," *The Annals of Statistics*, pp. 439–460, 1999. *(Cited on pages 109 and 117)*

[173] X. Liu and H.-G. MÃŒller, "Functional convex averaging and synchronization for time-warped random curves," *Journal of the American Statistical Association*, pp. 687–699, 2004. *(Cited on page 109)*

[174] N. Malfait and J. Ramsay, "The historical functional linear model," *Canadian Journal of Statistics*, pp. 115–128, 2003. *(Cited on page 109)*

[175] C. Crambes, A. Kneip, and P. Sarda, "Smoothing splines estimators for functional linear regression," *The Annals of Statistics*, pp. 35–72, 2009. *(Cited on page 109)*

[176] A. Kneip and T. Gasser, "Convergence and consistency results for self-modeling nonlinear regression," *The Annals of Statistics*, pp. 82–112, 1988. *(Cited on page 109)*

[177] G. Gervini and T. Gasser, "Self-modelling warping functions," *Journal of the Royal Statistical Society - Series B*, pp. 959–971, 2004. *(Cited on page 109)*

[178] H. Sakoe and S. Chiba, "Dynamic Programming Algorithm Optimization for Spoken Word Recognition," *IEEE Trans. Acoust., Speech, Signal Processing*, vol. 26, pp. 43–49, 1978. *(Cited on page 110)*

[179] B. Vahabzadeh and R. Sameni, "The Notion of Cardiac Phase and its Applications in Electrophysiological Studies," in *Biomedical Engineering (BioMed 2012)*, Innsbruck, Austria, February 15–17 2012. *(Cited on page 110)*

[180] J. O. Ramsay and X. Li, "Curve registration," *J R Stat Soc Series B Stat Methodol*, pp. 351–363, 1998. *(Cited on page 113)*

A

PUBLICATIONS

Journal:

1. **E. Kheirati Roonizi** and R. Sassi "A Signal Decomposition Model-Based Bayesian Framework for ECG Components Separation", IEEE Transactions on Signal Processing, VOL. 64 No. 3, pp. 665 – 674, 2016.
2. **E. Kheirati Roonizi** and R. Sassi "An Extended Nonlinear Bayesian Framework for Atrial and Ventricular Activity Separation", IEEE Journal of Biomedical and Health Informatics, In Press.
3. R. Abacherli, R. Twerenbold, R. Sassi, M.W. Rivolta, **E. Kheirati Roonizi**, L.T. Mainardi and T. Reichlin "Diagnostic and Prognostic Value of the $\mathcal{V}$-index, a novel 12-lead ECG marker of Repolarization Heterogeneity, in Patients with Symptoms suggestive of Acute Myocardial Infraction", Under review.

Conference:

1. **E. Kheirati Roonizi** and R. Sassi "A Signal Decomposition Approach to Morphological Modeling of P wave", Computing in Cardiology 2014; 41 : 341 – 344.
2. **E. Kheirati Roonizi**, L.T. Mainardi and R. Sassi "A New Algorithm for Estimating the $\mathcal{V}$-index Using Sinusoidal Basis Functions", Engineering in Medicine and Biology Society (EMBC), 37th Annual International Conference of the IEEE, pp. 386 – 389, 2015.
3. **E. Kheirati Roonizi**, M.W. Rivolta, L.T. ainardi and R. Sassi "A Comparison of Three Methodologies for the Computation of $\mathcal{V}$-index",Computing in Cardiology 2015; 42 : 593 – 596.
4. **E. Kheirati Roonizi** and R. Sassi "A Signal Decomposition Based Kalman Smoother for T-Wave Alternans Detection", AEIT International Annual Conference (AEIT), 2015, 1 – 4.

5. **E. Kheirati Roonizi** and R. Sassi "Dominant Atrial Fibrillatory Frequency Estimation using an Extended Kalman Smoother", Computing in Cardiology 2016; Accepted for publication.

B

APPENDIX A

B.1 AN ADVANCED TIME WARPING METHOD FOR SIGNAL REGISTRATION

Curve registration is one of the significant problems in functional data analysis (fda). When studying some processes (*e.g.*, biological or physical processes in different subjects), we usually see that the observed signals have a common structural pattern, but there are variations in both amplitude and phase (timing) between observation curves, which leads to many other problems.

Due to these problems, the issue of curve registration has been approached differently by researchers. A process of finding the monotone transformation to align the features of sample of one curve with another is named curve registration in literature review. It has been one of the most challenging problems during the last two decades [163, 164, 165, 166]. For more details see the monograph by Ramsay and Silverman [167]. For an overview, consider the set of curves shown in Fig. B.1. These curves differ from each other on the grounds of heights and locations of their peaks and valleys. So we can distinguish the amplitude variability from phase variability by defining the former as associated with the height and the latter with the location of peaks and valleys.

Many developments in curve alignment (curve registration) have been proposed in the related literature:

Estimating Smooth Monotone Functions [168], Continous Monotone Registration [165], Pairwise Curve Synchronization [169], Local Regression and Locally Estimate Monotone Transformation [170, 164], Curve alignment by equating the moments of a given set of curves [171], Curve alignment by Dynamic Time Warping [166], Synchronizing Sample Curves Nonparametrically [172], Functional Convex Synchronization [173], Functional Linear Regression [174, 175] and Self Modeling Warping Function (which is a curve alignment, based on a semi-parametric model for the warping functions) [176, 177].

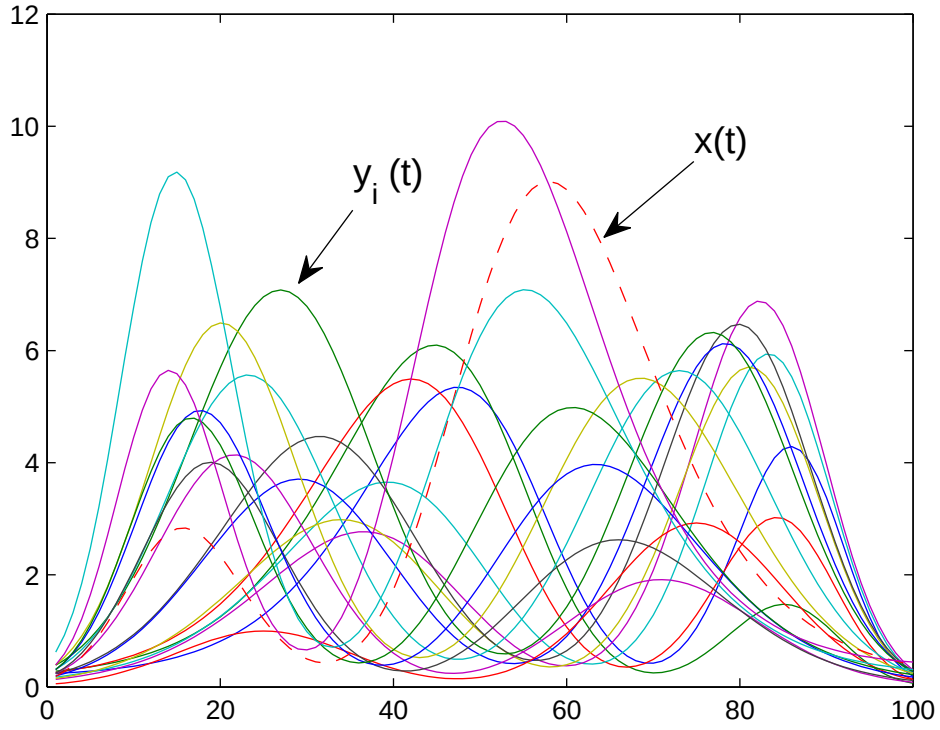

Figure B.1: 21 random unregistered curves with a two-dimensional structure generated from curves (B.18) and warping functions (F1)

One of the early works in using time warping was done by Sakoe *et al.* to synchronize speech signals [178]. In their work, they used dynamic time warping, which is a technique that warps the two time series nonlinearly in a way that similar events are aligned by minimizing the distance between them. It is better to point out that dynamic time warping in contrary to its name, uses nothing dynamic in the process. In this section, we propose a new method for estimating warping functions. The application of dynamic time warping in *cardiac phase* estimation has been studied in [179]. the estimated *cardiac phase* then can be used for calculating the heart rate (HR) signal. The main advantage of the estimated HR using *cardiac phase* is that the estimated HR will be continuous in time against HR estimated by RR-interval which is non-uniformly sampled. Several time warping methods have been used for estimating *cardiac phase* in [179]. The proposed model in this section can be used for estimating *cardiac phase*.

B.2 A NONLINEAR DIFFERENTIAL EQUATION FOR GENERATING WARPING FUNCTION

Let's consider $N+1$ functions $y_i(t)$, $1 \leqslant i \leqslant N$ and $x(t)$ be defined on the close real interval $[0,1]$. Suppose that $x(t)$ is the reference function and $y_i(t)$ is the function which warped to $x(t)$ with some specific warping function $h_i(t)$. Generally the objective is to find the function $h_i(t) \in [0,1]$, which aligns the two functions $y_i(t)$ and $x(t)$. In the simplest case the above definition is given as:

$$y_i(t) = a_i x\left[h_i(t)\right] \quad i = 1, ..., N \tag{B.1}$$

We assume a_i being an unknown with low changes in time ($\frac{\Delta a_i}{a_i^2} << 1$).

First a linear combination of basis functions is used for representing the observations $x(t)$ and $y_i(t)$:

$$\hat{x}(t) = \sum_{k=0}^{N-1} p_k \phi_k(t), \tag{B.2}$$

$$\hat{y_i}(t) = \sum_{k=0}^{N-1} q_k \phi_k(t), \tag{B.3}$$

where

- N is the number of basis functions in the expansion.
- $\{\phi_k(t)\}_{k=0}^{N-1}$ should be called the basis of the expansion.
- $\{p_k, q_k\}_{k=0}^{N-1}$ are the set of corresponding coefficients of the expansions, which are computed from $x(t)$ and $y_i(t)$, respectively.
- $\hat{x}(t)$ and $\hat{y}_i(t)$ design an "acceptable" model for $x(t)$ and $y_i(t)$.

A very important property for an "acceptable" model is its ability in function approximation, *i.e.*, the model error $e(t) = x(t) - \hat{x}(t)$ should be within an acceptable range. Considering the fact that the observation $x(t)$ might be rather noisy, an ideal model does not necessarily have a zero error. In fact, while the model $\hat{x}(t)$ should overall resemble $x(t)$, there are always some noisy fluctuations within $x(t)$ that should be neglected by the model. In other words, denoising is somewhat intrinsic to modeling. Nevertheless, the basis functions should generally have the property that the energy of approximation error converges to zero as the model order increases ($N \to \infty$). This property is guaranteed for $\{\phi_k(t)\}$ that form an orthogonal basis (*e.g.*, sinusoidal basis).

According to what was said, we can have the following definition for a good approximation.

$$\hat{y}_i(t) \equiv a_i \hat{x}\left[h_i(t)\right]$$

and

$$\sum_{k=0}^{N-1} q_k \phi_k(t) = a_i \sum_{k=0}^{N-1} p_k \phi_k [h_i(t)] \tag{B.4}$$

Taking the derivative of both sides of (B.4) yields:

$$\sum_{k=0}^{N-1} q_k \psi_k(t) = \frac{d}{dt} a_i + a_i \frac{d}{dt} h_i(t) \sum_{k=0}^{N-1} p_k \psi_k [h_i(t)] \tag{B.5}$$

where $\psi_k(t) = \frac{d}{dt}\phi_k(t), k = 0, ..., N-1$.

From (B.4 and B.5) the following equation is achived:

$$\frac{\sum_{k=0}^{N-1} q_k \psi_k(t)}{\sum_{k=0}^{N-1} q_k \phi_k(t)} = \frac{\frac{d}{dt} a_i}{a_i} + \frac{d}{dt} h_i(t) \frac{\sum_{k=0}^{N-1} p_k \psi_k [h_i(t)]}{\sum_{k=0}^{N-1} p_k \phi_k [h_i(t)]} \tag{B.6}$$

Assuming $\frac{\frac{d}{dt} a_i}{a_i} << 1$, then eq. (B.6) can be written as:

$$\frac{\sum_{k=0}^{N-1} q_k \psi_k(t)}{\sum_{k=0}^{N-1} q_k \phi_k(t)} = \frac{d}{dt} h_i(t) \frac{\sum_{k=0}^{N-1} p_k \psi_k [h_i(t)]}{\sum_{k=0}^{N-1} p_k \phi_k [h_i(t)]} \tag{B.7}$$

which is nonlinear with respect to $h_i(t)$, but no longer depends on a_i.

(B.7) can also be represented in matrix notation:

$$\frac{q^T \Psi(t)}{q^T \Phi(t)} = \frac{d}{dt} h_i(t) \frac{p^T \Psi(h_i(t))}{p^T \Phi [h_i(t)]} \tag{B.8}$$

where

$$\begin{aligned} p &= [p_0, p_1, ..., p_{N-1}]^T \\ q &= [q_0, q_1, ..., q_{N-1}]^T \\ \Phi(t) &= [\phi_0(t), \phi_1(t), ..., \phi_{N-1}(t)]^T \\ \Psi(t) &= \frac{d}{dt}\Phi(t). \end{aligned} \tag{B.9}$$

After simplifying, we get the following non-linear differential equation

$$\frac{d}{dt} h_i(t) = \frac{q^T \Psi(t) p^T \Phi [h_i(t)]}{p^T \Psi [h_i(t)] q^T \Phi(t)}. \tag{B.10}$$

The warping function $h_i(t)$ is considered as a strictly monotone function which has a strictly positive first derivative. Built upon the idea of Ramsay, a smooth monotone

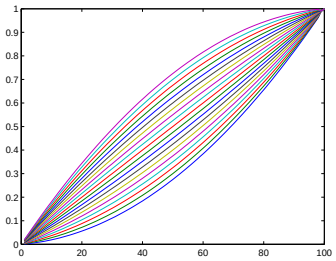

(a) the true time transformations $h_i(t)$ (F1)

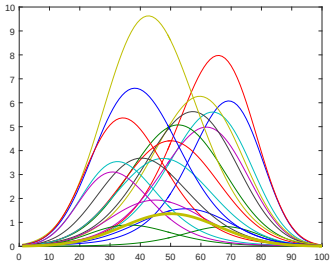

(b) the 21 sample curves before alignment;

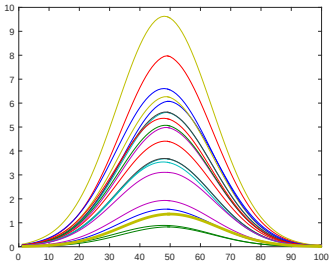

(c) the curves after alignment

Figure B.2: A typical run of the simulations with model (F1) for $h_i(t)$ and z_i with distribution $N(5, 1.25)$ for $x(h_i(t))$, Reference function (blue dashed line), average curve(Orange solid line)

.

function $h_i(t)$ can be defined by expressing its derivative, $\frac{d}{dt}h_i(t)$, as the exponential of an unconstrained function W of the form

$$\frac{d}{dt}h_i(t) = \exp[W]. \tag{B.11}$$

This idea was originally presented by Ramsay, in his landmark paper [180], which has ever since been used for various monotone spline modeling [167, Ch. 6].

Unconstrained function W can also be considered as a linear combination of B-spline basis functions:

$$W = c^T B(t) \tag{B.12}$$

where $B(t) = [B_0(t), B_1(t)..., B_m(t)]$ is the set of basis functions and $c = c_0, c_1, ..., c_m$ is the unknown corresponding coefficients. The B-spline basis functions consist of polynomial pieces that are smoothly connected together. So the warping functions are of the form

$$h_i(t) = \beta_0 + \beta_1 \int \exp[c^T B(t)]dt. \tag{B.13}$$

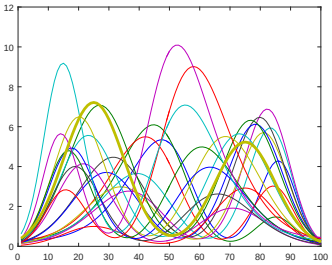

(a) the 21 sample curves before alignment;

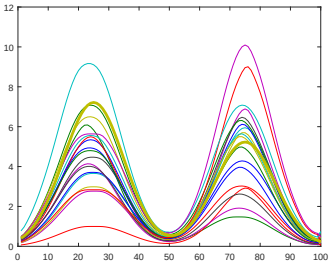

(b) the curves after alignment

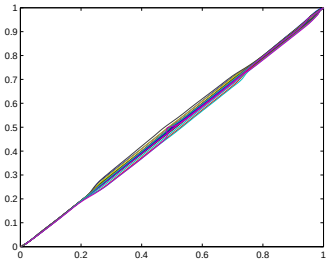

(c) the plot of the functions estimated warping functions $\hat{h}_i(h_i(t))$, which should be $\hat{h}_i(h_i(t)) = t$ for all i;

Figure B.3: A typical run of the simulations with model (F1) for $h_i(t)$ and z_i with distribution $N(5, 1.25)$ for $x(h_i(t))$, Reference function (blue dashed line), average curve(Orange solid line)

.

where β_0 and β_1 are constant value related to the boundary conditions. Also the derivative of (B.13) can be expressed as:

$$\frac{d}{dt}h_i(t) = \exp[c^T B(t)]. \tag{B.14}$$

By substituting (B.13) and (B.14) in (B.8) the fitting criterion is defined as:

$$\frac{q^T\Psi(t)}{q^T\Phi(t)} = \exp[c^T B(t)]\frac{p^T\Psi\left(\beta_0 + \beta_1\int\exp[c^T B(t)]dt\right)}{p^T\Phi\left(\beta_0 + \beta_1\int\exp[c^T B(t)]dt\right)} \tag{B.15}$$

The error function is defined as:

$$\rho(t) = \frac{q^T\Psi(t)}{q^T\Phi(t)} - \exp[c^T B(t)]\frac{p^T\Psi\left(\beta_0 + \beta_1\int\exp[c^T B(t)]dt\right)}{p^T\Phi\left(\beta_0 + \beta_1\int\exp[c^T B(t)]dt\right)} \tag{B.16}$$

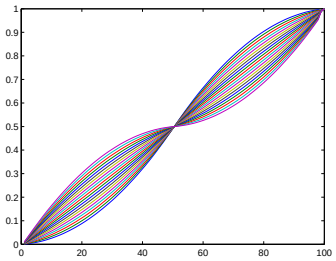

(a) the true time transformations $h_i(t)$ (F2)

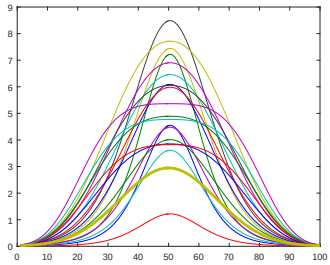

(b) the 21 sample curves before alignment;

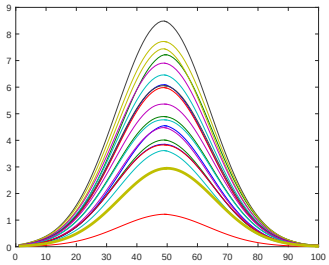

(c) the curves after alignment

Figure B.4: A typical run of the simulations with model (F2) for $h_i(t)$ and z_i with distribution $N(5, 1.25)$ for $x(h_i(t))$, Reference function (blue dashed line), average curve(Orange solid line)

.

Table B.1: Parameters of simulated model in (B.18)

Parameters	N = 1	N = 2
t_k	0.5	[0.25 0.75]
b_k	0.1581	[0.1 0.1]

The only unknown parameters is the coefficients vector c. The unknown coefficient c is obtained minimizing the corresponding LS criterion:

$$\sigma^2 = \int_0^1 \left[\frac{q^T\Psi(t)}{q^T\Phi(t)} - \exp[c^TB(t)] \frac{p^T\Psi\left(\beta_0 + \beta_1 \int \exp[c^TB(t)]dt\right)}{p^T\Phi\left(\beta_0 + \beta_1 \int \exp[c^TB(t)]dt\right)} \right]^2 dt + \lambda \int_0^1 \left(1 - \exp[c^TB(t)]\right)^2 dt \tag{B.17}$$

Thus the numerical solution of minimizing Eq. (B.17) estimates the warping functions (*e.g.*, the Matlab function `nlinfit.m` or `lsqnonlin.m` performs the required implementation of this nonlinear least-squares optimization).

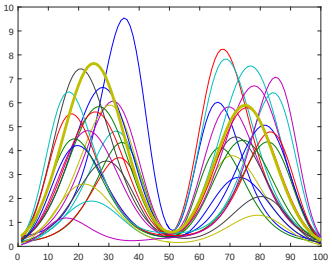

(a) the 21 sample curves before alignment;

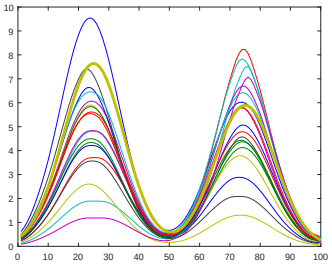

(b) the curves after alignment

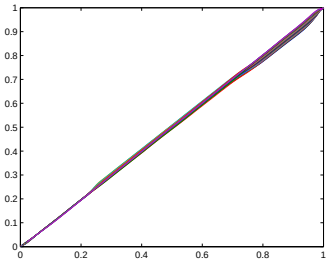

(c) the plot of the functions estimated warping functions $\hat{h}_i(h_i(t))$, which should be $\hat{h}_i(h_i(t)) = t$ for all i;

Figure B.5: A typical run of the simulations with model (F2) for $h_i(t)$ and z_i with distribution $N(5, 1.25)$ for $x(h_i(t))$, Reference function (blue dashed line), average curve(Orange solid line)

.

B.2.1 SIMULATED DATA ILLUSTRATION

The proposed algorithm was implemented in Matlab. To study the performance of the proposed method several simulation data sets were used. We generated four sets of 21 curves over the interval $[0, 1]$, which exhibit variation in amplitude and phase simultaneously:

$$y_i(t) = \sum_{k=0}^{N-1} z_{ik} \exp[-\frac{(t - t_k)^2}{2b_k^2}] \tag{B.18}$$

where N is the number of Gaussian functions, b_k and t_k are width, and center parameters of the Gaussian terms and the expansion coefficients z_{ik} were randomly generated from the distribution $N(5, 1.5)$.

These functions are suitable for describing many processes in mathematics, science, and engineering such as modelling the signals (*e.g.*, ECG). That is why we used these functions for simulates data. Some typical values of these parameters are listed in Table B.1.

We consider two forms of the time transformations $h_i(t)$:

Table B.2: The results of Sinusoidal and B-spline Models with Percentage root mean square differences, for different order of model for simulated curves (B.18) with 1000 samples

Method	Order						
	10	15	20	30	35	40	45
B-Spline	2.38%	2.22%	1.33%	1.013%	0.97%	0.83%	0.79%
Sinusoidal	2.87%	1.99%	1.32%	0.98%	0.88%	0.84%	0.78%

1. **F1:** Quadratic transformations $h_i(t) = t + b_i t(1-t)$, and the coefficients b_i were equally spaced between -1 and 1 .
2. **F2:** $h_i(t) = t + b_i sin(2\pi c_i t)$ where $c_i \in \{0, 1, 2, 3\}$. For more details see [172] .

Different examples of the curves $y_i(t)$ are shown in figures B.2 and B.4.

In this study, we employed the sinusoidal and B-spline basis alternatively for $\Phi(t)$ to model the unregistered curves $y_i(t)$. For performance evaluation, we used the percentage root-mean-square difference (PRD):

$$PRD \equiv 100 \sqrt{\frac{\sum_{k=1}^{N} (\hat{y}_{i,k} - \hat{x}(\hat{h}_{i,k}))^2}{\sum_{k=1}^{N} \hat{y}_{i,k}^2}}, \tag{B.19}$$

where, h_i and $\hat{h_i}$ are original and estimated warping functions. A lower PRD value indicates that the estimated function approximates the original more closely and is therefore better. The results of comparing the performance of Sinusoidal and B-spline basis functions are summarized in table B.2. Considering that the original curve has 1000 samples, the number of coefficients in (B.12) vary between ($N = 10 : 5 : 45$). The results show that the value of PRD decreases while the order of the model increases.